Wissenschaftszentrum Weihenstephan für Ernährung, Landnutzung und Umwelt

Lehrstuhl für Molekulare Ernährungsmedizin

Functional phenotype and metabolic properties of brite and brown adipocytes

Sabine Schweizer

Vollständiger Abdruck der von der Fakultät Wissenschaftszentrum Weihenstephan für Ernährung, Landnutzung und Umwelt der Technischen Universität München zur Erlangung des akademischen Grades eines

Doktors der Naturwissenschaften

genehmigten Dissertation.

Vorsitzender:	Prof. Dr. Michael Schemann
Prüfer der Dissertation:	1. Prof. Dr. Martin Klingenspor
	2. Prof. Dr. Martin Hrabě de Angelis

Die Dissertation wurde am 19.07.2017 bei der Technischen Universität München eingereicht und durch die Fakultät Wissenschaftszentrum Weihenstephan für Ernährung, Landnutzung und Umwelt am 29.11.2017 angenommen.

Table of contents

I. List of figures

II. List of tables

III. Abbreviations

2-DG	2-deoxy-D-glucose
2-DG-P	2-deoxy-D-glucose-phosphate
4-AAP	4-aminoantipyrine
AC	adenylate cyclase
Ache	acetylcholinesterase
Acot11	acyl-coenzyme A thioesterase 11
Acot4	acyl-coenzyme A thioesterase 4
Acot5	acyl-coenzyme A thioesterase 5
Acss2	acyl-coenzyme A synthetase
Agpat2	1-acyl-sn-glycerol-3-phosphate acyltransferase 2
Agpat3	1-acyl-sn-glycerol-3-phosphate acyltransferase 3
Akap6	a-kinase anchor protein 6
AMP	adenosine monophosphate
ANT	adenine nucleotide translocator
AR	adrenergic receptor
Aspg	asparaginase
Asph	aspartate-beta-hydroxylase
ATF-2	activating transcription factor 2
ATGL	adipose trigyceride lipase
ATP	adenosine triphosphate
Atp1b1	sodium/potassium-transporting ATPase subunit beta-1
Atp2a1	sarcoplasmic/endoplasmic reticulum calcium ATPase 1
Atp2a3	sarcoplasmic/endoplasmic reticulum calcium ATPase 3
BAT	brown adipose tissue
BCFA	branched chain fatty acid
BMI	body mass index
brite	brown in white
BSA	bovine serum albumin
Cacna1s	voltage-dependent l-type calcium channel subunit alpha-1s
Cacna2d1	voltage-dependent calcium channel subunit alpha-2/delta-1
Cacnb1	voltage-dependent l-type calcium channel subunit beta-1
Cacng1	voltage-dependent calcium channel gamma-1 subunit
Cacng6	voltage-dependent calcium channel gamma-6 subunit
Camk2a	calcium/calmodulin-dependent protein kinase type-6-subunit alpha
cAMP	cyclic adenosine monophosphate
Capn3	calpain-3
Casq1	calsequestrin-1
Casr	extracellular calcium-sensing receptor
Cav3	caveolin-3
cDNA	complementary DNA
Cds2	cdp-diacylglycerol synthase (phosphatidate cytidylyltransferase) 2
Chkb	choline kinase beta
Cidea	cell death-inducing DFFA-like effector a

Cidec	cell death-inducing DFFA-like effector c
Ckm	creatine kinase muscle type
Ckmt2	creatine kinase S-type, mitochondrial
CoA	coenzyme A
Coro1a	coronin-1a
Cox7a1	cytochrome c oxidase polypeptide 7a1
cpm	counts per minute
Cpt1a	carnitine palmitoyltransferase 1a
Cpt1b	carnitine palmitoyltransferase 1b
Cpt1c	carnitine palmitoyltransferase 1c
Cpt2	carnitine palmitoyltransferase 2
CREB	cAMP response element binding protein
Crhr2	corticotropin-releasing factor receptor 2
Ct	threshold cycle
Cth	cystathionine gamma-lyase
DAG	diacylglycerol
DAP	dihydroxyacetone phosphate
Dapk1	death-associated protein kinase 1
dd	day of differentiation
Dhrs7c	dehydrogenase/reductase sdr family member 7c
DIO-2	deiodinase 2
Dmd	dystrophin
DMEM	Dulbecco's Modified Eagle's Medium
DNA	deoxyribonucleic acid
dNTP	deoxyribonuleotide
dpm	disintegrations per minute
dsDNA	double-stranded DNA
ECAR	extracellular acidification rate
ER	endoplasmic reticulum
ERK	extracellular signal regulated kinase
Ero1l	ero1-like protein alpha
ESPA	sodium N-ethyl-N-(3-sulfopropyl) m-anisidine
Etnk1	ethanolamine kinase 2
Eva1	Eva-1 homolog a
eWAT	epididemal white adipose tissue
F2r	proteinase-activated receptor 1
FA	fatty acid
FADH2	dihydroflavine-adenine dinucleotide
FAME	fatty acid methyl esters
Fasn	fatty acid synthase
FCCP	carbonyl cyanide-4-(trifluoromethoxy)phenylhydrazone
FFA	free fatty acid
G1P	glycerol-1-phosphate
G3P	glycerol-3-phosphate
Glo1	glyoxalase i
Gnpat	dihydroxyacetone phosphate acyltransferase

Gpam	glycerol-3-phosphate acyltransferase 1, mitochondrial
GPAT1	glycerol-3-phosphate acyltransferase 1, mitochondrial
GPL	glycerophospholipid
gWAT	gonadal white adipose tissue
HBSS	Hank's Balanced Salt Solution
$HCO3^-$	hydrogen carbonate
hMADS cells	human multipotent adipose-derived stem cells
Hrc	sarcoplasmic reticulum histidine-rich calcium-binding protein
HSL	hormone sensitive lipase
iBAT	interscapular brown adipose tissue
IMM	inner mitochondrial membrane
IMS	intermembrane space
IP3	inositol 1,4,5-triphosphate
IP3R	inositoltriphoshate receptor
iWAT	inguinal white adipose tissue
Jph2	junctophilin-2
Jsrp1	junctional sarcoplasmic reticulum protein 1
LC/MS	liquid chromatography/mass spectrometry
LCFA	long chain fatty acid
LD	lipid droplet
LDH	lactate dehydrogenase
LPA	lysophosphatidic acid
Lpcat4	lysophospholipid acyltransferase lpcat4
Lpin1	Lipin1
Lpin3	Lipin3
LSC	liquid scintillation counting
Lypla1	lysophospholipase 1
MAPK	mitogen activated pathway kinase
MCU	mitochondrial calcium transporter
MEHA	3-methyl-N-ethyl-N-(β-hydroxyethyl)-aniline
MGL	monoacylglycerol lipase
MUFA	monounsaturated fatty acid
MW	molecular weight
mWAT	mesenteric white adipose tissue
Myf5	myogenic factor 5
Myh1	myosin-1
Myh4	myosin-4
Myh7	myosin-6-related
Mylk2	myosin light chain kinase 2, skeletal/cardiac muscle
Myo5b	unconventional myosin-vb
NADH	nicotinamide adenine dinucleotide, reduced
NCLX	sodium calcium transporter
NE	norepinephrine
NGS	next generation sequencing
NIC	normalized ion count
Nos1	nitric oxide synthase, brain

Nrxn2	neurexin-2
NST	non shivering thermogenesis
Nt5c	5', 3'-nucleotidase, cytosolic
Obscn	obscurin
OCFA	odd chain fatty acid
OCR	oxygen consumption rate
ORO	Oil Red O
Pacsin3	protein kinase c and casein kinase substrate in neurons protein 3
PAGE	polyacrylamide gel electrophoresis
PBS	phosphate buffered saline
PCR	polymerase chain reaction
Pcyt2	phosphate cytidylyltransferase 2, ethanolamine
Pde4d	cAMP-specific 3',5'-cyclic phosphodiesterase 4d
PET	positron emission tomography
Pfkm	ATP-dependent 6-phosphofructokinase, muscle type
PGC1α	PPARγ coactivator 1α
Phka1	phosphorylase b kinase regulatory subunit alpha, skeletal muscle isoform
Phkg1	phosphorylase b kinase gamma catalytic chain, skeletal muscle/heart isoform
Pik3r1	phosphatidylinositol 3-kinase regulatory subunit alpha
Pik3r2	phosphoinositide-3-kinase regulatory subunit 2
Pisd	phosphatidylserine decarboxylase
PKA	protein kinase A
PKC	protein kinase C
PL	phospholipid
Pla2g15	phospholipase a2, group 15
Pla2g4b	phospholipase a2, group 4 beta
Plbd1	phospholipase B domain containing 1
PLC	phospholipase C
PLIN	perilipin
Pnpla7	patatin-like phospholipase domain containing 7
Pnpla8	patatin-like phospholipase domain containing 8
PPARγ	peroxisome proliferator-activated receptor gamma
PPR	proton production rate
Prkcb	protein kinase c beta type
PSC-MPCs	human pluripotent stem-cell derived mesenchymal progenitor cells
PUFA	polyunsaturated fatty acid
Pvalb	parvalbumin alpha
qPCR	quantitative real-time polymerase chain reaction
Ramp1	receptor activity-modifying protein 1
RISK	RNA-induced silencing complex
RNA	ribonucleic acid
RNA-Seq	next generation sequencing of the transcriptome
RPKM	reads per 1000 base pairs transcript length and million reads
RQ	respiratory quotient
RT	room temperature
rWAT	retroperitoneal white adipose tissue

RYR	ryanodine receptor
SA	specific activity
Scd1	stearoyl-CoA desaturase 1
SDS	sodium dodecyl sulfate
SERCA	sarcoplasmic/endoplasmic reticulum calcium ATPase
siRNA	small (or short) interfering RNA
Slc30a1	zinc transporter 1
Slc8a3	sodium/calcium exchanger 3
Slc8b1	sodium/potassium/calcium exchanger 6, mitochondrial
Smtnl1	smoothelin-like protein 1
Srl	sarcalumenin
SVF	stroma vascular fraction
T2D	type 2 diabetes
T3	triiodothyronine
T4	thyroxine
TAG	triacylglyceride
TBS	tris buffered saline
TBST	tris buffered saline with tween
TCA	tricarboxylic acid
Tmem38a	trimeric intracellular cation channel type a
Trdn	triadin
Ttn	titin
UCP1	uncoupling protein 1
UTP	uridine 5'-triphosphate
VDAC	voltage-dependent anion channel
WAT	white adipose tissue
WB	Western Blot
WHO	World Health Organisation
Zic1	zinc finger protein of the cerebellum 1

IV. Summary

Worldwide, obesity is a major public health problem and the main cause of type 2 diabetes. Obesity can be treated by decreasing energy intake or increasing energy expenditure or both. In the last decade, anti-obesity and anti-diabetes effects of brown adipose tissue has become a major focus of scientific research. While white adipocytes store excess energy, brown adipocytes dissipate food energy by non-shivering thermogenesis. This process is mediated by mitochondrial uncoupling protein 1 (UCP1), located in the inner mitochondrial membrane. Beside the classical types of adipocytes, UCP1-expressing brown adipocyte like cells (brite, brown-in-white) can appear in white adipose tissue, in response to cold exposure and a variety of pharmacological or endocrine signals. This phenomenon has been coined browning. Since brown and brite adipocytes can be found in humans, their recruitment and activation represents an attractive treatment strategy. Knowledge of the basic biology of target cells is crucial for developing effective therapeutic tools. However, the functional and metabolic characteristics of brown and especially of brite cells are still not fully clarified.

In the present work, the functional phenotype and metabolic properties of brite and brown adipocytes was characterized using *in vitro* differentiated primary cultures.

Respirometric measurements confirmed the thermogenic capacity of brite adipocytes. Regarding the functional phenotype of these cells, we could show that lipolytic activity and lactate release in brite adipocytes were not affected by UCP1 abundance or activity. In contrast, a UCP1 dependent metabotype, mainly characterized by an altered FFA profile, was present in these cells. Combining metabolite profiling data and transcriptome data sets several candidate genes were identified which could play a crucial role in thermogenic function. Both in brite and in brown adipocytes, glucose uptake was completely independent of UCP1. UCP1 expressing brown adipocytes showed a reduced lactate release and activity of UCP1 diminished the release of lipolytic products. Interestingly, an alternative, ATP dependent thermogenic mechanism could be observed in brown adipocyte cultures from UCP1$^{-/-}$ mice which represents an exciting topic for future research. Moreover, within this project, from measured and deduced parameters, a model of metabolic fluxes was created that describes and predicts how an adrenergic stimulus changes metabolic reactions in a brown fat cell.

In summary, this PhD study provides new insights into the thermogenic capacity and functional characteristics of brite and brown adipocytes.

V. Zusammenfassung

Adipositas stellt eines der größten Gesundheitsprobleme weltweit dar und ist zudem Hauptursache für Typ 2 Diabetes. Adipositas kann entweder durch eine reduzierte Energieaufnahme und oder einen gesteigerten Energieverbrauch behandelt werden. Im vergangenen Jahrzehnt sind die positiven Effekte von braunem Fettgewebe im Zusammenhang mit Adipositas und Diabetes in den Fokus der Wissenschaft gerückt. Während weiße Adipozyten überschüssige Energie speichern, nutzen braune Adipozyten Energie zur zitterfreien Wärmebildung. Dieser Prozess wird über das in der inneren Mitochondrienmembran lokalisierte entkoppelnde Protein UCP1 vermittelt.

Neben klassischen Adipozyten können UCP1-expremierende, den braunen ähnlichen (englisch: brite, brown-in-white) Fettzellen im weißen Fettgewebe erscheinen. Dieses als browning bezeichnete Phänomen tritt in Folge von Kälteexposition und verschiedener pharmakologischer oder endokriner Signale auf. Da braune sowie brite Adipozyten beim Menschen vorkommen, stellen ihre Rekrutierung und Aktivierung eine attraktive Behandlungsstrategie dar. Für die Entwicklung wirksamer therapeutischer Maßnahmen ist Wissen um die fundamentale Biologie der Zielzellen essentiell. Jedoch, sind die funktionellen und metabolischen Charakteristika von braunen und ins Besondere von brite Adipozyten nicht vollständig bekannt.

Im Rahmen dieser Arbeit wurden *in vitro* differenzierte brite und braune Adipozyten hinsichtlich ihres funktionellen Phänotyps und metabolischen Eigenschaften untersucht.

Respirationsmessungen bestätigten die thermogene Fähigkeit von brite Adipozyten. Hinsichtlich ihrer funktionellen Eigenschaften konnte gezeigt werden, dass die lipolytsche Aktivität und die Freisetzung von Laktat nicht durch Vorkommen und Aktivität von UCP1 beeinflusst wurden. Allerdings, konnte ein UCP1 abhängiger Metabotype festgestellt werden, der hauptsächlich durch ein verändertes Fettsäureprofil gekennzeichnet war. Die Vereinigung von Metabolite Profiling Daten und Transkriptom Datensätzen ermöglichte die Identifizierung mehrerer Kandidatengene, die eine entscheidende Rolle in der thermogenen Funktion spielen könnten. Sowohl in brite als auch in braunen Fettzellen war die Glukoseaufnahme völlig unabhängig von UCP1. UCP1 exprimierende braune Fettzellen zeigten eine reduzierte Laktatfreisetzung. Zudem führte eine UCP1-Aktivität zu einer verminderten Freisetzung lipolytischer Produkte. Interessanterweise, konnte ein alternativer, ATP-abhängiger thermogener Mechanismus in braunen Adipozytkulturen von UCP1$^{-/-}$ Mäusen beobachtet werden. Dieser könnte einen spannenden Gegenstand

zukünftiger Forschung sein. Im Rahmen dieser Arbeit wurde zudem, mit Hilfe gemessener und abgeleiteter Parameter, ein metabolisches Fluxmodell generiert, welches die Veränderung metabolischer Reaktionen einer braunen Fettzelle in Folge eines adrenergen Stimulus beschreibt und vorhersagt.

Zusammenfassend lässt sich sagen, dass diese Dissertation neue Einblicke in die themogene Kapazität und funktionellen Eigenschaften von brite und braunen Adipozyten aufzeigt.

1 Introduction

1.1 Adipose tissue – white, brite and brown

In mammals, there exist two classical types of adipose tissues, white (WAT) and brown adipose tissue (BAT) (Cinti, 2005). WAT is one of the most abundant tissues in mammals and occurs mainly as subcutaneous and visceral depots. The distribution of WAT not only varies strongly among species, but also between individuals of one species and sex (Gesta and Kahn, 2012; Gesta et al., 2007). In rodents, major sites of subcutaneous WAT are the cervical and inguinal region whereas visceral fat can be found as mesenteric, perigonadal and retroperitoneal fat (Cinti, 1999). The primary function of WAT is the storage of excess energy, derived from food, mainly in form of triacylglyceride (TAG). In times of energy deprivation accumulated lipid stores can be mobilized to meet the energy demand of non-adipose tissues (Greqoir et al., 1998). In addition, WAT possesses an endocrine function. Through the production and secretion of adipokines WAT plays a crucial role in the regulation of whole body energy homeostasis (Cinti, 2005, 2012; Kuryszko et al., 2016; Unger and Scherer, 2010).

BAT occurs in rodents as visceral tissue in the mediastinic and perirenal region as well as subcutaneous depots in the cervical, axillary, subscapular and interscapular region (Heldmaier and Neuweiler, 2004). Like WAT, BAT is capable of accumulating energy as fat. However, its major purpose is to mobilize and catabolize this fat to produce heat and maintain body temperature in a cold environment (Nicholls and Locke, 1984).

Besides preadipocytes, endothelial cells, fibroblasts and immune cells WAT and BAT are mainly composed of white and brown adipocytes, respectively (Barneda et al., 2013; Cinti, 2005). In accordance with their distinct physiological function, white and brown adipocytes differ in morphology. White adipocytes are globular cells with a single large lipid droplet (LD) that occupies most of the intracellular space leaving only a thin rim of cytoplasm with a nucleus squeezed into a peripheral position. In contrast, brown adipocytes represent multilocular cells, storing fat within numerous small vacuoles. They have a central nucleus and are rich in mitochondria containing uncoupling protein 1 (UCP1) that mediates heat production (Cinti, 1999).

Interestingly, in response to cold exposure, adrenergic stimulation, peroxisome proliferator-activated receptor gamma (PPARγ) agoinist treatment or during postnatal development, UCP1-expressing brown adipocyte-like brite cells (“brown in white”, also

beige adipocytes) appear in WAT. This process has been termed browning (Cousin et al., 1992; Guerra et al., 1998; Himms-Hagen et al., 2000; Lasar et al., 2013; Xue et al., 2007; Young et al., 1984). Many transcriptional regulators, proteins and secreted factors have been associated with browning of WAT (Lo and Sun, 2013). Despite remarkable progress, the developmental origin, transcriptional control and physiological function of brite cells are still not fully understood.

In mice, interscapular BAT (iBAT) represents the largest brown fat depot (Rauch and Hayward, 1969). It contains classic brown adipocytes. In contrast, gonadal WAT (gWAT) is predominantly composed of white adipocytes, while in inguinal WAT (iWAT) white and brite adipocytes can be found (Figure 1) (de Jong et al., 2015; Waldén et al., 2012).The abundance of brite adipocytes depends on age, strain and environmental factors such as temperature and diet (Bonet et al., 2013; Garcia-Ruiz et al., 2015; Kozak and Koza, 2010; Rogers et al., 2012). In humans, BAT is present in the supraclavicular, suprarenal, paraaortic, paravertebral and neck region (Figure 1). Human BAT is more heterogenous. It is often mixed with white and brite adipocytes (Cypess et al., 2009; Virtanen et al., 2009; Zingaretti et al., 2009). This composition is for example present in the superclavicular region (Jespersen et al., 2013). A depot of classic brown adipocytes can be found deep in the neck, whereas brite adipocytes are enriched in the fat pad between the deep neck and subcutaneous WAT (Cypess et al., 2013). The characteristics of human BAT observed in the paravertebral, paraaortic and suprarenal region remain to be clarified.

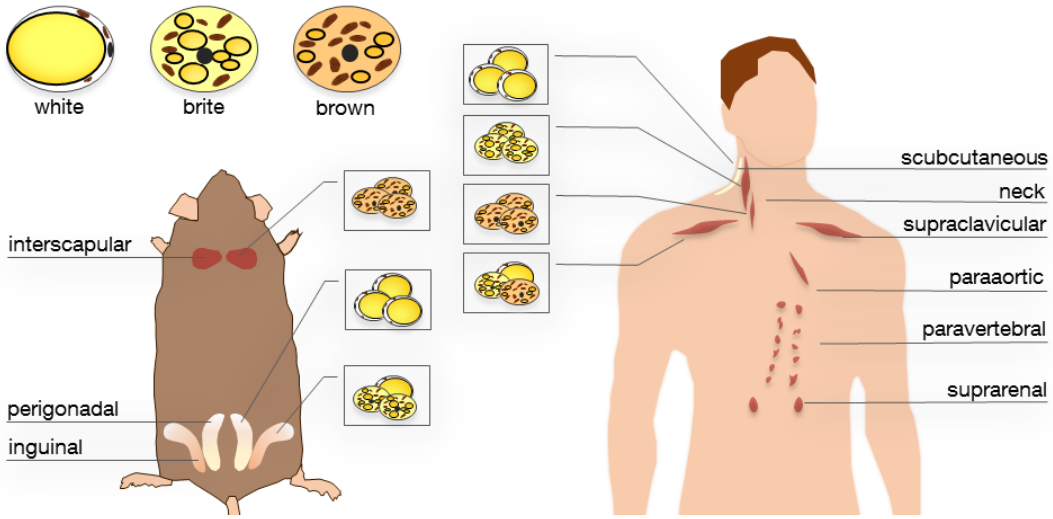

Figure 1: Anatomical location of brown, white and brite adipocytes in mice and humans. In mice, interscapular BAT contains classic brown adipocytes. Gonadal WAT is predominantly composed of white adipocytes. In the inguinal WAT a mixture of white and brite cells is present. The abundance of brite cells depends on intrinsic and environmental factors. In adult humans the subcutaneous fat has characteristics of classic WAT. Supraclavicular BAT contains brown, brite and white adipocytes, whereas classic BAT occcurs in the deep neck, close to muscle.

1.2 Origin and recruitment of brite adipocytes

In mice, the extent of browning varies among WAT depots as well as among inbred mouse strains. A large proportion of brite adipocytes can be found in iWAT, but these cells are rather rare in gWAT. An intermediate brite cell abundance is present in retroperitoneal WAT (rWAT) (Almind et al., 2007; Kozak and Koza, 2010). Mice of several strains, such as C57BL/6J, exhibit only minor induction of brite adipocytes upon adrenergic stimulation. In contrast, other inbred stains such as A/J and 129SV/S6, show a much larger response to this stimulus (Collins et al., 1997; Kozak and Koza, 2010; Vitali et al., 2012).

Currently, the developmental origin of brite cells is under debate. Lineage tracing experiments revealed that, in contrast to white adipocytes, classical brown adipocytes are derived from myogenic factor 5 (Myf5) positive precursors and thus developmentally related to skeletal muscle cells (Seale et al., 2008). Depending on anatomical location, brite cells arise either from Myf5 negative or positive precursor cells. While brite adipocytes in iWAT were found to be descendent of a Myf5 negative lineage (Seale et al., 2008), most of the brite cells in rWAT originate from Myf5 positive progenitors (Sanchez-Gurmaches et al., 2012).

For the recruitment of brite cells two concepts have been proposed. The first so-called transdifferentiation concept is based on the hypothesis that brite cells arise from mature white adipocytes by interconversion (Barbatelli et al., 2010; Himms-Hagen et al., 2000; Rosenwald et al., 2013; Vitali et al., 2012). The second hypothesis involves the *de novo* differentiation of brite cells from existing progenitor cells (Wang et al., 2013). The first concept is supported by the fact that brite recruitment under cold exposure or adrenergic treatment happens rather fast. Increased Ucp1 RNA expression is already visible after three hours and reaches its maximum after 48 hours (Kozak and Koza, 2010). Furthermore, upon cold exposure the total number of adipocytes in a WAT depot stays the same, while the proportion of brite cells increases (Barbatelli et al., 2010) and most brite adipocytes do not emerge by mitosis (Himms-Hagen et al., 2000). Aditionally, a brite phenotype change is reversible. When the cold stimulation ceases, brite adipocytes seem to be reconverted into cells with a white morphology and gene expression pattern. These white-like adipocytes can be again converted into brite adipocytes by an additional cold stimulus (Rosenwald et al., 2013). Therefore, brite adipocytes might occur at a basal state camouflaged as white-like adipocytes with the propensity to turn into multilocular cells upon stimulation and become re-camouflaged when this stimulation ends (Li et al., 2014c). The second concept is supported by identification of putative brite progenitor cells with

distinct surface markers (Lee and Granneman, 2012; Schulz et al., 2011; Steinbring et al., 2017). Thus, for both the transdifferentiation as well as the *de novo* differentiation concept, experimental evidence has been presented. It remains to be clarified which mechanism is dominant in recruitment of brite cells in WAT.

Taken together, brite adipocytes represent a novel type of fat cells that are heterogenous in their ontogeny and possess a similar morphology to brown adipocytes.

1.3 Thermogenic function of brown and brite adipocytes

To maintain a constant body temperature independent of environmental conditions, endothermic animals have developed thermoregulatory mechanisms (Scholander et al., 1950). Adaptive heat production becomes necessary when ambient temperature is below the thermoneutral zone. The thermoneutral zone is defined as a range of ambient temperatures at which temperature regulation is achieved only by control of heat loss and metabolic rate is basal. The thermoneutral zone varies between species and is around 30 °C in laboratory mice and unclothed humans (Gordon, 2012; IUPS, 2001; Kingma et al., 2014). Adaptive heat production is achieved by shivering and non-shivering thermogenesis (NST). Shivering involves increased involuntary contractile activity of skeletal muscles without physical work, whereas heat production through NST is characterized by metabolic energy transformation without any muscle contractions (IUPS, 2001). NST occurs almost exclusively in BAT and is mediated by UCP1, located in the inner mitochondrial membrane (IMM), where it uncouples respiration from adenosine triphosphate (ATP) synthesis.

UCP1 function

In a cell, most ATP is produced via the ATP synthase, complex V of the respiratory chain, in the IMM (Jonckheere et al., 2012). ATP production is driven by a flux of protons from the intermembrane space (IMS) through transmembrane into the mitochondrial matrix along a proton gradient. This proton motive force is due to an unequal distribution of protons across the IMM that is maintained by the proton pumps of the respiratory chain, powered by electrons from reduction equivalents reduced nicotinamide adenine dinucleotide (NADH) and dihydroflavine-adenine dinucleotide ($FADH_2$) generated in tricarboxylic acid (TCA) cycle and β-oxidation (Mitchell, 1961; Rich and Marechal, 2010). The final step within the electron transport chain is catalyzed by complex IV. It oxidizes cytochrome c and thereby reduces oxygen to water (Figure 2). Due to proton leak, oxygen consumption is not completely coupled to ATP synthesis. When this uncoupling happens,

energy stored in the proton gradient is not transformed into chemical energy in form of ATP but released as heat (Busiello et al., 2015). Basal proton leak occurs in all mitochondria and accounts for more than 20 % of total oxygen consumption in mammals (Rolfe and Brand, 1996). However, mitochondria of brown adipocytes, can dissipate up to 100 % of their proton motive force to produce heat by regulated uncoupling via UCP1 (Nicholls and Locke, 1984).

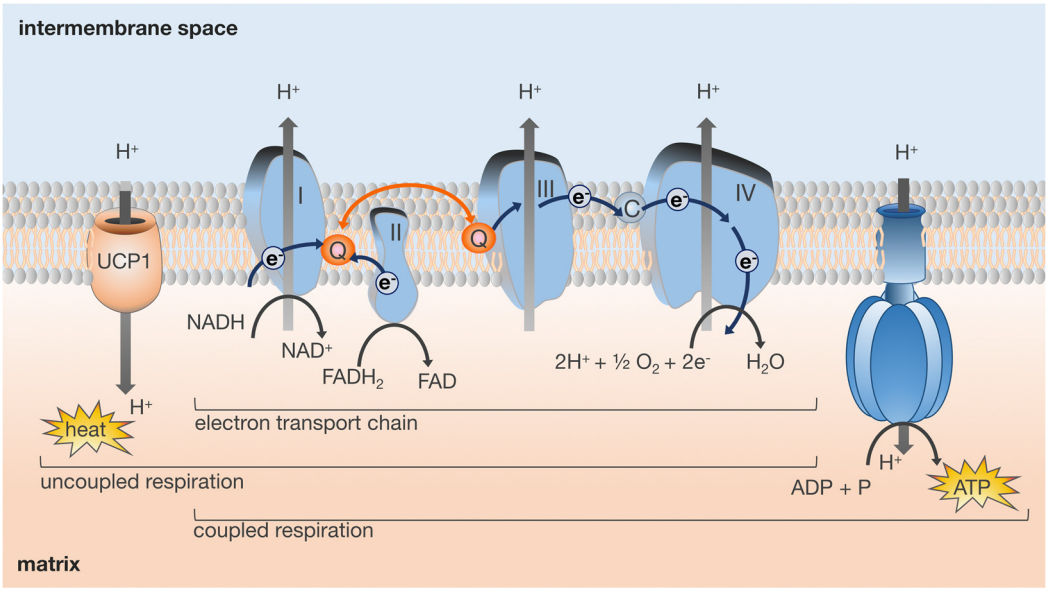

Figure 2: Mitochondrial coupled and uncoupled respiration. The respiratory chain generates a proton gradient across the inner mitochondrial membrane by translocation of protons from the matrix into the intermembrane space via complex I, III and IV. This process is driven by energy-rich electrons (e^-) from reduction equivalents NADH and $FADH_2$. e^- are passed through proton pumps facilitated by mobile carrier molecules ubiquinone (Q) and cytochrome c (C). Thereby they release stepwise their energy and are finally combined with oxygen and protons to form water. Protons can reenter the matrix by ATP synthase or by proton leak, catalyzed by UCP1. Thus, proton motive force is either chemically fixed in the form of ATP (coupled respiration) or dissipated as heat (uncoupled respiration by UCP1).

UCP1 is a 32 kDa protein that in cold acclimated rodents accounts for 5.8 – 7.7 % of mitochondrial protein and 15–20 % of the extractable membrane protein fraction of brown adipocytes (Lin and Klingenberg, 1980). High concentrations of cytosolic purine nucleotides constitutively inhibit UCP1. In contrast, free fatty acids (FFA) represent positive regulators of UCP1 activity. The exact molecular mechanism of UCP1 activation and action is still unclear. UCP1 may act as direct translocase that channels protons along negatively charged amino acid residues from the IMS to the matrix. In this case, FFA could act as a cofactor (Winkler and Klingenberg, 1994). Fedorenko et al. (2012) proposed a symport of protons and long chain fatty acid (LCFA) anions that cannot dissociate from UCP1 due to hydrophobic interactions established by their hydrophobic tails. Hence, UCP1 would effectively operate as an H^+ carrier activated by LCFA. Another model is that UCP1 can translocate protons without a cofactor but is inhibited by bound nucleotides.

FFA counteract inhibition by competing for an overlapping binding site without being transported through the membrane (Huang, 2003; Shabalina et al., 2004). Conversely, FFA anions themselves could be the transported substrate. In the IMS in the presence of high proton concentrations FFA would be protonated and in their neutral form enter the mitochondrial matrix by an uncatalyzed flip-flop mechanism. The low proton concentration of this compartment would lead to a release of the proton from the carboxyl group, creating a net proton flux across the IMM. In this model the function of UCP1 is the export of FFA anions out of the mitochondrial matrix and perhaps additionally the facilitation of flip-flop events (Garlid et al., 1996; Skulachev, 1991). All these concepts of molecular mechanisms can explain the observed increase in UCP1 mediated leak respiration upon release of FFA.

Activation and recruitment of thermogenic capacity

Upon a cold stimulus, norepinephrine (NE) is released from the sympathetic nervous system. It activates adrenergic receptors (ARs) of brown and brite adipocytes (Figure 3). Brown and brite cells express G_s-coupled β1-, β2- and β3-AR as well as the G_q and G_i coupled α1-AR and α2-AR, respectively. In rodents, β3-AR seems to be the most relevant AR (Lafontan and Berlan, 1993). Stimulation of G_s-coupled AR induces cyclic adenosine monophosphate (cAMP) formation via adenylate cyclase (AC), which in turn stimulates the protein kinase A (PKA). Hormone sensitive lipase (HSL) and the LD coating protein perilipin (PLIN) are phosphorylated and lipolytic rate increases (Holm, 2003; Stralfors and Belfrage, 1983). Additionally, lipolytic activity is initiated by activation of the adipose trigyceride lipase (ATGL) and further elevated via the extracellular signal regulated kinase (ERK) cascade (Greenberg et al., 2001; Pagnon et al., 2012; Robidoux et al., 2006). The released FFA can enter mitochondria, counteract the UCP1-inhibitory cytosolic purine nucleotides or are combusted in β-oxidation. Thus, FFAs released by lipolysis serve both as activators and fuel of non-shivering thermogenesis (Cannon and Nedergaard, 2004; Ellis et al., 2012). The acute activation of thermogenesis, mainly mediated via the β3-AR, is modulated by activation of α1-AR and α2-AR. α1-AR-binding activates phospholipase C (PLC) which leads to generation of diacylglycerol (DAG) and inositol 1,4,5-triphosphate (IP3). DAG activates protein kinase C (PKC) that further promotes lipolysis (Carmen and Víctor, 2006; Flechtner-Mors et al., 2002; Fricke et al., 2004). IP3 signaling mediates an increase in cytosolic calcium levels that can further modulate thermogenic function.

In parallel to the acute activation of UCP1 via increased lipolytic rate, NE initiates recruitment of NST capacity by elevating transcription of Ucp1 and other thermogenic

genes. Induction of the PKA-pathway via cAMP activates the transcription factor cAMP response element binding protein (CREB) and leads to activation of the mitogen activated pathway kinase (MAPK) p38 (Bonet et al., 2013; Cao et al., 2004).

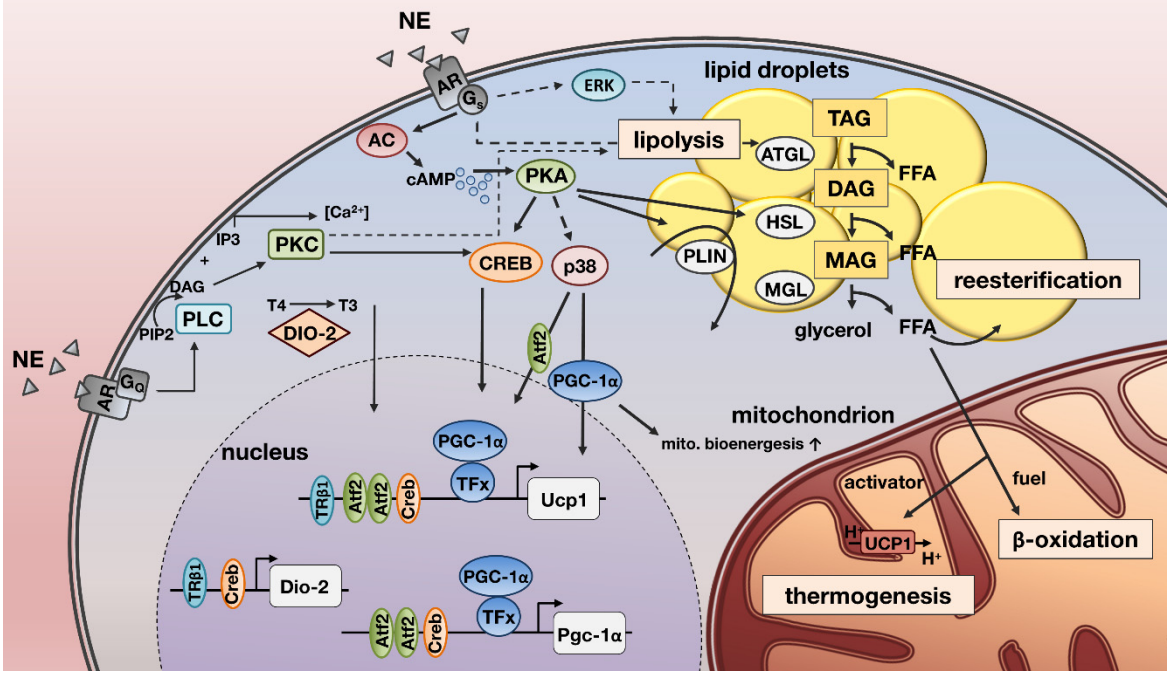

Figure 3: Signaling pathways involved in the regulation of non-shivering thermogenesis activity and capacity. At the plasma membrane, released norepinephrine (NE) activates G-protein coupled adrenoreceptors (AR). Gs-coupled-AR mediated signaling via PKA activation induces lipolytic release of fatty acids from lipid droplets. These free fatty acids (FFAs) are fuel and activators of UCP1 mediated non-shivering thermogenesis. Recruitment of thermogenic capacity in response to NE is mediated by a complex network of transcriptional control processes. Within this network adaptive gene expression is primarily initiated by the transcription (co-) factors CREB, ATF-2 and PGC1α. For detailed description and abbreviations please refer to the main text. Dashed arrows indicate pathway segments with interconnections unknown or deliberately left out. (modified from Klingenspor et al. (2017).

CREB binds to the promoter region of genes such as Ucp1, PPARγ coactivator 1α (Pgc1α) or thyroid hormone converting enzyme deiodinase 2 (Dio-2) (Canettieri et al., 2000; Rim et al., 2004). Besides its activation via PKA, part of CREB phosphorylation is mediated by a α1-ARs dependent pathway that involves PKC (Thonberg et al., 2002). The MAPK p38 phosphorylates the activating transcription factor 2 (ATF-2) which binds to the Ucp1 enhancer and the Pgc1α promoter. Besides its transcriptional regulation, PGC1α is also activated post-translationally by MAPK p38. In its active phosphorylated form, PGC1α is a potent transcriptional coactivator of Ucp1 and induces transcription of many genes involved in mitochondrial biogenesis. DIO-2 converts the thyroid prohormone thyroxine (T4) to its bioactive form triiodothyronine (T3). T3 binds and activates nuclear thyroid hormone receptors. Via the T3 receptor β1 (TR β1) isoform, T3 promotes Ucp1 and Dio-2 transcription (Golozoubova et al., 2004; Martinez de Mena et al., 2010). Taken together,

thermogenic capacity is recruited via an interwoven self-amplifying network of transcriptional control processes that include several positive feedback loops (Klingenspor et al., 2017).

Thermogenesis in brite adipocytes

Under cold exposure, when NST is required, browning occurs (Young et al., 1984). In cold exposed mice, in iWAT, Ucp1 mRNA expression is around 20 % and protein expression about 10 % of those in iBAT, respectively (Nedergaard and Cannon, 2013; Waldén et al., 2012). It is a subject of debate whether the UCP1 expressed in brite adipocytes contributes to thermogenesis. Isolated mitochondria from iWAT of cold-exposed mice contain similar amounts of UCP1 protein as mitochondria derived from iBAT. They are thermogenically active but show a lower thermogenic capacity compared to iBAT mitochondria (Shabalina et al., 2013). *In vivo,* browning of iWAT in response to cold is not reflected in increased metabolic activity, assessed by glucose and FFA uptake or oxidative activity (Labbe et al., 2016). Nevertheless, paucity of BAT was compensated by browning of WAT (Schulz et al., 2013). UCP1 in *in vitro* differentiated brite adipocytes as well as in brite cell lines was shown to be functionally thermogenic (Li et al., 2014b; Wu et al., 2012). Due to the limited amount of data, there is a need for directly assessing the functional phenotype and metabolic properties of brite adipocytes.

1.4 Health promoting effects of brown and brite fat in the context of obesity and diabetes

During the last decades, global obesity incidence has more than doubled. In 2014, 39 % of adults were overweight (body mass index, BMI ≥ 25) and 13 % were obese (WHO, 2016). If this epidemic trend continues, 60 % of the worldwide population will be overweight (2.2 billion) or obese (1.1 billion) in 2030 (Kelly et al., 2008). Overweight and obesity are the result of a prolonged positive energy balance. Besides genetic factors, this energy imbalance is mainly caused by excessive energy intake from food accompanied by a reduction of energy expenditure in the form of physical activity (Hill et al., 2012). Nowadays, more people die from overweight than from underweight and according to the World Health Organization (WHO), overweight and obesity represent the fifth leading risk for global deaths (WHO, 2009). Excessive body weight is associated with multiple comorbidities including cardiovascular diseases, diabetes, and cancer (Clark, 2013). In most European countries, overweight and obesity are responsible for around 80 % of cases of type 2 diabetes (T2D), 35 % of ischaemic heart disease and 55 % of

hypertensive disease among adults (Fruhbeck et al., 2013; Tsigos et al., 2011). T2D represents the most abundant form of diabetes (Alberti and Zimmet, 1998) and is characterized by reduced insulin sensitivity, hyperinsulinemia and progressive pancreatic β-cell failure (Kahn, 1998; Kasuga, 2006; Prentki, 2006). Over time, it can cause cardiovascular diseases, retinopathy, chronic kidney disease and neuropathy (Bailey et al., 2014; Bourne et al., 2013; Pasnoor et al., 2013; Sarwar et al., 2010).

The existence of BAT in adult humans had been questioned until studies based on positron emission tomography (PET) in combination with computed tomography confirmed the presence of significant amounts of metabolically active BAT in healthy adult humans (Cypess et al., 2009; van Marken Lichtenbelt et al., 2009; Virtanen et al., 2009). Based on glucose uptake it was estimated that approximately 60 g of BAT in healthy adults can burn 1-2 kg of fat tissue (Virtanen et al., 2009). Recently it was shown that in BAT positive subjects more than 300 ml of BAT tissue can be detected (Gerngroß et al., 2017). Human BAT depots are heterogenous and can contain white and brite adipocytes (Cypess et al., 2009; Virtanen et al., 2009; Zingaretti et al., 2009). In the last decade, anti-obesity and anti-diabetes effects of BAT have been demonstrated. In humans, cold-induced BAT activity is negatively correlated with BMI (Orava et al., 2013; van Marken Lichtenbelt et al., 2009). In addition, subjects with cold-activated detectable BAT have higher whole-body insulin sensitivity than BAT-negative subjects (Chondronikola et al., 2014; Orava et al., 2013). In streptozotocin-induced diabetic mice, BAT transplants resulted in improved glucose tolerance and reversal of clinical diabetes markers such as polyuria or polydipsia (Gunawardana and Piston, 2012). Thus, there is evidence that BAT is a promising therapeutic target.

In summary, brown and brite adipocytes are present in humans. Their recruitment and activation could be a useful therapeutic tool in the fight against the global health burden of obesity and T2D.

1.5 Objective of the present work

Obesity and associated comorbidities such as T2D are a global health burden. In this context, the recruitment and activation of brite and brown adipocytes are attractive treatment strategies. The development of successful therapeutic tools relies on understanding the basic biology of the target cells. However, the functional and metabolic properties, especially of brite adipocytes, are not clarified.

Adipose tissues are composed of mature adipocytes, preadipocytes and several other non-adipocyte cells including immune cells, fibroblasts, pericytes, endothelial cells, and other progenitor cells (Barneda et al., 2013). Besides systemic influences, non-adipocyte cells within the tissue can affect functional and metabolic properties. Isolation of preadipocytes and their differentiation *in vitro* represents a useful model to study fundamental and intrinsic biological properties and functions of brite and brown adipocytes independent from influences from tissue and organism.

The aim of this PhD thesis is to characterize *in vitro* differentiated brite and brown primary adipocytes in terms of their functional phenotype and metabolic properties.

In the first part, brite adipocytes cultures with differential browning capacities are characterized. For this study cultures of 129SV/S6 (high browning propensity) and C57BL/6J UCP1$^{+/+}$(low browning propensity) as well as C57BL/6J UCP1$^{-/-}$ mice are included. This model allows the examination of functional and metabolic parameters in presence of gradual UCP1 abundance. First, the finding that browning propensity varies between inbred strains and that this strain difference is maintained in primary cell culture on a molecular level has to be reproduced. Afterwards, morphological studies should clarify if the brite adipose cultures, compared in this study, have a similar differentiation capacity. In the next step, the thermogenic function of brite adipocytes is explored using microplate-based respirometry which allows a high throughput assessment of mitochondrial bioenergetics in adherent intact cells. It is important to clarify if the differential expression of UCP1 is reflected in UCP1 mediated uncoupled respiration, since this relationship is the perquisite for other functional analysis. Besides oxygen, thermogenic activity requires the supply of fatty acids and glucose. Thus, further functional phenotyping will include the assessment of lipolytic activity and glucose uptake as well as the release of lactate as a marker for glycolytic activity. To gain more information on the functional biochemical state of brite cells non-targeted metabolite profiling will be applied. The resulting metabolite profiling dataset will be combined with transcriptome analysis data. This approach can facilitate the identification of new metabolic pathways involved in the thermogenic function of brite adipocytes. Genes involved within these pathways represent putative candidates. Their role in the browning process and NST can be investigated by siRNA knockdown experiments.

The second part of this work focusses on the functional and metabolic characteristics of brown adipocyte cultures derived from UCP1$^{+/+}$ as well as UCP$^{-/-}$ mice. Since thermogenesis is the primary function of brown adipocytes, they have an increased

oxidative capacity and express UCP1 in much higher amounts than brite adipocytes. Ablation of UCP1 in these cells might have a lager impact on functional phenotype than in brite cells. Like in brite adipocytes, functional parameters such as oxygen consumption, lipolysis and lactate release will be measured. From crucial measured and deduced parameters, a model of metabolic fluxes will be created that describes and predicts how an adrenergic stimulus changes metabolic reactions in a brown fat cell.

This project provides an important opportunity to advance the understanding of the basic biology of brite and brown adipocytes. The assessment of the intrinsic functional and metabolic properties of these cells contributes to the evaluation of their use as therapeutic targets for obesity and T2D.

2 Material and Methods

A complete list of all chemicals and reagents including manufacturer and order number, can be found in appendix 6.2. Kit systems are available in appendix 6.3. For antibodies, disposables as well as devices and other equipment, consult appendices 6.4, 6.5 and 6.6 respectively. Software and internet resources are listed in appendix 6.7. All buffer and media compositions are given below the respective text sections.

2.1 Inbred mouse strains

For the functional phenotyping and metabolite profiling of brite adipocytes, C57BL/6J UCP1$^{+/+}$ and UCP1$^{-/-}$ mice (Hofmann et al., 2001) as well as 129SV/S6 were used. For the functional phenotyping of brown adipocytes, 129SV/S1 UCP1$^{+/+}$ and UCP1$^{-/-}$ mice were employed (Enerbäck et al., 1997). All mice were bred at the specified pathogen free animal facility of Technical University of Munich in Weihenstephan in accordance with the German animal welfare law.

2.2 Primary cell culture

Male mice, aged five to six weeks, were used to prepare primary cultures of brown and brite adipocytes. Depots of interscapular brown adipose tissue (iBAT) and inguinal white adipose tissue (iWAT) were dissected and transferred into prewarmed (37 °C) phosphate buffered saline (PBS) with 1 % v/v antibiotics (2:2:1 gentamycine, penicillin/streptomycin, fungizone). Depots were carefully minced, treated with collagenase containing digestion buffer and incubated at 37 °C under continuous vortex mixing in an orbital shaker for 45 minutes. Digestion was stopped by adding wash buffer. The homogenate was filtered through a 250 µm nylon mesh and centrifuged at 250 g for five minutes. The layer of mature adipocytes was disrupted, to achieve a complete separation of the stromal vascular fraction (SVF) from the primary mature adipocytes. Centrifugation was repeated, the supernatant was discarded and the pellet resuspended in wash buffer, followed by centrifugation at 500 g for five minutes. Supernatant was discarded and the remaining SVF was resuspended in culture medium and seeded to cell culture plates. On the next day, cells were washed twice with prewarmed PBS to remove the debris. Then fresh culture medium was added. After reaching confluency, induction medium was added for two days. Afterwards cells were maintained in differentiation medium for seven days. Medium was changed every two days (Figure 4).

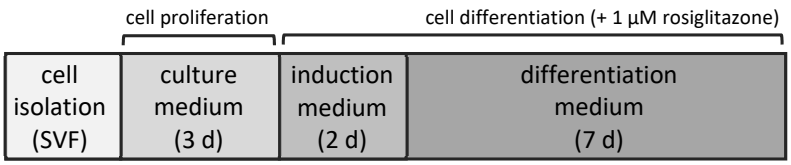

Figure 4: Cell culture scheme. Isolated stroma vascular fraction (SVF) was seeded to cell culture plates and maintained in culture medium until confluence. Then medium was changed to induction medium that was replaced by differentiation medium after two days.

Digestion buffer: 1x HBSS w/Mg;Ca, 3.5 % bovine serum albumin (BSA), 0.55 mM, glucose, 0.1 % collagenase A

Wash buffer: 1x HBSS w/Mg;Ca, 3.5 % BSA

Culture medium: DMEM, 20 % v/v FBS, 1 % v/v penicillin/streptomycin, gentamycin, fungizone (2:2:1)

Induction medium: DMEM, 10 % v/v FBS, 0.5 % v/v penicillin/streptomycin, 0.5 % v/v gentamycin, 0.5 mM isobutylmethylxanthine, 125 nM indomethacin, 1 mM dexamethasone, 850 nM insulin, 1 nM T3, 1 µM rosiglitazone

Differentiation medium: DMEM, 10 % v/v FBS, 0.5 % v/v penicillin/streptomycin, 0.5 % v/v gentamycin, 0.5 mM 850 nM insulin, 1 nM T3, 1 µM rosiglitazone

Volume of media: 6-well plate: 2 ml/well; 12-well plate: 1 ml/well, F96-V3PS-microplate: 180 µl/well

2.3 RNA extraction and quantification

Ribonucleic acid (RNA) isolation was carried out using a combined phenol extraction and column purification protocol. For cell cultures, medium was removed and 1 ml TRIsure (Bioline, London, UK) was added per 10 cm^2 growth area. After a brief incubation step, samples were homogenized by pipetting up and down. Cell lysates were collected and processed immediately or stored at -80 °C for several days. When RNA was isolated from tissue, frozen tissue samples were homogenized in 1 ml TRIsure using a dispersing instrument (Ultra-Turrax D-1, Miccra GmbH, Mühlheim, Germany).

For further extraction, samples were incubated at room temperature (RT) for two minutes. Then 200 µl of chloroform per 1 ml TRIsure were added to the sample-TRIsure mixture and the tubes were vigorously shaken by hand for 15 s. After an incubation at RT for three minutes samples were centrifuged at 12,000 g and 4 °C for 15 minutes to obtain phase separation. The upper aqueous phase, containing RNA, was mixed with 75 % ethanol in RNAse free water (500 µl per 1 ml TRIsure) and transferred to columns of the SV total RNA isolation system (Promega, Fitchburg, USA). Subsequent steps of RNA purification, including deoxyribonucleic acid (DNA) digestion, were carried out according to the kit manual.

RNA was eluted from the column in 30 - 40 µl of RNAse free water and concentration was determined by sample extinction at 260 nm using an infinite M200 microplate reader (Tecan, Männedorf, Switzerland). RNA was stored at -80 °C.

2.4 Quantitative real time PCR

Fluorescence based quantitative real-time polymerase chain reaction (qPCR) was used to measure mRNA abundance. To use this method, reverse transcription of mRNA into complementary DNA (cDNA) has to be performed beforehand. The cDNA can then be amplified by PCR using gene specific primers, deoxyribonuleotides (dNTPs) as components for the new synthesized strands and a heat-stable DNA polymerase for replication as well as an adequate buffer solution. For quantification a non-specific fluorescent dye, here SybrGreen, that intercalates with double-stranded DNA (dsDNA) is added to the reaction mix. When bound to dsDNA, this fluorophore shows greatly increased fluorescence. Fluorescence signal is measured after every cycle and is directly proportional to the generated amount of dsDNA. The number of cycles at which the fluorescence exceeds background is called threshold cycle (C_t) or quantitative cycle (C_q). The higher the initial amount of target cDNA, the earlier the C_t-value is reached in the course of amplification. For assigning a relative concentration out of the detected C_t-values, a standard curve is used.

cDNA synthesis

RNA is not a suitable template for PCR amplification. Thus, RNA has to be transcribed into cDNA before qPCR. To do so, either the QuantiTect Reverse Transcription Kit (Qiagen, Venlo, Netherlends) or the SensiFAST cDNA Synthesis kit (Bioline, London, UK) was used. Both kits include the retroviral enzyme reverse transcriptase, an oligo-dT primer mix and random hexamers. Reverse transcription was conducted in accordance with manufactures instructions (Table 1). 500 ng total RNA were used in a 10 µl reaction. Obtained cDNA was stored at -20 °C.

Table 1: Reverse transcription protocols.

QuantiTect Reverse Transcription kit		
Components	Volume (µl)	Program
RNA (500 ng)	x	
gDNA wipeout buffer	1	
Nuclease-free water	up to 7	
		42 °C, 3 min
RT	0.5	
5x RT buffer	2	
Primermix	0.5	
		42 °C, 30 min
		95 °C, 3 min

SensiFAST cDNA Synthesis kit		
Components	Volume (µl)	Program
RNA (500 ng)	x	
Nuclease-free water	up to 7.5	
RT	0.5	
5x TransAmp buffer	0.5	
		25 °C, 10 min
		42 °C, 15 min
		85 °C, 5 min

Primer design for qPCR

Primers were designed with the Primer3 web tool (http://primer3.ut.ee). Sequences of target genes were obtained from ENSEMBLE (http://www.ensembl.org). In order to prevent gDNA amplification primers were designed to span at least one large intron. It was preferred to include one of the last introns, since 3' end is reverse transcribed more efficiently due to the use of oligo-dT primers. Primers were designed to have a melting temperature around 60 °C, a GC content near 50 % and an amplicon size of 100 - 250 bp. To check for specificity of the primers an *in silico* PCR was conducted (http://genome.ucsc.edu/). Primers were ordered from MWG biotech as unmodified DNA oligonucleotides. Before qPCR, products of a conventional PCR were loaded on an agarose gel to confirm product size and specificity.

Primers:

Ucp1:	for	5'-GTACACCAAGGAAGGACCGA-3'
	rev	5'-TTTATTCGTGGTCTCCCAGC-3'
Ucp1[1]:	for	5'-GGATTGGCCTCTACGACTCA-3'
	rev	5'-GCATTCTGACCTTCACGACC-3'
TfIIb:	for	5'-TGGAGATTTGTCCACCATGA-3'
	rev	5'-GAATTGCCAAACTCATCAAAACT-3'
Gpam:	for	5'-GAGGTGCTCTGGAGGGTC-3'
	rev	5'-CTCTGCCACTGTGAGAATGC
Fabp4:	for	5'-GATGGTGACAAGCTGGTGGT-3'
	rev	5'-TTTATTTAATCAACATAACCATATCCA-3'
Cidea:	for	5'-TGCTCTTCTGTATCGCCCAGT -3'
	rev	5'-GCCGTGTTAAGGAATCTGCTG-3'
Cox7a1:	for	5'-GCCGACAATGACCTCCCAGTA-3'
	rev	5'-TGTTTGTCCAAGTCCTCCAA-3'

[1]Primer pair targeting exon 2 for comparing samples from UCP1$^{+/+}$ and UCP1$^{-/-}$ mice.

Quantitative PCR

For qPCR 384 multiwell plates and the LightCycler 480 device (Roche applied Science, Penzberg, Germany) were used. Samples were measured in triplicates and standards in duplicates. The cDNA samples were diluted 10-fold. For the standard curve a cDNA pool of all samples was diluted 1:2, 1:4, 1:8, 1:16, 1:32 and 1:64. Mastermixes were composed of SensiMix SYBR no Rox (Bioline, London, UK), primer pairs and water. The premixed sensimix solution contained SYBR Green I dye, dNTPs, buffer and a hot start polymerase. 11.5 µl of mastermix and 1 µl of template were used per well. The plate was sealed with a transparent foil and centrifuged at 500 g for five minutes. Then the plate was transferred to the thermal cycler. After 45 cycles of amplification, a melting curve was generated (Table 2).

Table 2: PCR program for q-PCR.

Step	Temperature (°C)	Time (s)	
Initial denaturation	95	420	
Denaturation	97	10	
Annealing	53	15	45x
Elongation	72	20	
Melting curve	60 - 95	1200	

2.5 Protein extraction and quantification

Cells were scraped on ice in radioimmunoprecipitation assay buffer (RIPA) buffer containing 1 % v/v protease inhibitor and 0.5 % v/v phosphatase inhibitor cocktail. Afterwards, suspensions were transferred to reaction tubes, vigorously shaken for 30 minutes at 4 °C and centrifuged at 16,000 g at 4 °C for 15 minutes. Thereby, samples separated into three phases: a lipid layer, a nuclear fraction and a protein-containing liquid phase. The protein containing phase was collected and the amount of protein was quantified using a bicinchoninic acid (BCA) protein assay kit. In a 96-well plate, 200 µl Working Reagent (Reagent A and Reagent B, 50:1) were added to 25 µl diluted samples or 25 µl of standard (2, 1.5, 1, 0.5, 0.25 mg/mL) followed by an incubation at 37 °C for 30 minutes. Then absorbance at 562 nm was measured with the spectrophotometer. The calculated standard curve was used to determine sample protein concentrations.

RIPA buffer: 50 mM Tris, 1 % v/v NP-40 substitutent, 0.25 % Na-desoxycholate, 150 mM NaCl, 1 mM EDTA, adjusted to pH 7.4

Volume of RIPA buffer: 12-well: 50 µl/well, 96-well: 5 µl/well

2.6 Western Blot

The Western Blot (WB) encompasses gel electrophoresis to separate proteins by their size, their transfer to a membrane and their detection with specific antibodies. With the help of a secondary antibody coupled to a reporter system the first antibody and thereby the target epitope of the protein of interest can be visualized.

SDS-PAGE

Sodium dodecyl sulfate (SDS) polyacrylamide gel electrophoresis (PAGE) was applied to separate proteins according to their size. During this step, protein samples migrate to the anode through the polyacrylamide gel, leading to their separation by size.

On the day prior to the experiment, polyacrylamide gels were generated. Glass plates and spacers were assembled in a casting stand and leak tightness was tested. Then separation gel mixture (5 ml/ mini gel) was prepared and quickly pipetted between the glass plates and carefully layered with water. After 45 minutes, the stacking gel was cast onto the running gel. A comb was inserted and gel was left to polymerize for 45 minutes. Gels were wrapped in wet tissue paper and cling film and stored at 4 °C overnight. For protein separation, gels were inserted in an electrophoresis chamber. Then chamber was filled with running buffer. Samples containing 30 µg protein were mixed 1:2 with 2x loading buffer and boiled at 95 °C for five minutes in order to achieve a complete protein denaturation. Afterwards samples and molecular weight (MW) marker were loaded. Then an electric field was applied at constant 80 V for approximately one hour.

12.5 % separation gel:	12.5 % v/v polyacrylamide, 0.1 % v/v SDS, 375 mM Tris pH 8.8, 0.05 % v/v TEMED, 0.05 % v/v AMPS
5 % stacking gel:	5 % v/v polyacrylamide, 0.1 % v/v SDS, 125 mM Tris pH 6.8, 0.1 % v/v TEMED, 0.06 % v/v AMPS
1x SDS running buffer:	25 mM Tris, 250 mM glycine, 0.1 % v/v SDS, adjusted to pH 8.3 with glycine
2x loading buffer:	13.13 % v/v 0.5 M Tris-HCl pH 6.8, 26.25 % v/v glycerin, 2.1 % v/v SDS, 0.01 % v/v bromophenol blue and 0.5 % v/v mercaptoethanol

Protein transfer

Proteins were transferred and immobilized on to a nitrocellulose membrane using a semi-dry transfer method. To do so, the gel was removed from the glass plates and put into transfer buffer. Membrane and filter papers (Whatman) of the same size as the gel were wetted with transfer buffer. Then membrane, gel and filter papers were placed into the blotting chamber between positive and negative electrodes in the following order:

anode - three papers - gel - membrane -three papers – cathode

Air bubble formation between layers was avoided. An electric field was applied at a constant 1 mA per cm^2 membrane surface for one hour.

1x transfer buffer: 48 mM Tris, 1.3 mM SDS, 20 % v/v methanol, adjusted to pH 9.2 with glycine

Tris buffered saline: 20 mM Tris, 140 mM NaCl, adjusted to pH 7.6

Antibody incubation and detection

After blotting, the membrane was washed with tris buffered saline (TBS) and incubated with 25 ml blocking solution at RT for two hours. Afterwards the membrane was incubated with primary antibodies, diluted in TBS with tween (TBST), at 4 °C overnight. Primary antibody solution was removed and the membrane was washed five times with TBST for five minutes. Secondary antibodies, which were directed against the host species of primary antibodies were diluted 1:20,000 in TBST and incubated at RT for two hours. Then the membrane was washed six times with TBST for five minutes. Finally, the blot was scanned using an infrared imaging system (Odyssey®, LI-COR). For signal quantification, odyssey software was used. UCP1 signal intensity was normalized to β-actin signal intensity. Primary and secondary antibodies including manufacturer and order number are listed in appendix 6.4.

TBS: Tris, NaCl

TBST: 0.1 % v/v Tween20 in TBS

Blocking solution: 3% BSA in TBS

2.7 Oil-Red-O staining

The degree of cellular lipid accumulation, as marker of differentiation of a fat cell, was visualized by Oil Red O (ORO) staining on day seven of differentiation. A 0.5 % ORO stock solution was prepared in isopropanol. Before use, the stock solution was diluted to a 0.3 % working solution with H_2O and filtered through a 45 µm syringe filter. Cells were washed with PBS and fixed in 3.7 % formaldehyde at RT for one hour. Then they were stained with ORO working solution for one hour, followed by washing twice with PBS. Then cells were covered with PBS and staining was checked under the microscope. At that point, representative pictures were taken.

2.8 Lipid droplet size distribution

LD size distribution was determined algorithmically (LipidDroplet module, Wimasis). On day seven of differentiation, representative pictures of cell cultures were taken and analyzed.

2.9 Respiration measurement

Oxygen consumption rates (OCRs), extracellular acidification rate (ECAR) and proton production rates (PPR) were measured simultaneously at 37 °C using a XF-96 extracellular flux analyzer (Agilent Technologies, Santa Clara, USA). This instrument enables the measurement of bioenergetics of adherent cells in a 96-well format. The assay kit is composed of a 96-well cell culture plate and a sensor cartridge that is placed on top of the culture plate during the measurement. The sensor cartridge comprises a sensor spot with two fluorophores on the bottom of each of the probe sleeve that measures oxygen consumption and extracellular acidification. During the measurement, the cartridge is moved down toward the cells creating a transient microchamber (Figure 5).

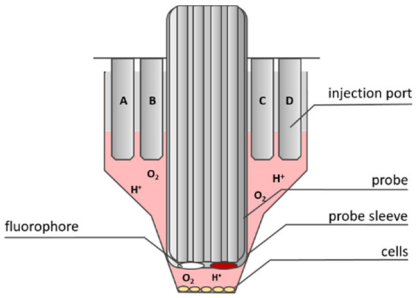

Figure 5: Seahorse micro chamber during the measurement.

Fiber optic bundles are inserted into the plastic sleeves. The optical fluorescent biosensors are excited and their emission represents changes in oxygen or proton concentrations inside the microchamber. Afterwards, the sensor cartridge is lifted, allowing the concentrations to return to baseline. It is possible to inject four different components into the cell culture plate during the experiment. The drugs have to be loaded into injection ports that surround the probe sleeves of the sensor cartridge.

Isolated primary cells were seeded into F96-V3PS-microplate and differentiated into mature adipocytes. At day seven of differentiation, the cell culture medium was replaced with prewarmed unbuffered respiration medium (180 µl/well) supplemented with 2 % essentially fatty acid free BSA and incubated at 37 °C in a non-CO_2 incubator for one hour. First basal respiration of untreated cells was measured. Coupled respiration was inhibited by oligomycin treatment (20 µl/well), which blocks ATP-Synthase. UCP1 mediated

uncoupled respiration was determined after isoproterenol injection (22 µl/well). Afterwards FCCP, a chemical uncoupler that allows assessment of maximal respiratory capacity, was added (24 µl/well). Finally, antimycin A was injected to block complex III of the electron transport chain, leaving only non-mitochondrial OCR to be measured (26 µl/well) (Table 3). OCR, ECAR and PPR were automatically calculated by the Seahorse XF-96 software.

Table 3: Protocol for measurement of UCP1 activity with XF96 analyzer

Step	Command	Duration	Loop
1	Calibrate probes		
2	Equilibrate	12	
3	Mix	2	
4	Delay	2	3
5	Measure	3	
6	**Inject port A (20 µl)** 5 µM oligomycin		
7	Mix	2	
8	Delay	2	3
9	Measure	3	
10	**Inject port B (22 µl)** 0.5 µM isoproterenol		
11	Mix	2	
12	Delay	2	5
13	Measure	3	
14	**Inject port C (24 µl)** 1 µM FCCP		
15	Mix	2	
16	Delay	2	3
17	Measure	3	
18	**Inject Port D (26 µl)** 5 µM antimycin A		
19	Mix	2	
20	Delay	2	3
21	Measure	3	
22	Program end		

Respiration medium: DMEM, 25 mM glucose, 2 mM sodium pyruvate, 31 mM NaCl, 2 mM GlutaMax, 15 mg/l phenol red, adjusted to pH 7.4

2.10 Extracellular acidification calculations

Proton production by CO_2

CO_2 is metabolically produced during substrate combustion. In aqueous solution generated CO_2 gets hydrated to carbonic acid (H_2CO_3), which subsequently dissociates to hydrogen carbonate (HCO_3^-) and H^+ at physiological pH (Garrett and Grisham, 2009; Mookerjee et al., 2015). Acidification by CO_2 can be calculated from the OCR, the production of H^+ per consumed O_2 (Net H^+/O_2) or respiratory quotient (RQ).

$$CO_{2\,(aq)} + H_2O \leftrightarrows H_2CO_3 \leftrightarrows HCO_3^- + H^+ \qquad (1)$$

Maximal H^+ released during complete oxidation of a substrate was calculated from its balanced reaction equation:

Complete oxidation of palmitate (RQ = 0.70):

$$C_{16}H_{31}O_2^- + H^+ + 23O_2 \rightarrow 16CO_2 + 16H_2O \quad (2)$$

$$16CO_2 + 16\,H_2O \rightarrow 16HCO_3^- + 16\,H^+ \quad (3)$$

$$\max H^+/O_2 = (16\text{-}1)/23 = 0.65 \quad (4)$$

Complete oxidation of glucose (RQ = 1.00):

$$C_6H_{12}O_6 + 6O_2 \rightarrow 6CO_2 + 6H_2O \quad (5)$$

$$6CO_2 + 6H_2O \rightarrow 6HCO_3^- + 6\,H^+ \quad (6)$$

$$\max H^+/O_2 = 6/6 = 1.00 \quad (7)$$

Complete oxidation of glutamine (RQ = 1.11):

$$C_5H_{10}N_2O3 + 4.5O_2 \rightarrow 5CO_2 + 2H_2O + 2NH_3 \quad (8)$$

$$5CO_2 + 2NH_3 + 5H_2O \rightarrow 5HCO_3^- + 2NH_4^+ + 3H^+ \quad (9)$$

$$\max H^+/O_2 = 3/4.5 = 0.67 \quad (10)$$

Hydration of CO_2

Dissolved CO_2 is not completely hydrated at equilibrium. The fraction of hydrated CO_2 can be calculated with the overall pKa for CO_2 in aqueous solution at 37 °C = 6.093 (Garrett and Grisham, 2009):

$$HCO_3^-/(CO_{2\,(\text{non dissolved})} + HCO_3^-) \quad (11)$$

$$= 10^{(\text{pH-pK})}/(1 + 10^{(\text{pH-pK})}) \quad (12)$$

$$= 10^{(7.4\text{-}6.093)}/(1 + 10^{(7.4\text{-}6.093)}) \quad (13)$$

$$= 0.953$$

Net H^+ production is calculated as max H^+/O_2 multiplied by the fraction of CO_2 hydrated:

$$\text{Net } H^+/O_2 = 0.953 \text{ x } O_{2(\text{mito})}\,[\text{nmol/min/cm}^2] \text{ x max } H^+/O_2 \quad (14)$$

Proton production by lactic acid and FFA

Lactic acid is glycolytically produced and FFA are derived from lipolysis. In aqueous solution, under physiological conditions these organic acids dissociate into their conjungated base and release H^+ stoichiometrically:

$$\text{lactic acid} \leftrightarrows \text{lactate} + H^+ \ (\text{pKa} = 3.86) \quad (15)$$

$$\text{FFA} \leftrightarrows \text{FFA}^- + H^+ \ (\text{pKa} \approx 4.80 - 5.00) \quad (16)$$

Further model calculations are based on palmitate as sole substrate (RQ = 0.7).

Maximal FFA amount used for β-Oxidation

$$\text{FFA}_{\text{oxidized}} = \text{O}_{2(\text{mito})} \ [\text{nmol/min/cm}^2] \ \text{x CE} \ [\mu\text{J/nmol O}_2]/\Delta\text{G} \ [\mu\text{J/nmol}] \quad (17)$$

for palmitate caloric equivalent (CE) = 431 µJ /nmol O_2; ΔG = 9.8 µJ/pmol (Gnaiger and Kemp, 1990; Olmsted and Williams, 1997)

Hydrolyzed triglyceride amount

The amount of hydrolyzed triacylglyceride (TAG) can be estimated from the total amount of FFA.

$$\text{FFA}_{\text{total}} = \text{FFA}_{\text{exported}} + \text{FFA}_{\text{oxidized}} \quad (18)$$

$$\text{TAG} \ [\text{nmol}] = \text{FFA}_{\text{total}} \ [\text{nmol}]/3 \quad (19)$$

$$\text{TAG} \ [\text{nmol}] \ \text{x MW} = \text{TAG} \ [\text{ng}] \quad (20)$$

MW of tripalmitin is 307,34 g/mol.

2.11 Lipolysis Assay

Lipolytic activity was assessed by the measurement of glycerol and non-esterified free fatty acid (FFA) released into the medium (Schweiger et al., 2014). The quantitative detection of lipolysis products is based on enzymatic spectrophotometric method.

Glycerol

Glycerol concentration is determined by a coupled enzyme assay. In the first step, glycerol is phosphorylated into glycerol-1-phosphate (G1P) by glycerol kinase. Then G1P is oxidized by glycerol phosphate oxidase forming dihydroxyacetone phosphate (DAP) and hydrogen peroxide (H_2O_2). In the final step peroxidase catalyses the coupling of H_2O_2 with 4-aminoantipyrine (4-AAP) and sodium N-ethyl-N-(3-sulfopropyl)-m-anisidine (ESPA) which leads to the production of a quinoneimine dye with an absorbance maximum at 540 nm. Increase in absorbance at 540 nm is directly proportional to the glycerol concentration of the sample (Equation 21-23).

$$\text{glycerol} + \text{ATP} \xrightarrow{glycerol\ kinase} \text{G-1-P} + \text{ADP} \quad (21)$$

$$\text{G-1-P} + O_2 \xrightarrow{glycerol\ phosphate\ oxidase} \text{DAP} + H_2O_2 \quad (22)$$

$$H_2O_2 + \text{4-AAP} + \text{ESPA} \xrightarrow{peroxidase} \text{quinoneimine dye} + H_2O \quad (23)$$

FFA

FFA levels are also measured by coupled enzymatic reactions. First, in the presence of coenzyme A (CoA) and ATP, FFAs are converted to acyl-CoA by acyl-CoA-sythetase. The produced acyl-CoA is further oxidized to 2,3-trans-enoyl-CoA and H_2O_2 by acyl-CoA-oxidase. Then the peroxidase catalyzes the oxidative condensation of H_2O_2 with 3-methyl-N-ethyl-N-(β-hydroxyethyl)-aniline (MEHA) and 4-aminoantipyrin to a blue purple pigment. The increase in absorbance at 546 and 660 nm is directly proportional to FFA concentration of the sample (Equation 24-26).

$$\text{HCOOH (FFA)} + \text{ATP} + \text{CoA} \xrightarrow{acyl-CoA\ synthetase} \text{Acyl} - \text{CoA} + \text{AMP} + \text{PPi} \quad (24)$$

$$\text{Acyl-CoA} + O_2 \xrightarrow{acyl-CoA\ oxidase} 2,3 - \text{trans} - \text{Enoyl} - \text{CoA} + H_2O_2 \quad (25)$$

(26)

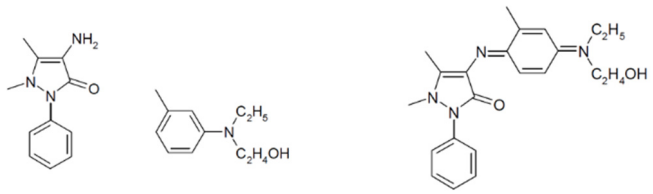

$$H_2O_2 + \text{4-aminoantipyrin} + \text{MEHA} \xrightarrow{peroxidase} \text{blue purple pigment} + 3\ H_2O$$

On day seven of differentiation, cells were washed with assay medium and, in the case of brite adipocytes, stimulated with 0.5 µM isoproterenol in assay medium and incubated for one hour. Then medium was replaced with identical fresh medium and the incubation step was repeated. After one hour medium was collected for further analysis. Cells were washed with PBS and used for protein determination. In contrast, brown adipocytes were pretreated with or without 5 µM oligomycin for 30 minutes. Then medium was replaced and cells were stimulated with 0.5 µM isoproterenol either in the presence of oligomycin or not. After one hour medium was collected.

The amount of glycerol was detected using a free glycerol reagent and glycerol standard solution from Sigma (cat. no. F6428, G7793; Sigma-Aldrich). 10 µl of blank, standard or

samples were pipetted into the wells of a 96-well plate. Blank and standards, ranging from 4 to 260 µg glycerol/ml, were measured in duplicates. Samples were analyzed in triplicates. Subsequently, 100 µl of free glycerol reagent was added. The plate was protected from light and incubated at RT for 15 minutes. The determination of the absorption at 540 nm was conducted using a plate reader (Tecan, Männedorf, Switzerland). Finally, the glycerol concentrations of the samples were calculated from the slope of the standard curve.

The concentration of FFA was determined using the NEFA-HR(2) R1 and R2. kit (Wako Chemicals). Due to different volume requirements samples with low (e.g. basal conditions) and high FFA concentration (e.g. stimulated conditions) have to be measured on separate plates. For basal lipolysis, 50 µl of blank, palmitate standard (Wako Chemicals) or samples were pipetted into a 96-well plate in duplicates (blank, standard) or triplicates (samples). Measurement was performed in a microplate reader (Tecan, Männedorf, Switzerland) at 37 °C. Plates were preheated to 37 °C. Then, 100 µl of R1 were injected followed by vigorously shaking the plate for three seconds. The plate was visually examined and air bubbles removed. Absorbance was measured at 546 nm (main wavelength) and 660 nm (sub wavelength) as sample baseline. Afterwards samples were incubated for three minutes before 50 µl of R2 were injected into each well. The plate was again vigorously shaken and air bubbles were removed. After an incubation step of 3.5 minutes absorbance at 546 and 660 nm was measured. Differences of main and sub wavelengths as well as of the first and second measurement were calculated. For measurement of stimulated samples, 20 µl of blank, standard or samples were used. 150 µl R1 and 75 µl R2 were injected. Besides these different volumes, the same protocol as for basal samples was applied. Unknown FFA concentration was calculated using a calibration curve of palmitate ranging from 0.025 to 1 mM.

Assay medium: DMEM without glucose or pyruvate, 5.55 mM glucose, 2 % essentially fatty acid free bovine serum albumin (BSA), pH 7.4

2.12 Glucose uptake with 2-Deoxy-D-[1-^{3}H]-glucose

Radiometric glucose uptake assays are commonly used to measure glucose transport. The uptake can be studied using radiolabeled glucose itself, or radiolabeled glucose analogs such as 2-deoxy-D-glucose (2-DG). In this study, ^{3}H labeled 2-DG was used. The glucose analog 2-DG is phosphorylated by hexokinase. The resulting 2-DG-phosphate (2-DG-P) cannot be further metabolized by glucose-6-phosphate isomerase and thus accumulates within the cell. Radioactivity of trapped labeled 2-DG-P can then be

quantified by liquid scintillation counting (LSC), a standard laboratory method to quantify radioactivity of low energy radioisotopes. After exposure to labeled 2-DG, adherent cells are washed to separate radiochemical that has not been taken up by the cells. Cells are then lysed and a LSC cocktail is added. This cocktail absorbs the energy emitted by radioisotopes and reemits it as light pulses which are detected by the photomultiplier tube of the scintillation counter. The number of light flashes registered per minute are expressed as counts per minute (cpm).

If not stated otherwise, glucose uptake studies were made in the following way: All experiments were performed on day seven of differentiation in 12-well plates. On day six insulin was removed from medium. To reduce basal glucose uptake, the medium was changed to serum-free DMEM containing 0.5 % BSA for two hours (1 ml/well). Then this medium was replaced by unbuffered assay medium (600 µl/well) and cells were incubated at 37 °C in a non-CO_2 incubator. After one hour cells were stimulated with 1 µM isoproterenol, 1 µM insulin or both in combination (additional 400 µl/well) for 30 minutes. Then medium was changed to fresh assay medium containing stimulants and trace amounts (3 µCi) of 2-deoxy-d-[1-^{3}H]-glucose (500 µl/well). After three minutes, glucose uptake was terminated by washing cells with ice-cold stop solution (PBS, 25 mM glucose). Cells were lysed with 0.2 M NaOH at 60 °C for one hour. Incorporated radioactivity was determined by LSC (Perkin Elmer, Waltham, USA). Resulting cpm values were transformed into disintegrations per minute (dpm) values and with the help of the specific activity (SA) the absolute amount of glucose taken up from the cells was calculated (Equation 27-29).

$$\text{mmol glucose} = (\text{dpm}/(2.22 \times 10^{12})) \times (1/\text{SA [mCi/mmol]}) \quad (27)$$

$$\text{SA [mCi/mmol]} = \text{total glucose [mM]}/\text{total mCi} \quad (28)$$

$$1\,[\text{Ci}] = 2.22{\times}10^{12}\,[\text{dpm}] \quad (29)$$

Assay medium: DMEM, 5.55 mM glucose, 2 mM sodium pyruvate, 31 mM NaCl, 2 mM GlutaMax, 15 mg/l phenol red, 2 % BSA, adjusted to pH 7.4

Stop solution: PBS, 25 mM D-glucose

2.13 Lactate measurement

Lactate release into supernatant was measured by an endpoint enzymatic assay which is based on the conversion of lactate to pyruvate by lactate dehydrogenase (LDH) in the presence of NAD^+. The amount of NADH formed is measured spectrophotometrically at 340 nm with a microplate reader (Tecan, Männedorf, Switzerland). For quantitative conversion of lactate, a high pH and the presence of hydrazine are required. In the

presence of hydrazine, a nonenzymatic conversion of pyruvate to pyruvate hydrazone takes place. The coupled reaction prevents reversibility of NADH production and decreases the likelihood of product inhibition (Equation 30-31).

$$\text{lactate} + \text{NAD}^+ \xleftrightarrow{lactate\ dehydrogenase} \text{pyruvate} + \text{NADH} + \text{H}^+ \quad (30)$$

$$\text{pyruvate} + \text{hydrazine} \rightarrow \text{pyruvate hydrazone} \quad (31)$$

Briefly, brite cells were washed with PBS and incubated with assay medium with or without 0.5 µM isoproterenol for one hour. Then medium was saved for further analysis. Cells were washed with PBS and lysed. Cell lysates were used for protein determination. Brown adipocytes received a pretreatment with or without 5 µM oligomycin for 30 minutes. Then medium was replaced and cells were stimulated with 0.5 µM isoproterenol either in the presence of oligomycin or not.

For quantification of lactate concentration samples were diluted 1:2 with 6 % PCA, vortexed for five seconds and centrifuged at 3000 g for 15 minutes. Then in a 96-well plate, per well, 10 µl of sample were mixed with 100 µl of reagent mix (98,8 % hydrazine buffer, 0.2 % NAD^+, 1 % LDH) and incubated at RT for 30 minutes. The amount of lactate was calculated using a calibration curve and standardized to the amount of protein per well.

Assay medium: DMEM without glucose or pyruvate, 5.55 mM glucose, 2 % essentially fatty acid free bovine serum albumin (BSA), pH 7.4

2.14 Metabolite profiling

Non-targeted metabolomics was applied to characterize brite adipocytes. On day seven of differentiation, cells were treated with or without 0.5 µM isoproterenol for 30 minutes. Then cells were washed with PBS and extraction solvent containing four standard compounds was added (-80 °C, 500 µl/6-well). Cells were scraped in extraction solvent, transferred to pre-cooled tubes and stored at -80 °C until further analysis. Non-targeted metabolomic analysis was conducted at the Genome Analysis Center, Helmholtz Zentrum München. Cell suspensions, supplied with 80 mg 0.5 mm glass beads (Precellys, Berlin, Germany) were homogenized twice using a Precellys24 (PeqLab Biotechnology, Erlangen, Germany) at 4 °C for 25 seconds at 5500 rpm with a five seconds break. After homogenization, 80 µl of homogenates were taken for fluorescence-based DNA cell number determination, whereas the rest of homogenate was used for ultra-high performance LC/MS (UPLC-MS/MS) in positive as well as negative electrospray ionization

mode. Resulting data were matched to a chemical database library (Metabolon, Inc., Durham, USA) based on retention index, precursor mass, and MS/MS spectra. Relative signal intensities of identified metabolites were normalized to cell number.

Extraction solvent: 80 % v/v methanol, 1 % 1.2 M tridecanoic acid, 1 % 1.34 M DL-2-fluorophenylglycine, 1 % 6.4 Md6-cholesterol, 1 % 5 M DL-4-chlorophenylalanine

2.15 Fatty acid analysis

Fatty acid (FA) analysis was performed as described previously (Ecker et al., 2012). Briefly, FA methyl esters (FAME) were generated with acetyl-chloride and methanol for one hour at 95°C and extracted with hexane. Total FA analysis was carried out using a 2010-GC-MS system (Shimadzu, Duisburg, Germany). FAMEs were separated by a column (BPX70, SGE, Trajan Scientific and Medical, Australia) of 10 m length, 0.10 mm diameter and 0.20 µm film thickness using helium as carrier gas. The FAs were quantified by single-ion monitoring mode detecting the specific fragments of saturated and unsaturated FAs. As an internal standard, non-naturally occurring C21:0 iso was used.

2.16 Transcriptome analysis

Next generation sequencing (NGS) of the transcriptome (RNA-Seq) was performed by Dr. Christine Wurmser, Chair of Animal Breeding (Technichal University of Munich, Weihenstephan Freising) using a HiSeq 2500 platform (Illumina).

For RNA-Seq analysis, RNA of *in vitro* differentiated brown and brite adipocytes as well as RNA of iBAT were used. RNA integrity was checked with RNA 6000 Nano Kit using a 2100 Bioanalyzer (Agilent Technologies, Santa Clara, USA). Sequencing libraries were prepared (Stranded TNA LT kit, Illumina) and clustered onto a sequencing flow cell (TruSeq SR Cluster Kit v3 and TruSeq SBS Kit v3-HS, Illumina). By multiplexing 7-8 samples per lane 15-25 million single reads per sample were generated. Quality control and mapping were performed by a software package (Mining Station and Genome Analyzer, Genomatix, Munich, Germany). All quantifications of transcript abundance are given in ‘reads per 1000 base pairs transcript length and million reads’ (RPKM).

2.17 siRNA Transfection

Target gene in *in vitro* differentiated adipocytes was knocked down with a small (or short) interfering RNA (siRNA) reverse transfection protocol (Isidor et al., 2015). The approach is used for transient silencing of protein coding genes in mature adipocytes. siRNA is an artificial RNA duplex designed to specifically target a mRNA for degradation. It is

composed of two RNA strands, an antisense or guide strand and a sense strand of 19 to 25 bp in length. When siRNAs are transfected into cells RNA interference is triggered. The guide strand is loaded into the RNA-induced silencing complex (RISC). Once RISC is formed and activated this multiprotein and nucleic acid complex can produce gene silencing by specific binding to a particular mRNA sequence, thereby targeting it for cleavage and degradation (Patzel, 2007).

On day five of differentiation, adipocytes were reverse transfected with siRNA in the following way: siRNA and Lipofectamine RNAiMAX (Life Technologies, Carlsbad, USA) were diluted in Opti-MEM I reduced serum medium (Life Technologies, Carlsbad, USA) separately and then mixed. This transfection mix was added to 24-well cell culture plates or XF-96 cell culture microplates and left to incubate at RT for 25 minutes. The final concentrations of Lipofectamine RNAiMAX and siRNA were 5 µl/ml and 50 nM, respectively. The final volume of medium was 600 µl per well in a 24-well plate and 90 µl in a XF-96 cell culture microplate.

Transfection-Mix: Optimem, Lipofectamin 5 µl/ml, 50 nM siRNA

2.18 Statistics and data analysis

Graphs were created using GraphPad Prism version 6.00 for Windows (GraphPad Software, La Jolla, USA). Data are presented as individual values with the group mean indicated as bar or as mean ± standard deviation (SD). Statistical analyses were performed with SigmaPlot 12.5 (Systat Software Inc., San Jose, USA). Statistical tests were conducted as indicated in figure legends. P-values <0.05 were considered significant. Significant differences are indicated by asterisks or printed characters. Normal distribution was tested using the Shapiro-Wilk normality test. Three normally distributed groups were compared by One Way analysis of variance (ANOVA). When two variables were present Two Way ANOVA and Tuckey post-test was used. For Multiple comparisons Tukey post-hoc-test was performed. Two normally distributed groups were compared by t-test whereas non-normally distributed groups were compared using Mann-Whitney Rank Sum test. Differential RNA expression analysis (DESeq algorithm, Genome Analyzer, Genomatix, Munich, Germany) was used applying a log2 fold change of |0.5| with a p-value threshold of 0.05 corrected for multiple testing. Integrated enrichment analysis of RNA trascriptome and metabolite profiling data was accomplished with the Incromap tool (Center for Bioinformatics Tübingen (ZBIT), Germany). Thereby a log2 fold change of 2.0 was used for RNA data and a log2 fold change of 0.2 was applied for metabolite data.

3 Results

3.1 Functional phenotyping and metabolite profiling of brite adipocytes

In response to cold exposure and a variety of pharmacological or endocrine signals, brown adipocyte-like cells, so-called brite adipocytes, appear in white adipose tissue (WAT). This process has been coined browning. To date, the functional and metabolic properties of brite cells are still not fully clarified and their contribution to thermogenesis is a matter of debate. Thermogenic activity requires supply of oxygen, fatty acids (FAs) and glucose. Thus, functional phenotyping should include investigation of themogenic potential as well as oxygen consumption, lipolytic activity and glucose uptake.

In this project, preadipocytes, isolated from the iWAT of 129SV/S6 (high browning propensity), C57BL/6J UCP1$^{+/+}$ (low browning propensity) and C57BL/6J UCP1$^{-/-}$ mice were used and differentiated *in vitro* in presence of the PPARγ agonist rosiglitazone. Functional parameters were evaluated in the basal or in the adrenergic stimulated state in order to differentiate between effects of UCP1 abundance and activity. Adrenergic stimulation was achieved by treatment with the non-selective β-adrenoreceptor agonist isoproterenol, a sympathomimetic that is stable under cell culture conditions.

3.1.1 Browning propensity is maintained in vitro

The extent of browning of *in vitro* differentiated primary adipocytes can be accessed by measuring mRNA expression levels of Ucp1 and other brown fat-specific genes by qPCR. In the differentiated state, cultures from 129SV/S6 compared to C57BL/6J mice had a significant higher Ucp1 mRNA abundance (Figure 6A). On average, 129SV/S6 cells had four times more Ucp1 mRNA than C57BL/6J UCP1$^{+/+}$ cells. As other markers of a brown fat like phenotype, expression of the subunit 7a1 of cytochrome c oxidase (Cox7a1) and the lipid droplet (LD) coating protein cell death-inducing DFFA-like effector a (Cidea) were analyzed. The level of mRNA of Cox7a1 and Cidea tended to be higher in cultures of C57BL/6J UCP1$^{-/-}$ mice. However, this difference was not statistically significant. The expression of fatty acid binding protein 4 (Fabp4), a differentiation marker for both brown and white adipocytes, did not differ significantly between the groups, indicating a comparable degree of adipogenic differentiation in all cell cultures types (Figure 6B).

Expression of UCP1 on the protein level was confirmed by Western Blot (WB) (Figure 7A). Similar to mRNA levels, 129SV/S6 cultures had a significantly higher UCP1 protein levels

compared to C57BL/6J UCP1$^{+/+}$ cultures. This was reproducible in WBs with different antibodies against UCP1 and Actin. Normalized UCP1 protein expression in 129SV/S6 cultures was 1.58 – 4.4-fold higher than in C57BL/6J UCP1$^{+/+}$ cultures (Figure 7B). As expected C57BL/6J UCP1$^{-/-}$ cells did not express any intact Ucp1 mRNA or UCP1 protein (Figure 6 and Figure 7).

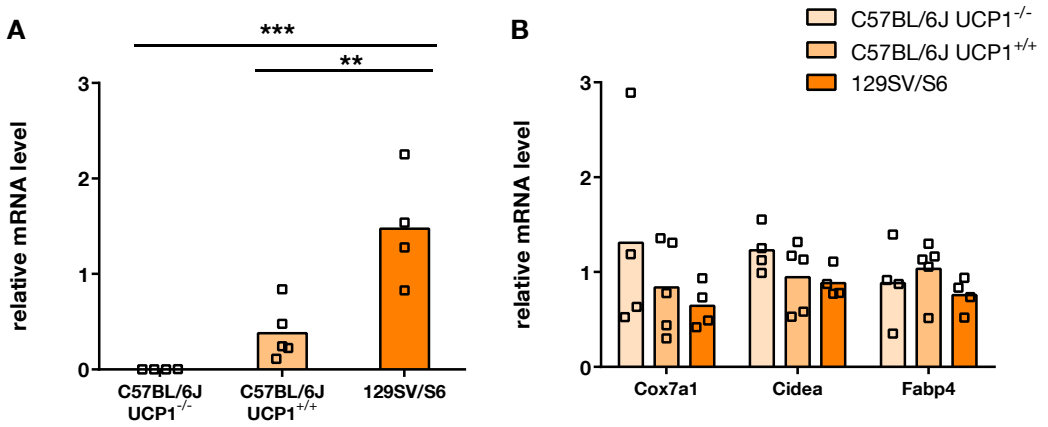

*Figure 6: RNA Expression of Ucp1(A) and other brown fat marker genes (B) in brite adipocyte cultures. Data was analyzed by One Way ANOVA and Tukey post-hoc-test (** p<0.01, *** p≤0.001).*

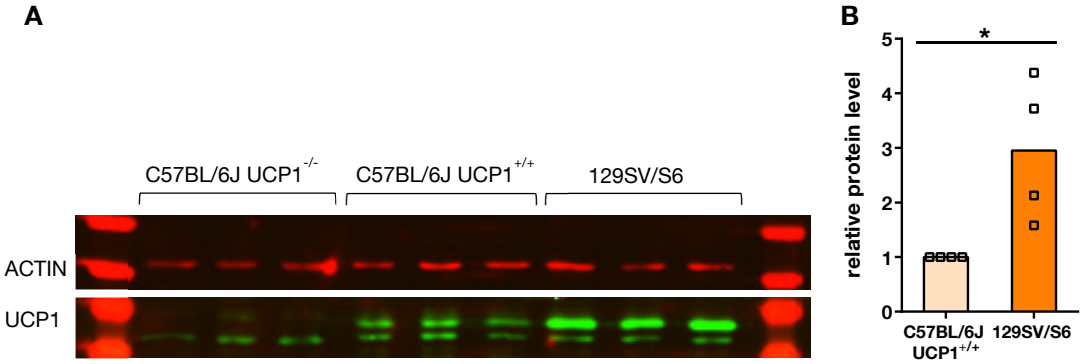

Figure 7: UCP1 protein expression in brite adipocyte cultures. Representative Western Blot (A). Quantification of four Western Blots with different biological replicates. Data presented as fold change of C57BL/6J Ucp1$^{+/+}$ (B). Data was analyzed by Mann-Whitney Rank Sum Test (p<0.05).*

Together, mRNA and protein data clearly show that, on the molecular level, *in vitro* differentiated 129SV/S6 and C57BL/6J cells express a brite phenotype. Furthermore, the results indicate that strain specific differences in brite adipogenesis observed *in vivo* could be pheno-copied in primary cultures *in vitro.*

3.1.2 Lipid droplet size positively correlates with UCP1 abundance

Cellular morphology may influence the functional phenotype of adipocyte cultures. On day seven of differentiation, the degree of cellular lipid accumulation, as a marker of adipocyte

differentiation, was visualized by Oil Red O (ORO) staining. Cell cultures showed a comparable degree of differentiation (Figure 8).

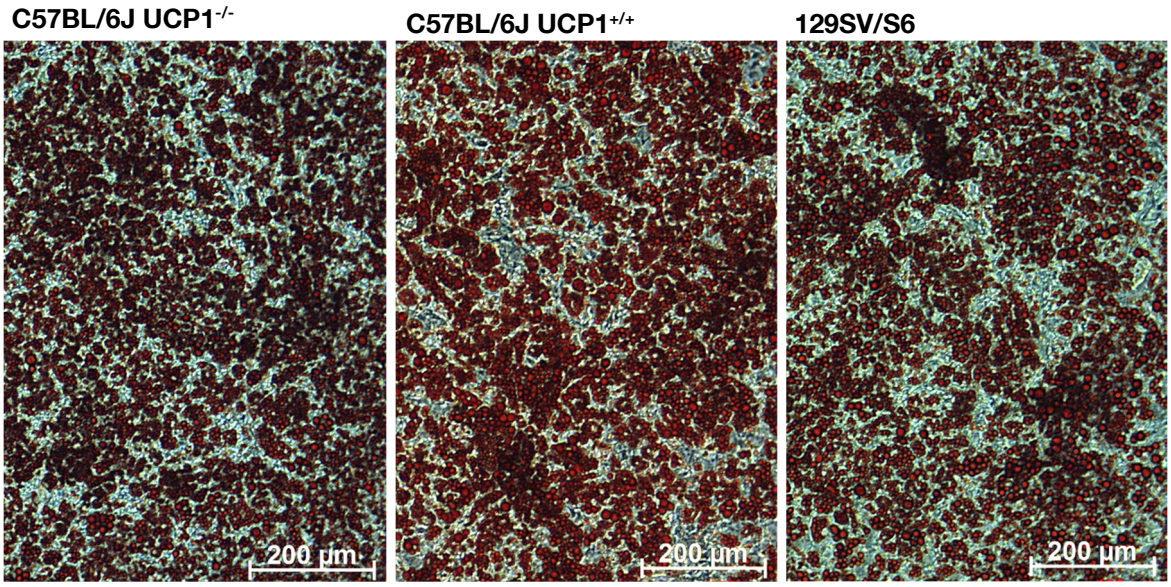

Figure 8: Oil Red O staining of brite adipocyte cultures.

In order to compare the morphology of different primary brite cell cultures, light microscope images were taken on day seven of differentiation. LD size was determined by an automatic algorithm (LipidDroplet module, Wimasis) (Figure 9). The mean LD size (Figure 10), was significantly lower in C57BL/6J UCP1$^{-/-}$ cells (60.35 µm2), compared to 129SV/S6 cells (78.97 µm^2, $p<0.01$). C57BL/6J UCP1$^{+/+}$ cells had an intermediate mean LD size (70.17 µm^2). What could be already observed in the mean value gets clearer in the LD size distribution (Figure 11A). C57BL/6J UCP1$^{-/-}$ cultures had more small (<40 µm^2) and less big LDs (>230 µm^2) than C57BL/6J UCP1$^{+/+}$ cultures. In contrast, cells derived from 129SV/S6 mice showed the lowest and the highest percentage of these respective classes of LDs (Figure 11 B, C).

C57BL/6J UCP1$^{-/-}$

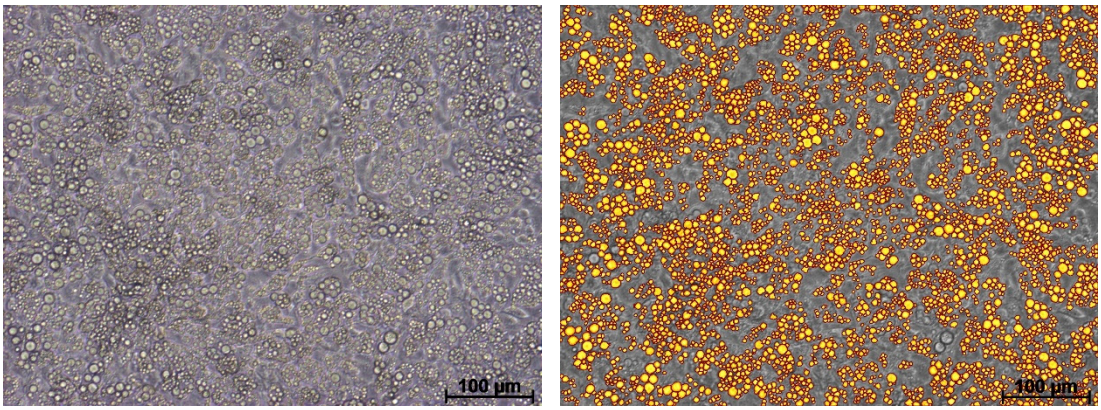

C57BL/6J UCP1$^{+/+}$

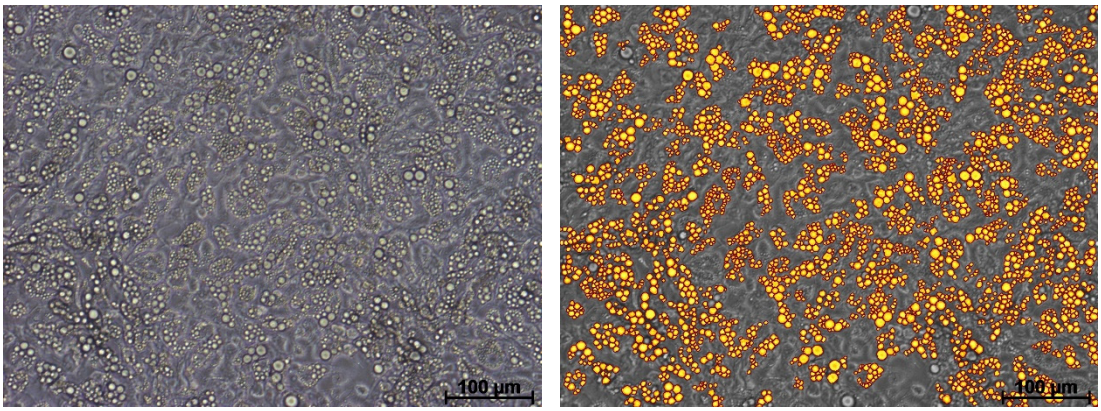

129SV/S6

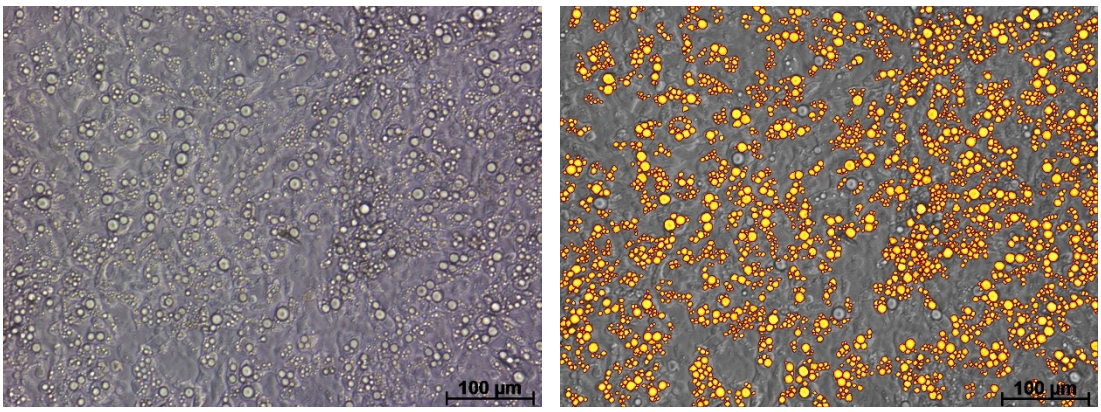

Figure 9: Morphology of brite adipocyte cultures. Representative light microscope images of C57BL/6J UCP1$^{-/-}$, C57BL/6J UCP1$^{+/+}$ and 129SV/S6 cultures (left panel). Lipid droplets were detected by an algorithm of the web-based LipidDroplet module of Wimasis online software (right panel).

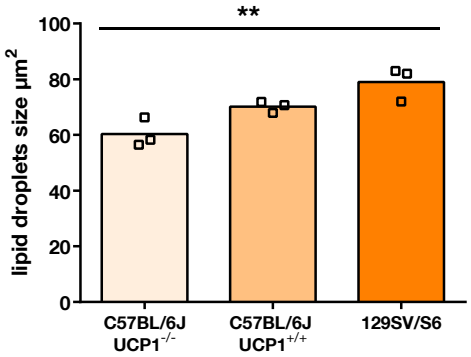

*Figure 10: Mean lipid droplet size in µm². Bars represent mean value of three independent experiments. Data was analyzed by One Way ANOVA and Tukey post-hoc-test (** p<0.01).*

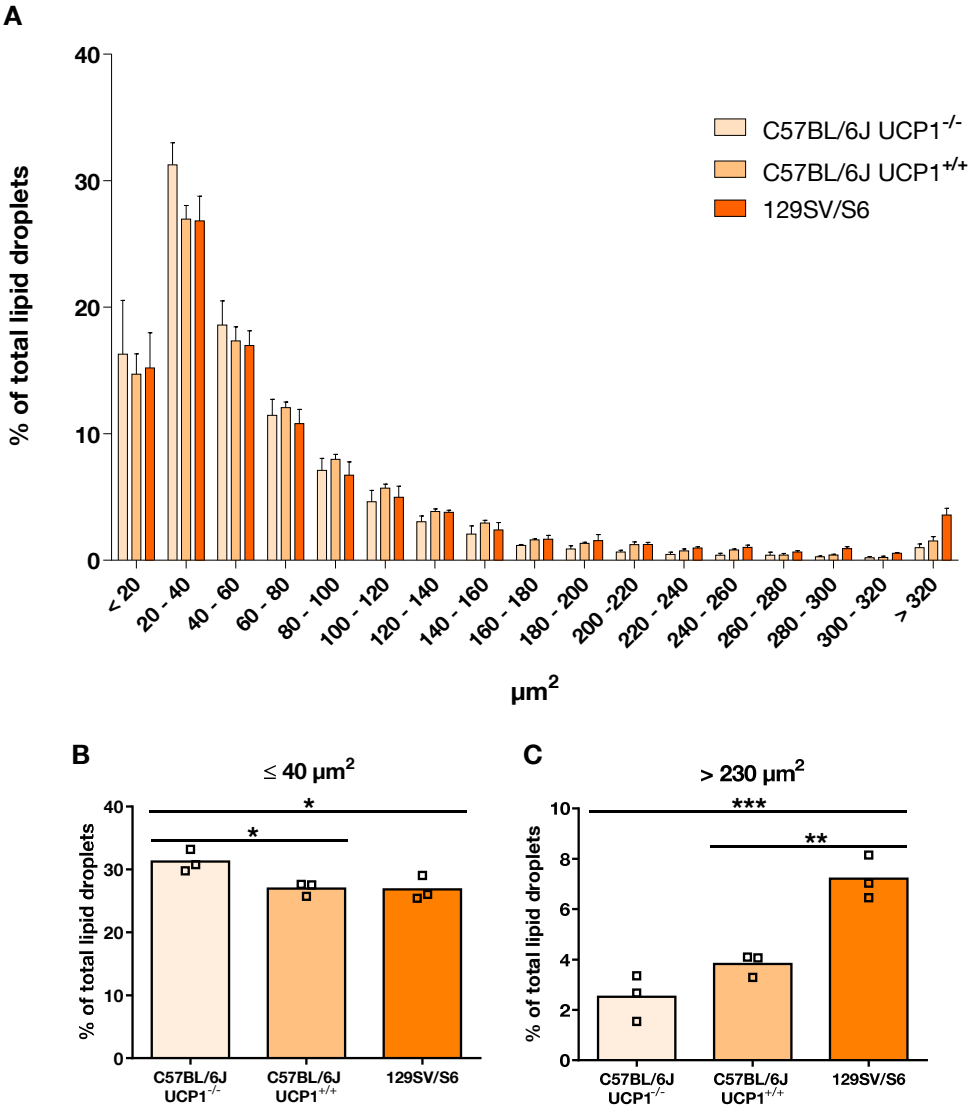

*Figure 11: Lipid droplet size distribution. Histogram of abundance of size classes in percentage of total lipid droplets (A). Percentage of lipid droplets with a size ≤ 40 µm² (B) or > 230 µm² (C). Bars represent mean value of three independent experiments. As statistical analysis was performed by One Way ANOVA and Tukey post-hoc-test (*p<0.05, **p<0.01, *** p<0.001).*

3.1.3 Respiration rates resemble differences in UCP1 expression

The physiological function of UCP1 is to uncouple respiration from ATP synthesis and dissipate energy as heat to maintain core body temperature in a cold environment (Klingenspor et al., 2012; Li et al., 2014c). The oxygen consumption of cells can be used as an indirect measure of their thermogenic function.

Respiration rates of *in vitro* differentiated C57BL/6J and 129SV/S6 cells were measured using a microplate extracellular flux analyzer. A representative time course of this experiment is shown in Figure 12A. First, basal respiration was detected. Then oligomycin was added, which inhibits ATP synthase and lowers OCR to basal leak respiration, a state where mitochondria maintain oxygen flux only to compensate for the basal proton leak. UCP1 mediated uncoupled respiration was determined after isoproterenol (0.5 µM) injection. Next FCCP, a chemical uncoupler was added. Finally, antimycin A was injected to block complex III of the electron transport chain, leaving only non-mitochondrial OCR to be measured. Primary cultures from 129SV/S6 compared to cultures from C57BLB/6J mice showed a lager increase of uncoupled respiration after isoproterenol injection. C57BLB/6J UCP1$^{+/+}$ have a higher OCR under isoproterenol than respective UCP1$^{-/-}$ cultures (Figure 12A). This pattern was visible in every single experiment. Respiration data under isoproterenol from independent experiments were expressed as a percentage of the respective OCR under basal (Figure 12B) and FCCP (Figure 12C) conditions. Additionally, the fold change of isoproterenol induced oxygen consumption over basal leak was calculated (Figure 12D). Comparing C57BLB/6J UCP1$^{-/-}$ with C57BLB/6J UCP1$^{+/+}$ cultures, the only significant difference was observed when isoproterenol induced respiration was expressed as a percentage of basal respiration. However, in each experiment oxygen consumption under isoproterenol was higher in UCP1$^{+/+}$ than in UCP1$^{-/-}$ cultures. In all ways of data normalization, a significantly higher isoproterenol induced and UCP1 mediated oxygen consumption of 129SV/S6 cells was present. Hence, differences observed on the molecular level (Figure 6 and Figure 7) are also visible on the functional level. 129SV/S6 cultures did not just have the highest expression of UCP1 but also showed the highest UCP1 activity. The more UCP1 is expressed, the higher is the capacity for thermogenic uncoupled respiration.

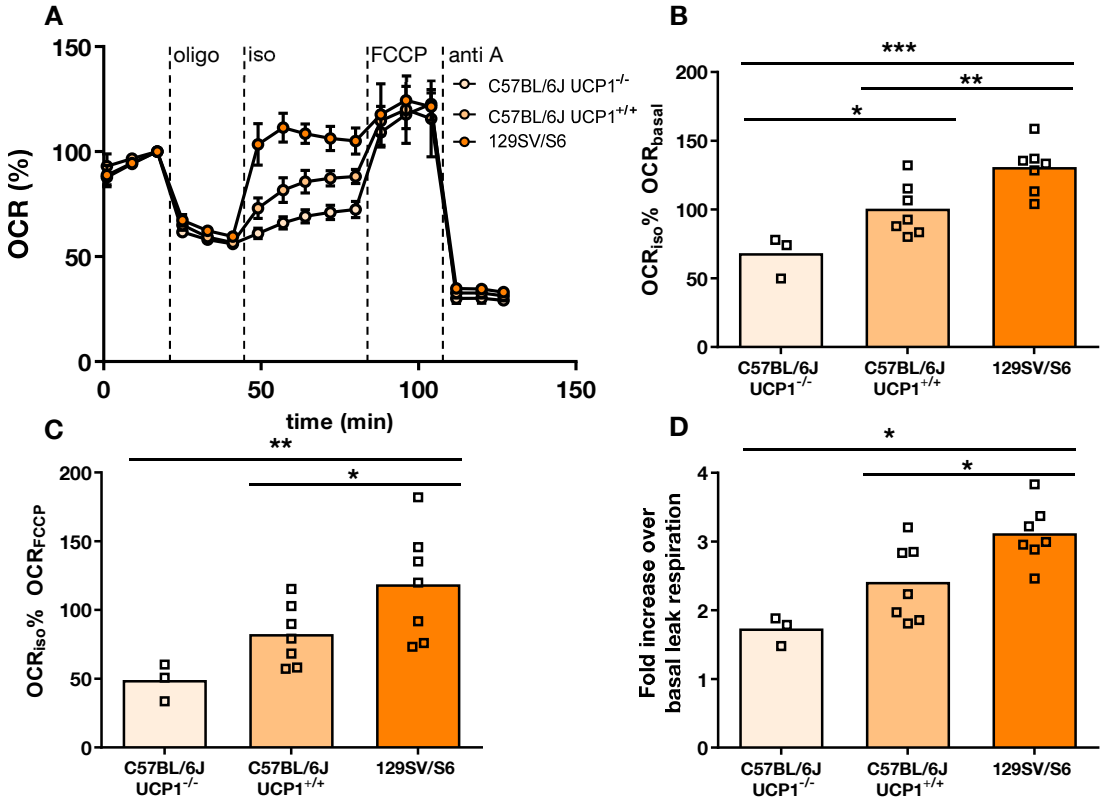

Figure 12: Oxygen consumption rates (OCR) of brite adipocytes from different inbred strains. Representative time course of OCR. First, basal respiration was detected. Then oligomycin (oligo) was added, to measure basal leak respiration. UCP1 mediated uncoupled respiration was determined after isoproterenol (iso, 0.5 µM) injection. Next FCCP, a chemical uncoupler, was added. Finally, antimycin A (anti A) was injected to block complex III of the electron transport chain, leaving only non-mitochondrial OCR to be measured. Data of one measurement with 16 – 32 technical replicates. Dots represent mean values ± SD (A). Maximal OCR under iso as a percentage of basal respiration (B) or as a percentage of OCR under FCCP (C). Fold increase of OCR under iso over basal leak respiration (D). Data of B, C and D represent three independent experiments with 16 – 32 technical replicates per group. Data was analyzed by One Way ANOVA and Student-Newman-Keuls post-hoc-test (p<0.05, **p<0.01, *** p<0.001).*

3.1.4 Release of lipolytic products is independent of UCP1 abundance or activity

Lipolysis and the release of free fatty acids (FFA) are a perquisite of fueling and activation of UCP1. Furthermore, the differences observed in LD size distribution of brite adipocyte cultures could have an impact on their lipolytic capacities. Accessibility of triglycerides to lipolytic enzymes can depend on surface area of the LD and its surface to volume ratio, which is higher in smaller as compared to bigger LDs. Therefore, lipolytic capacity was investigated. The release of lipolytic products FFA and glycerol were measured under basal and isoproterenol stimulated conditions. In response to the adrenergic stimulus, FFA and glycerol release significantly increased 2.43-fold ($p<0.001$) and 1.82-fold ($p<0.01$), respectively. The lipolytic capacities of 129SV/S6 and C57BLB/6J UCP1$^{+/+}$ cells were

comparable. Also, a complete knockout of UCP1 did not affect the release of FFA or glycerol (Figure 13). Thus, release of lipolytic products was independent from UCP1 abundance or activity.

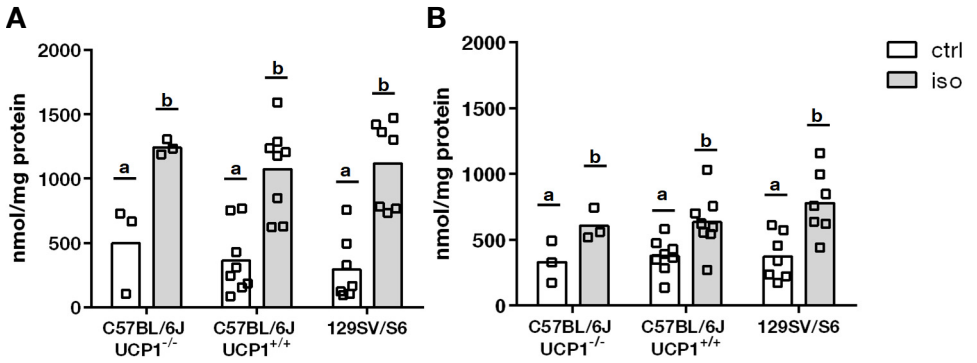

Figure 13: Lipolytic capacity of brite adipocytes. Concentration of free fatty acids (FFA) (A) and glycerol (B) in medium after one hour of incubation. Datasets represent 3 – 8 independent experiments with three technical replicates, analyzed by Two Way ANOVA and Tukey post-hoc-test. Printed characters indicate differences induced by treatment (FFA $p<0.001$; glycerol $p<0.01$).

3.1.5 Glucose uptake is not affected by UCP1 abundance or activity

High amounts of glucose are taken up by brown adipose tissue (BAT) (Shibata et al., 1989; Vallerand et al., 1990). It is used either as energy substrate or as a carbon source. Basically, the uptake can be triggered in two opposite metabolic states. During non-shivering thermogenesis, glucose uptake is stimulated by norepinephrine (NE), whereas in an anabolic state, when energy stores are replenished, glucose uptake is triggered by insulin through activation of GLUT4 translocation (Cannon and Nedergaard, 2004; Leto and Saltiel, 2012). Functional BAT and brite fat can improve blood glucose clearance in mice (Stanford et al., 2013; Tharp et al., 2015). It was hypothesized that adrenergically stimulated glucose uptake differs between cell cultures that express different UCP1 amounts

Establishing glucose uptake in brown adipocytes

Different protocols for glucose uptake using 2-[3H]-deoxy-D-glucose were tested in primary brown adipocytes in the basal and isoproterenol stimulated state. (Figure 14). In all cases, serum was replaced by 2 % BSA. Cells were stimulated with 1 µM isoproterenol for 30 minutes and then exposed to medium containing isoproterenol and trace amounts of 2-deoxy-D-[1-3H]-glucose. Uptake was performed in glucose free medium (Figure 14A) as described by Hutchinson et al. 2015, in the presence of 1 mM 2-deoxy-D-glucose (Figure 14B), or in presence of 5.55 mM D-glucose with (Figure 14C) or without a

pretreatment with 5 µM oligomycin for 30 minutes (Figure 14D). The absolute amount of glucose taken up strongly differed between different protocols with only trace amounts of glucose taken up when following protocols in which uptake was performed in medium without normal D-glucose (Figure 14A and B). Since the aim was to measure glucose uptake under conditions with reasonable D-glucose concentrations and in a state where ATP synthase is active, further measurements were performed in the presence of 5.55 mM D-glucose without a pretreatment with oligomycin. Additionally, the medium was switched to unbuffered assay medium.

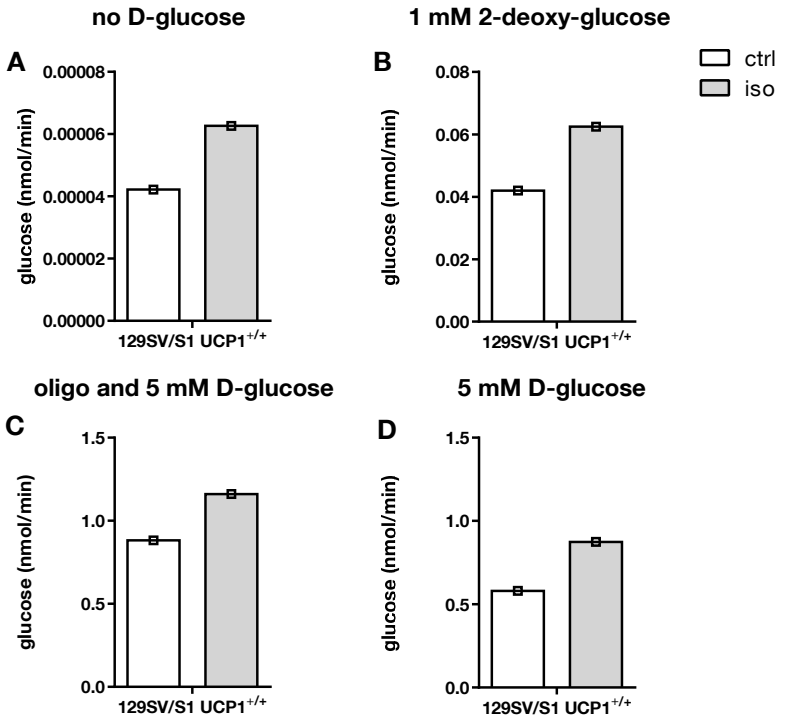

Figure 14:Testing of different glucose uptake protocols in brown adipocytes from 129SV/S1 mice. Serum was replaced by 2 % bovine serum albumin. Cells were stimulated with 1 µM isoproterenol (iso) for 30 min and then exposed to medium containing iso and trace amounts (3 µCi) of 2-deoxy-D-[1-^{3}H]-glucose for three minutes. Uptake was performed in glucose free medium (A), in the presence of 1 mM 2- deoxy-D-glucose (B), or in presence of 5.55 mM D-glucose with (C) or without a pretreatment with 5 µM oligomycin (oligo) for 30 min (D). Data point represents the mean of 3 technical replicates

Glucose uptake in brite adipocytes

The established glucose uptake protocol was used to measure glucose uptake in brite cultures. Cells were treated with 1 µM isoproterenol, 1 µM insulin or both in combination. Compared to controls, isoproterenol treatment caused an overall 1.6-fold increase in glucose uptake ($p<0.05$) whereas insulin treatment led to a 2.3-fold increase ($p<0.001$). A combination of isoproterenol and insulin did not further elevate glucose uptake (Figure 15). Basal and stimulated glucose uptake was comparable between brite adipocytes cultures.

In summary, UCP1 abundance and activity did not affect glucose uptake in brite adipocytes.

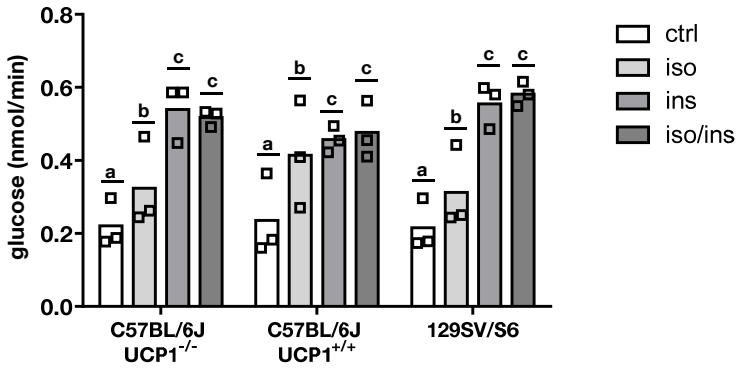

Figure 15: Glucose uptake in brite adipocytes. Uptake was measured in the basal state (ctrl) and when cells were stimulated with 1 µM isoproterenol (iso), 1 µM insulin (ins) or both in combination. Datasets represent 3 independent experiments with three technical replicates and were analyzed by Two Way ANOVA and Tukey post-hoc-test. Printed characters indicate differences induced by treatment (a compared to b p<0.05, to c p<0.001).

Glucose uptake in brown adipocytes

In brite adipocytes, no correlation between glucose uptake and UCP1 expression or activity could be observed. To further clarify if glucose uptake is also independent of UCP1 in brown adipocytes the same experiment was repeated in brown *in vitro* differentiated adipocytes derived from129SV/S1 UCP1$^{+/+}$ and UCP$^{-/-}$ mice. Again, cells were treated with 1 µM isoproterenol, 1 µM insulin or both in combination. Compared to controls, stimulation with isoproterenol or insulin caused a 1.6-fold ($p< 0.05$) and 2.5-fold ($p< 0.05$) increase in glucose uptake, respectively. A combination of these components did not further elevate glucose uptake (Figure 16). There was no difference between the genotypes, supporting the finding that glucose uptake *in vitro* is completely independent of presence or activity of UCP1.

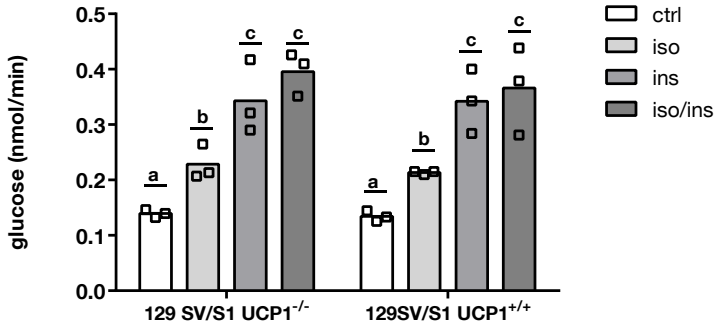

Figure 16: Glucose uptake in brown adipocytes from 129SV/S1 mice. Uptake was measured in the basal state (ctrl) and when cells were stimulated with 1 µM isoproterenol (iso), 1 µM insulin (ins) or both in combination. Datasets represent three independent experiments with 3 technical replicates and were analyzed by Two Way ANOVA and Tukey post-hoc-test. Printed characters indicate differences induced by treatment (a compared to b p<0.05, to c p<0.001).

3.1.6 Lactate release is affected by strain and not by UCP1expression or activity

During glycolysis, glucose is converted into pyruvate. In anaerobic conditions, pyruvate is transformed into lactate by the enzyme lactate dehydrogenase in the cytosol. The reaction regenerates NAD^+ and thereby allows continued glycolysis with the constant production of ATP. In the end, two ATP molecules per glucose molecule are gained. In the presence of oxygen, pyruvate is imported into mitochondria where it is used in TCA cycle and oxidative phosphorylation. Here, 32 ATP can be net produced per glucose molecule. In an uncoupled state, when UCP1 is active, ATP production via oxidative phosphorylation will be severely limited. Under these conditions, anaerobic glycolysis could occur even in the presence of oxygen to provide ATP. Therefore, it was hypothesized, that lactate release differs among brite adipocyte cultures that express UCP1 in different amounts.

Lactate concentration was determined under basal conditions and after stimulation with 0.5 µM isoproterenol. Under both conditions, lactate levels were elevated in the supernatant of 129SV/S6 cultures compared to those of C57BL/6J cultures. This was not the case between C57BL/6J $UCP1^{-/-}$ and C57BL/6J $UCP1^{+/+}$ cultures, indicating rather an effect of strain than of UCP1 abundance. Isoproterenol treatment significantly increased lactate release into the supernatant by almost 50 % (Figure 17). There was no statistically significant interaction between treatment and genetic background. Therefore, isoproterenol induced lactate release was independent of UCP1 activity. Thus, neither glucose uptake nor its use in glycolytic production of lactate were affected by UCP1.

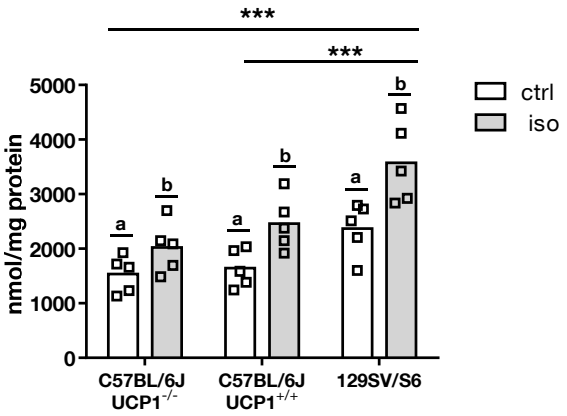

*Figure 17: Lactate release of brite adipocytes. Cells were treated with 0.5 µM isoproterenol (iso) and compared to controls (ctrl). Datasets represent five independent experiments with three technical replicates and were analyzed by Two Way ANOVA and Tukey post-hoc-test (*** p≤0.001). Printed characters indicate differences induced by treatment with isoproterenol (iso, p≤0.001).*

3.1.7 Metabolite profile depends on UCP1 activity

Non-targeted metabolite profiling was applied to further characterize the functional and metabolic properties of brite cells. Brite cultures were treated with isoproterenol to stimulate lipolysis and UCP1 activity and compared to non-treated controls. In a first pilot study, cell lysate samples of 129SV/S6, C57BL/6J UCP1$^{+/+}$ and UCP1$^{-/-}$ cultures from one experiment (E1; N=1, n=3) were analyzed. Cluster analysis revealed a dramatic change in metabolic profile after adrenergic stimulation. Relative signal intensities of saturated (SAFA) and unsaturated FFA were increased, whereas those of several amino acids, small peptides and nucleoside triphosphates were reduced (Figure 18). Metabolites were identified which were altered specifically in the presence of UCP1, constituted mainly by fatty acids, lysophospholipids and amino acids.

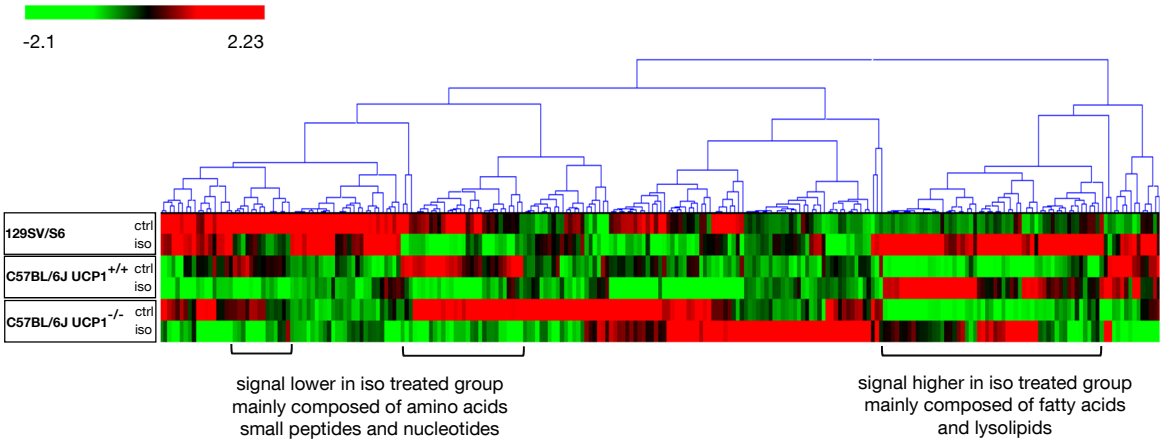

Figure 18: Hierarchical clustering heat map of metabolites from brite adipocyte cultures treated with or without 0.5 µM isoproterenol (iso) for 30 minutes (E1). Pilot experiment with three technical replicates per group. Clustering includes 245 metabolites. Similarity measures were based on Pearson Correlation Coefficient. Clusters correspond to a minimum similarity value of 0.35.

To validate the candidates found in the pilot study a second study was conducted which included two biological replicates (E2, E3; N=2, n=3). Again, adrenergic treatment altered the metabolite profile and also metabolites, altered specifically in the presence of UCP1, were present (Figure 19). In total for 40 metabolites an interaction of genotype and treatment could be detected (Table S1). Instrument performance strongly varied between the two measurements and relative signal intensities of metabolites were not comparable between the two datasets. Consequently, they had to be analyzed separately.

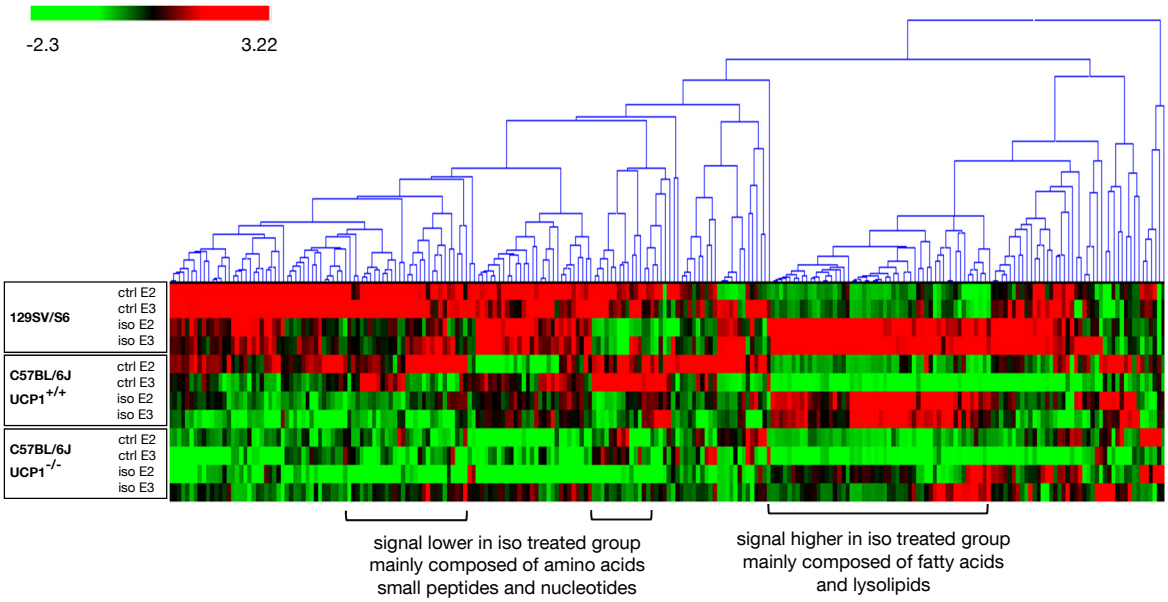

Figure 19: Hierarchical clustering heat map of metabolites from brite adipocyte cultures treated with or without 0.5 µM isoproterenol (iso) for 30 minutes (E2, E3). Each row represents mean of three technical replicates. In total the dataset is composed of two biologically independent experiments (N=2; n=3). Clustering includes 240 metabolites. Similarity measures were based on Pearson Correlation Coefficient. Clusters correspond to a minimum similarity value of 0.37.

In total 245 (E1) and 240 (E2, E3) metabolites could be detected. From these metabolites, 40 and 48, respectively, remained unknown. The overlap of metabolites that were detected in both studies encompassed 137 metabolites. 16 out of these 137 molecules could not be annotated (Figure 20).

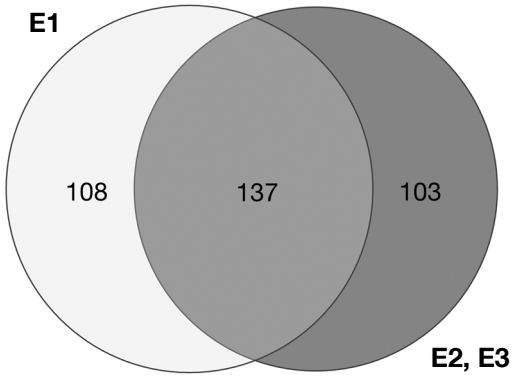

Figure 20: Total number of metabolites that were detected in E1 as well as in E2 and E3.

Six metabolites showed altered signal intensities under adrenergic stimulation that were independent of UCP1 activity in both datasets, (Figure 21A). The gamma-methyl ester of glutamate, oxidized glutathione, uridine 5'-triphosphate (UTP) and ATP were more abundant in untreated cultures of all genotypes. Conversely, AMP and 10-nonadecenoate (19:1n9) were present in higher concentrations in isoproterenol treated cultures (Table S2).

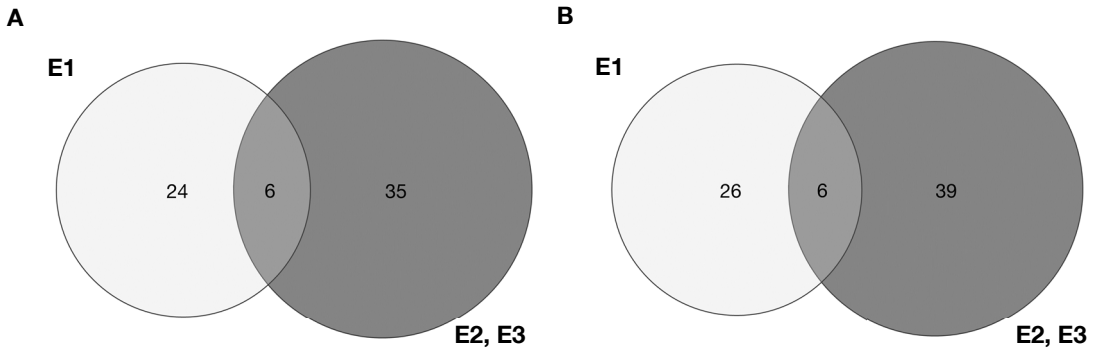

Figure 21: Metabolites that showed altered signal intensities in adrenergic treated groups (A). Metabolites present in distinct amounts between mouse strains (B).

In total, 6 metabolites could be identified that were present in distinct amounts in cultures from 129SV/S6 and C57BL/6J mice (Figure 21B). The gamma-glutamyl amino acids gamma-glutamylisoleucine, gamma-glutamylthreonine and gamma-glutamylvaline as well as the amino acid ophthalmate and the unknown metabolite X–2776 had higher signal intensities in 129SV/S6 cultures compared to C57BL/6J cultures. These differences were independent from treatment (Table S3). In contrast, strain dependent differences in the abundance of the polyunsaturated fatty acid (PUFA) dihomo-linolenate (20:3) were only visible in the isoproterenol-stimulated state. Under these conditions signal intensities were much higher in 129SV/S6 compared to C57BL/6J samples (Figure 22).

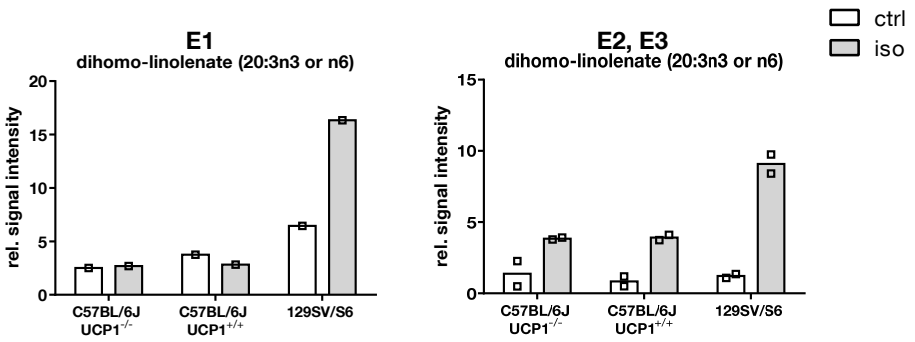

Figure 22: Relative signal intensities of dihomo-linolenate (20:3) in brite adipocytes. Cultures were treated with 0.5 µM isoproterenol (iso) for 30 minutesand compared to controls.

The most interesting metabolites are those that show a UCP1 activity dependent pattern. Metabolites that are altered specifically upon UCP1 activity could help to identify metabolic pathways that are up or down regulated in a thermogenically active cell.

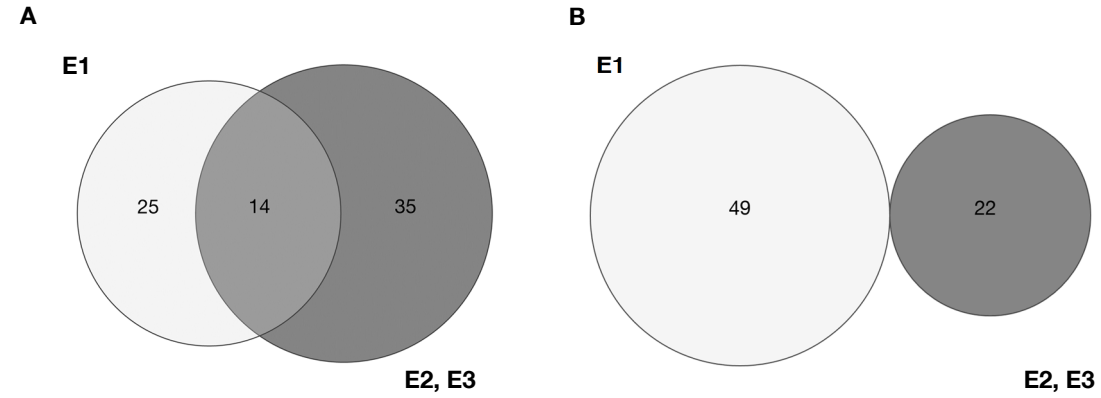

Figure 23: Metabolites that were altered specifically upon UCP1 activity. Signal intensities of respective metabolites were either increased (A) or decreased (B) under UCP1 activity. 14 metabolites showed the same signal intensity pattern in E1 as well as in E2 and E3.

Overall, 14 metabolites could be detected, that were upregulated in a UCP1 activity dependent manner in both datasets (Figure 23). Among these metabolites PUFAs were the most abundant class. The relative signal intensities of linoleate (18:2n6), linolenate (18:3n3 or 6), arachidonate (20:4n6) and docosapentaenoate (n3 DPA; 22:5n3), were elevated in the adrenergic stimulated condition. Although the increase was present in all brite adipocyte cultures, the extent of alteration was much more pronounced in UCP1 expressing cell cultures. In addition, the highest concentration of respective metabolites could be observed in the isoproterenol treated samples of those cultures that possess the highest UCP1 expression levels (Figure 24). These results indicate that several PUFAs are altered in a UCP1 activity dependent manner and that this relationship is not only true qualitatively but also quantitatively. Besides PUFAs, also the monounsaturated fatty acids (MUFA) 10-heptadecenoate (17:1n7), eicosenoate (20:1) oleate (18:1n9) palmitoleate (16:1n7) as well as the saturated fatty acids pentadecanoate (15:0), palmitate (16:0) and margarate (17:0) showed a UCP1 activity dependent pattern in their signal intensities (Table 4). Furthermore, the same pattern was observed in the amount of the branched chain fatty acid (BCFA) 15-methylpalmitate, the acyl glycine hippurate and the unknown metabolite X – 11909.

Taken together, the majority of metabolites that were altered in a UCP1 activity dependent manner are FFA that are either PUFAs, MUFAs, BCFAs or odd chain fatty acids (OCFA). The overall lipolytic activity does not vary between brite adipocyte cultures of distinct genetic background (3.1.4). Thus, higher FFA levels cannot be explained by a generally increased lipolytic release. There are three possibilities, why several FFA show a UCP1 dependent pattern. First, the FA composition of LDs could be different in UCP1 expressing cells. If the triacylglycerides (TAGs) contain more PUFAs, MUFAs, BCFAs or OCFAs more

of these metabolites are released during lipolysis. Second, increased signal intensities could be explained by reduced degradation. When UCP1 is active, β-oxidation is elevated. Thermogenically active adipocytes could preferentially oxidize other FFA. Subsequently, concentrations of the respective PUFAs, MUFAs, BCAFAs and OCFAs would rise in these cells. Third, cells that do not express UCP1 could preferentially reesterify the respective FFA with glycerol or FA-binding proteins and thereby decrease their concentration.

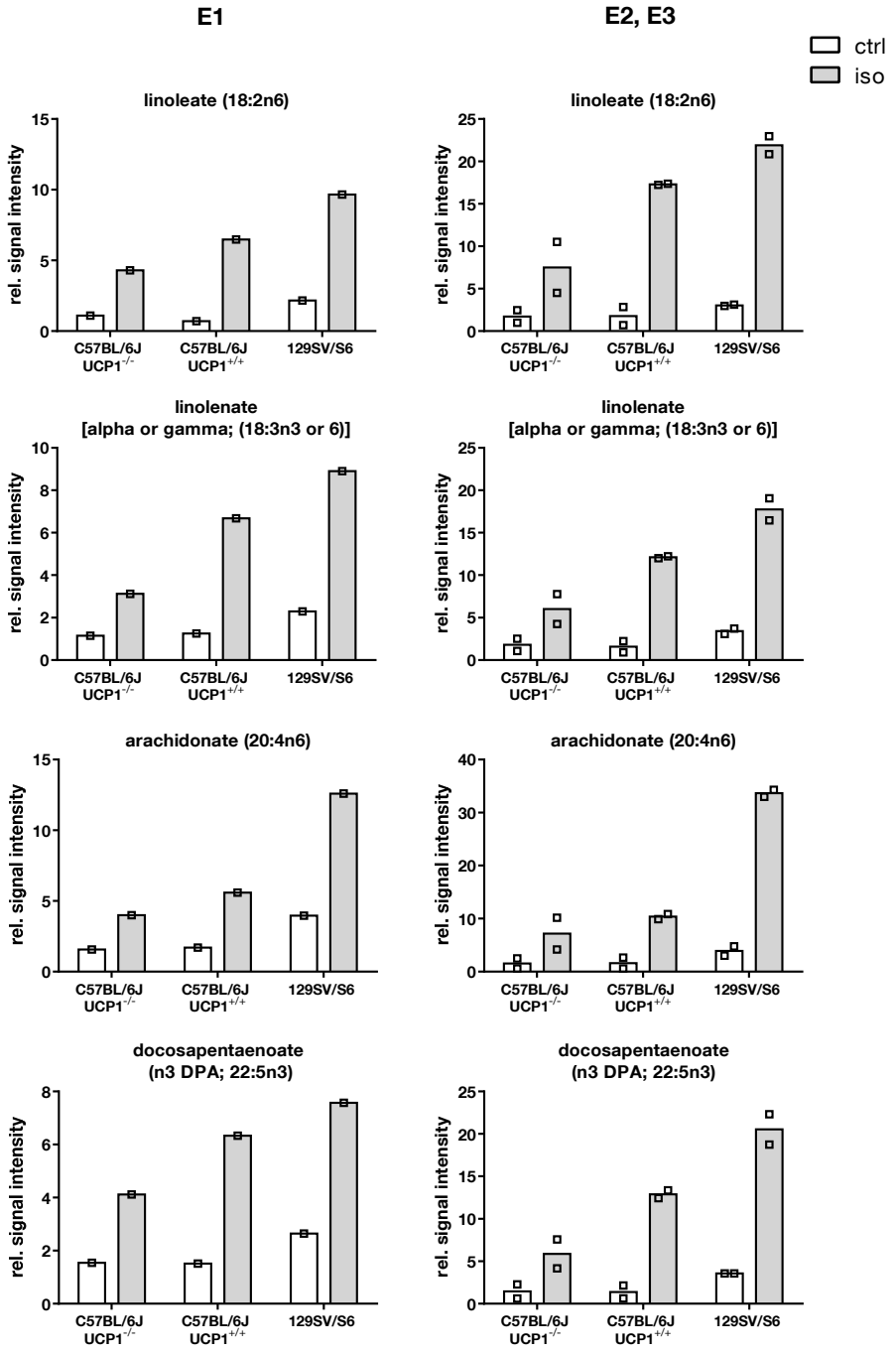

Figure 24: Polyunsaturated fatty acids that were specifically altered upon UCP1 activity.

Table 4: Relative signal intensities of metabolites that were altered specifically upon UCP1 activity

	129SV/S6						C57BL/6JUCP1 $^{+/+}$						C57BL/6JUCP1$^{-/-}$					
	ctrl			iso			ctrl			iso			ctrl			iso		
Biochemical	E1	E2	E3	E1	E2	E3	E1	E2	E3	E1	E2	E3	E1	E2	E3	E1	E2	E3
10-heptadecenoate (17:1n7)	1.45	2.92	4.98	5.29	88.74	108.08	0.47	3.83	0.53	7.58	97.93	106.10	0.34	2.87	0.66	4.49	40.49	5.54
15-methylpalmitate	1.35	3.08	5.26	6.58	17.90	21.48	0.51	3.71	1.13	5.37	14.27	11.68	0.38	2.05	0.79	4.06	7.21	4.26
eicosenoate (20:1)	1.68	2.59	4.49	7.72	33.26	45.78	0.46	3.45	0.59	7.79	55.06	42.80	0.32	2.37	0.46	3.45	22.28	6.76
hippurate	4.57	4.69	5.24	40.11	5.48	6.30	31.30	3.23	2.85	43.26	5.71	5.42	5.48	2.58	2.06	1.82	3.15	3.63
margarate (17:0)	3.45	3.40	5.30	5.66	11.88	14.92	1.22	4.73	1.33	10.64	16.85	14.17	0.99	1.99	0.87	4.84	8.66	6.60
oleate (18:1n9)	1.54	3.04	4.95	7.55	42.59	50.27	0.50	4.65	0.73	5.92	50.83	49.68	0.43	2.90	0.75	3.83	25.33	5.28
palmitate (16:0)	2.35	3.25	5.30	6.49	20.63	25.39	0.92	4.28	1.11	4.76	24.92	20.67	0.83	2.05	0.81	3.68	11.14	4.96
palmitoleate (16:1n7)	1.44	2.98	5.07	7.18	69.07	74.69	0.47	2.66	0.43	4.83	62.24	64.68	0.41	2.70	0.57	3.96	24.89	4.72
pentadecanoate (15:0)	2.00	3.17	5.73	5.20	23.01	31.45	0.66	4.27	1.14	8.32	26.58	21.84	0.48	1.97	0.96	5.62	10.15	5.56
X - 11909	2.76	3.51	3.30	9.98	20.25	15.02	1.56	2.72	0.60	6.82	19.77	20.83	1.23	3.09	0.67	4.82	5.52	5.75

The total FA composition of brite adipocytes was measured to further investigate FA composition. Brite adipocyte cultures were treated with or without 0.5 µM isoproterenol for 30 minutes. FAs of cell lysates were detected by GC/MS after complete hydrolysis of all lipids. Most abundant FAs were SAFAs (51.48 %) and MUFAs (47.87 %). PUFAs accounted on average for 0.65 % of all FA present in brite adipocytes. 129SV/S6 cultures tended to have less SAFAs and PUFAs than C57BL/6J UCP1$^{+/+}$ cultures whereas MUFAs seemed to be elevated (Figure 25). FAs which were altered specifically in the presence and activity of UCP1 (Figure 24, Table 4) did not show a UCP1 dependent pattern on total FA level (Table 5). Moreover, treatment with isoproterenol did not change the relative abundance of these FA in brite adipocytes (Table 5).

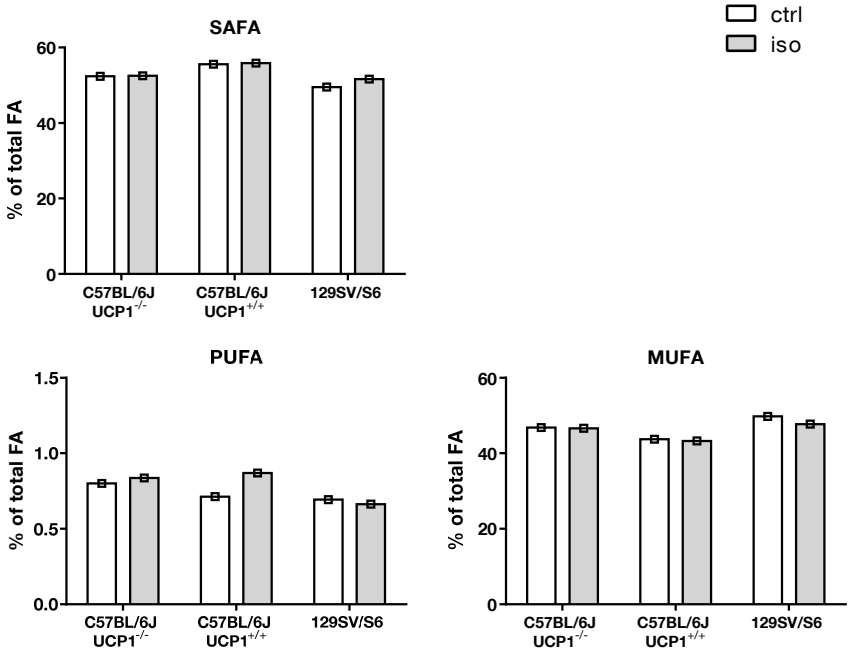

Figure 25: Proportion of different fatty acid classes on total fatty acid content of brite adipocytes. Saturated fatty acid (SAFA), mono- and polyunsaturated fatty acid (MUFA, PUFA). Cell cultures were treated with or without isoproterenol (iso) for 30 min. Datasets represent one biological experiment with three technical replicates.

Table 5: Abundance of certain fatty acids. Amount of fatty acids (FAs) expressed as a percentage of total FAs. Data represent one biological experiment with three technical replicates.

	129SV/S6				C57BL/6J UCP1$^{+/+}$				C57BL/6J UCP1$^{-/-}$			
	ctrl		iso		ctrl		iso		ctrl		iso	
FA	% FA	SD	% FA	SD	% FA	SD	% FA	SD	% FA	SD	% FA	SD
pentadeonate (15:0)	1.12	0.09	1.11	0.01	2.09	0.13	2.02	0.05	1.86	0.18	1.82	0.07
palmitate (16:0)	39.28	0.69	41.16	0.70	42.77	0.96	43.41	0.28	40.26	0.40	40.91	0.44
palmitoleate (16:1n7)	37.36	0.84	35.71	0.95	30.87	0.16	29.66	0.71	32.94	0.67	32.61	0.77
margarate (17:0)	0.17	0.01	0.17	0.01	0.38	0.02	0.37	0.01	0.32	0.03	0.32	0.02
linoleate (18:2n6)	0.14	0.00	0.14	0.00	0.17	0.02	0.18	0.02	0.16	0.00	0.17	0.00
linolenate (18:3n3)	0.01	0.00	0.01	0.00	0.02	0.00	0.01	0.00	0.01	0.00	0.02	0.00
eisoseoate (20:1)	0.08	0.00	0.07	0.00	0.09	0.01	0.09	0.00	0.10	0.00	0.10	0.00
arachidonate (20:4n6)	0.29	0.01	0.28	0.01	0.28	0.11	0.38	0.04	0.35	0.01	0.37	0.02

In summary, metabolite profile of brite adipocyte cultures differs among metabolic state and strain (Figure 21). Furthermore, themogenically active adipocytes have a distinct metabotype. This UCP1 dependent metabotype is mainly characterized by an altered FFA profile, which is not present in total FA composition.

3.1.8 Identification of candidate genes involved in browning

We combined the metabolite profile dataset with transcriptome analysis data in order to reveal metabolic pathways implicated in the thermogenic function of brite adipocytes. For this approach, seven preexisting NGS based transcriptome analysis data sets from human and murine samples were included (Figure 24). *In vitro* data sets were based on murine *in vitro* differentiated primary brite adipocyte cultures from different inbred strains (Li, 2013), into brite and white differentiated human multipotent adipose-derived stem (hMADS) cells (Loft et al., 2015) and into white and brown differentiated human pluripotent stem-cell derived mesenchymal progenitor cells (PSC-MPCs) (Moisan et al., 2015). *In vivo* data sets included samples from mice during postnatal browning and cold exposure. The postnatal browning data set is composed of retroperitoneal WAT samples from C57BL6/J and 129SV/S6 mice at postnatal day 10, 20 and 30 (Lasar, 2013). Cold exposure (5 °C) data sets include iBAT samples from six, 12 and 48 hours cold exposed mice (Fromme, 2013), iBAT samples of three days cold exposed mice (Marcher et al., 2015) as well as iBAT and iWAT samples of two and four days cold acclimated mice (Hao et al., 2015).

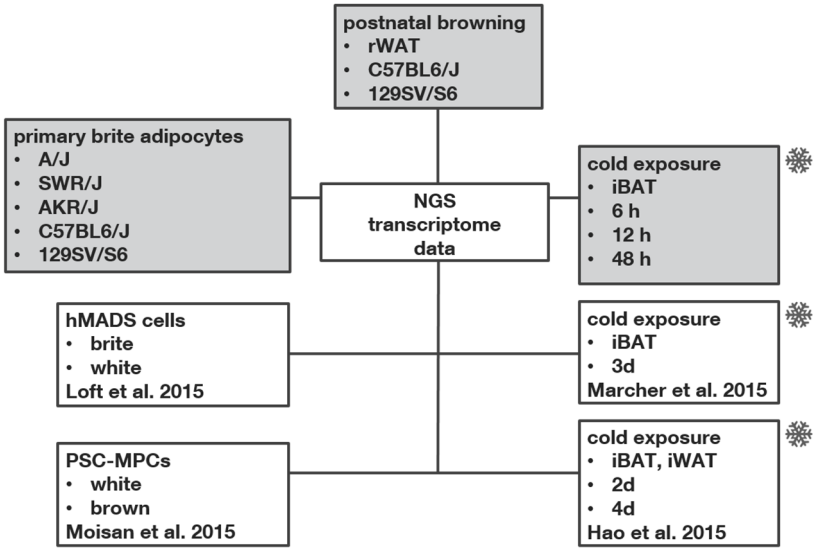

Figure 26: Next generation sequencing (NGS) based transcriptome analysis data sets that were included into analysis. White boxes represent public data sets. Grey boxes are data sets of the chair for molecular nutritional medicine.

As a first step, we conducted a pathway analysis of metabolite and NGS transcriptome data of 129SV/S6 and C57BL6/J primary brite adipocytes. Log2 fold changes of RNA and metabolite data were analyzed with an integrated enrichment tool (Incromap, ZBIT, Tübingen, Germany). For metabolite data log2 fold change of isoproterenol stimulated conditions were used to include the metabotype of an thermogenically active brite adipocyte. Pathway analysis revealed that in the isoproterenol treated samples glycerophospholipid (GPL) metabolism as well as biosynthesis of unsaturated fatty acids are upregulated in 129SV/S6 compared to C57BL6/J cultures ($p<0.05$). Also, as known from chapter 3.1.6, most metabolites that were altered in a UCP1 activity dependent manner were FFA that were either PUFAs, MUFAs, BCAFAs or odd chain fatty acids (OCFA). We concluded that genes within the GPL or FA metabolism could be putative candidate genes involved in thermogenic function of brite adipocytes.

In the next step, correlation analysis between the expression of these putative candidate genes and Ucp1 expression were performed. For this approach, the primary brite adipocyte NGS transcriptome data set was used that included five different inbred strains with distinct browning propensities. Additionally, log2 fold changes of respective genes in the remaining NGS data sets were evaluated in the context of thermogenic function. In total 33 candidate genes were identified (Table 6). With a correlation coefficient of 0.71 ($p<0.01$) and a score value of 3, Gpam represented one of the top candidate genes that could be involved in thermogenic function of brite adipocytes. In contrast to other

candidate genes this gene is abundantly expressed. Furthermore, Gpam has been already shown to be involved in mitochondrial function (Faris et al., 2014).

The gene Gpam encodes for a 94-kDa integral membrane protein, the glycerol 3-phosphate-acyltransferase-1 (GPAT1), located in the outer mitochondrial membrane. GPAT1 possesses two transmembrane domains where both NH_2 and COOH termini are oriented toward the cytosol and a loop is facing the intermembrane space (Gonzalez-Baro et al., 2001; Gonzalez-Baro et al., 2007). Together with other GPAT isoforms, GPAT1 catalyzes the conjugating of acyl-CoA with glycerol-3 phosphate (G3P) to lysophosphatidic acid (LPA), the first rate limiting step of de novo GPL and TAG synthesis via the glycerol phosphate pathway (Faris et al., 2014; Hammond et al., 2002; Igal et al., 2001) (Figure 27). So far four mammalian GPAT isoforms have been identified. GPAT1 and GPAT2 represent mitochondrial isoforms, whereas GPAT3 and GPAT4 are localized in the endoplasmic reticulum (ER) membrane (Takeuchi and Reue, 2009). Instead of being processed by GPAT-1, acyl-CoA can also be converted to fatty acyl carnitine by carnitine palmitoyltransferase-1 (CPT1), transported into the mitochondria and used for β-oxidation. Therefore, GPAT-1 and CPT1 compete for acyl-CoAs, thereby playing a role in determining the fate of a fatty acid: if it is used for energy production via β-oxidation or for GPL and TAG synthesis (Faris et al., 2014). GPAT1 and CPT1 are reciprocally regulated by AMPK, thus sensitive to cellular nutrient levels. When cellular energy stores are depleted or energy need is high, AMPK is activated and down-regulates GPAT1 activity, while promoting CPT1 activity via decreasing cellular malonyl-CoA, (Wendel et al., 2009; Winder and Thomson, 2007).

Table 6: Candidate genes involved in glycerophospholipid and fatty acid metabolism. Analysis is based on the following data sets: murine in vitro differentiated primary brite adipocyte cultures from different inbred strains (Li, 2013) [1], postnatal browning rWAT samples from C57BL6/J and 129SV/S6 mice at postnatal day 10, 20 and 30 (Lasar, 2013)[2], iBAT samples from 6, 12 and 48 hours cold exposure (Fromme, 2013)[3], iBAT sampels of three days cold exposure (Marcher et al., 2015)[4] as well as iBAT and iWAT samples of two and four days cold acclimation (Hao et al., 2015)[5], into brite and white differentiated human multipotent adipose-derived stem (hMADS) cells (Loft et al., 2015)[6] and into white and brown differentiated human pluripotent stem-cell derived mesenchymal progenitor cells (PSC-MPCs) (Moisan et al., 2015)[7]. Evaluation of log2 fold changes in context of thermogenic function (datasets [2-7]): 1 = log2 fold change ≥0.5. Score represents sum of log2 fold change evaluation and mitochondrial localization

Gene	Name	primary brite adipocytes[1]		Postnatal browning (rWAT)[2]	Cold exposure (iBAT)[3]	Cold exposure (iBAT)[4]	Cold exposure (iBAT, iWAT)[5]	hmads (white, brown)[6]	PSC-MPCs (white, brown)[7]	Mitochondial localization	Score
		Pearson r	p value summary								
Acss2	acyl-coa synthetase short-chain family member 2	0.87	****	0	0	0	1	0	0	0	1
Pla2g4b	phospholipase a2, group 4 beta	0.80	***	0	0	0	1	0	0	0	1
Fasn	fatty acid synthase	0.79	***	0	0	0	1	0	0	1	2
Acot11	acyl-coa thioesterase 11	0.79	***	0	1	1	1	0	0	0	3
Scd1	stearoyl-CoA desaturase 1	0.76	**	0	0	0	0	0	0	0	0
Lpin1	phosphatidate phosphatase 1	0.74	**	0	0	0	1	0	0	0	1
Gpam	glycerol-3-phosphate acyltransferase 1, mitochondrial	0.71	**	0	1	1	0	0	0	1	3
Pcyt2	phosphate cytidylyltransferase 2, ethanolamine	0.65	**	0	1	0	1	0	0	0	2
Plbd1	phospholipase B domain containing 1	0.65	**	0	1	0	1	1	0	0	3
Chkb	choline kinase beta	0.65	**	0	0	0	1	0	0	0	1
Pnpla8	patatin-like phospholipase domain containing 8	0.64	**	0	0	0	1	0	0	1	2
Cpt2	carnitine palmitoyltransferase 2	0.63	*	0	0	0	1	1	0	1	3
Agpat3	1-acyl-sn-glycerol-3-phosphate acyltransferase gamma	0.62	*	0	1	1	1	0	0	0	3
Gnpat	dihydroxyacetone phosphate acyltransferase	0.62	*	0	0	0	1	0	0	0	1
Cpt1b	carnitine palmitoyltransferase 1b	0.62	*	1	1	0	1	1	0	1	5
Lpin3	phosphatidate phosphatase 3	0.61	*	0	1	0	0	0	0	0	1
Etnk1	ethanolamine kinase 2	0.61	*	0	0	0	0	0	0	0	0
Agpat2	1-acyl-sn-glycerol-3-phosphate acyltransferase beta	0.60	*	0	0	0	1	1	0	0	2
Aspg	60 kda lysophospholipase	0.54	*	0	0	0	1	0	0	0	1
Glo1	glyoxalase 1	0.54	*	0	0	0	0	0	0	0	0
Lypla1	lysophospholipase 1	0.50	ns	0	0	0	1	1	0	0	2
Acot4	acyl-coenzyme a thioesterase 4	0.34	ns	0	1	0	1	0	0	0	2
Pnpla7	patatin-like phospholipase domain containing 7	-0.34	ns	0	1	0	1	0	0	0	2
Cpt1a	carnitine palmitoyltransferase 1a	-0.34	ns	0	0	0	0	0	0	1	1
Ache	acetylcholinesterase	-0.35	ns	0	1	0	1	0	1	0	3
Acot5	acyl-coenzyme a thioesterase 5	-0.57	*	0	0	0	0	0	0	0	0
Pisd	phosphatidylserine decarboxylase	-0.58	*	0	0	0	0	0	0	1	1
Pla2g15	phospholipase a2, group 15	-0.59	*	0	0	0	0	0	1	0	1
Cds2	cdp-diacylglycerol synthase (phosphatidate cytidylyltransferase) 2	-0.71	**	0	1	0	1	0	0	1	3
Cpt1c	carnitine palmitoyltransferase 1c	-0.74	**	0	0	1	1	1	0	1	4
Nt5c	5', 3'-nucleotidase, cytosolic	-0.75	**	0	1	0	0	0	1	0	2
Lpcat4	lysophospholipid acyltransferase 4	-0.79	***	0	0	0	0	1	0	0	1
Pik3r2	phosphoinositide-3-kinase regulatory subunit 2	-0.81	***	0	1	0	1	0	0	0	2

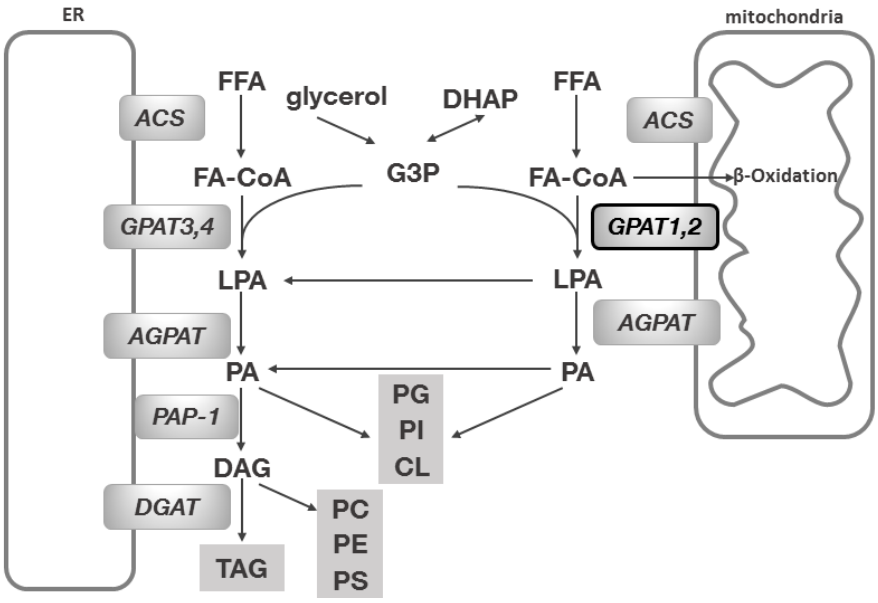

Figure 27: Gpat1 and its function in the glycerol phosphate pathway for de novo triacylglycerol (TAG) and glycerophospholipid synthesis. GPAT1 catalyzes the formation of lysophosphatidic acid (LPA) from glycerol-3 phosphate (G3P) and acyl-CoA. LPA is further acylated to phosphatidic acid (PA) which serves as a precursor for glycerophospholipid and triglyceride synthesis. For the last steps of TAG synthesis LPA and PA must be transported to the ER. GPAT, glycerol-3-phosphate acyltransferase; AGPAT, 1-acylglycerol-3-phosphate acyltransferase; PI, phosphatidylinositol; PG, phosphatidylglycerol; CL, cardiolipin; PC, phosphatidylcholine; PE, phosphatidylethanolamine; PS, phosphatidylserine; DAG, diacylglycerol; DGAT, diacylglycerol acyltransferase. Modified from Coleman and Lee (2004); Coleman et al. (2000).

3.1.9 Knockdown of Gpam increases Ucp1 expression on RNA but not on protein level

Gpam was identified as a candidate gene, possibly involved in thermogenic function of brite adipocytes. Gpam transcript levels in brite adipocytes across inbred strains correlated positively with the respective difference in Ucp1 expression. In addition, Gpam transcript levels in BAT were elevated upon cold exposure (Table 6). It was hypothesized that Gpam could be an essential functional component of brite adipocytes and that a knockdown of Gpam would impair thermogenic function. In a first experiment, a time course of Gpam expression in cultures derived from 129SV/S6 mice was established and compared to the Ucp1 expression profile (Figure 28). The highest mRNA level of Gpam was detected after two days of induction (day of differentiation 0, dd0). Afterwards, mRNA abundance decreased. The second highest mRNA level of Gpam occurred on dd5. Here the mRNA abundance is around 60 % of the abundance on dd0. In contrast, mRNA levels of Ucp1 reached a maximum on dd1 and dd3, decreased on dd5 and again increased at dd7. In the RNA data sets, a positive correlation between Gpam and Ucp1 was found on dd7. However, at this timepoint the lowest Gpam mRNA level is present during differentiation. During differentiation, a shift between Gpam and Ucp1 expression was

observable, indicating that in brite adipogenesis GPAT1 is required before UCP1. GPAT1 is pivotal for GPL synthesis. Thus, it could be involved in the production of lipid species for mitochondrial membranes, required for thermogenesis. To elucidate the consequences of lower Gpam abundance on Ucp1 expression and thermogenic function, siRNA mediated knock down experiments were performed.

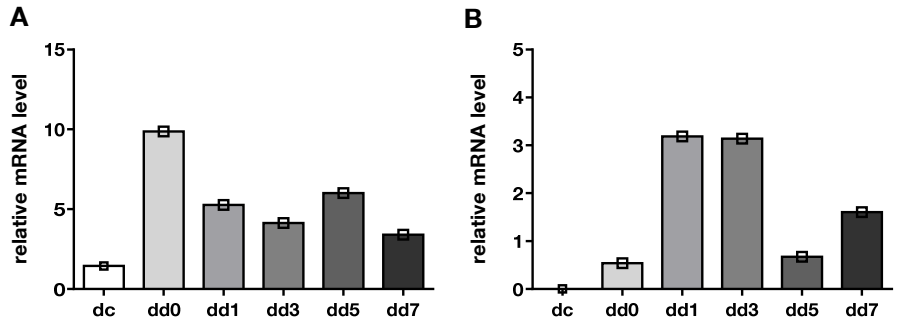

Figure 28: Time course of Gpam and Ucp1 gene expression. Relative RNA expression of Gpam (A) and Ucp1 (B) in brite adipocytes at different timepoints during differentiation (day of confluence, dc, day of differentiation, dd). Datasets represent one biological experiment with three technical replicates.

Since Gpam plays a crucial role in lipid formation and adipocyte differentiation, siRNA experiments were not performed on dd0 (highest expression of Gpam) but on dd5 when adipocyte differentiation was already in an advanced state. Knockdown of Gpam caused an almost 2-fold increased Ucp1 expression (Figure 29). If GPAT1 is required for thermogenic function this effect on Ucp1 expression could represent a compensatory reaction to defend thermogenic capacity diminished by a lower Gpam expression.

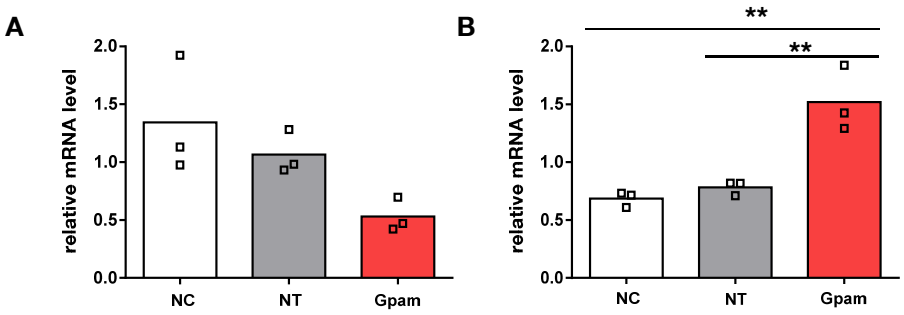

*Figure 29: relative RNA expression of Gpam (A) and UCP1 (B) in siRNA transfected brite adipocytes on differentiation day 8 (dd8). On dd5, cells received only transfection mix (negative control, NC) or transfection mix with non-targeting siRNA (non-targeting control, NT) or siRNA targeting Gpam. Values were normalized to Tf2b expression. Data represent 3 independent experiments and were analyzed by One Way Anova with Holm-Sidak post hoc test (** $p<0.01$).*

Subsequently, respiration experiments were performed to check if the observed elevated Ucp1 or reduced Gpam expression on mRNA level has an impact on UCP1 activity. To do so, cells were transfected on dd5 and oxygen consumption was assessed on dd8 using a

microplate extracellular flux analyzer. After injection of oligomycin and measurement of basal leak respiration, UCP1 mediated uncoupled respiration was induced by isoproterenol (Figure 30A). Thermogenic oxygen consumption on dd8 was not influenced by a knockdown of Gpam on dd5. No differences could be detected between Gpam targeting siRNA treated cells and controls when OCR data under isoproterenol of two independent experiments was expressed as a percentage of the respective OCR under basal (Figure 30B) or FCCP (Figure 30C) conditions. Neither was the fold change of isoproterenol induced oxygen consumption over basal leak was different between the groups (Figure 30D). These observations can be explained by two different hypotheses. First, impaired thermogenic function caused by knockdown of Gpam could be compensated by increased Ucp1 expression on mRNA and protein level. Second, knockdown of Gpam did not impair thermogenic function but increased Ucp1 expression on mRNA level but not on protein level, thereby not influencing its activity.

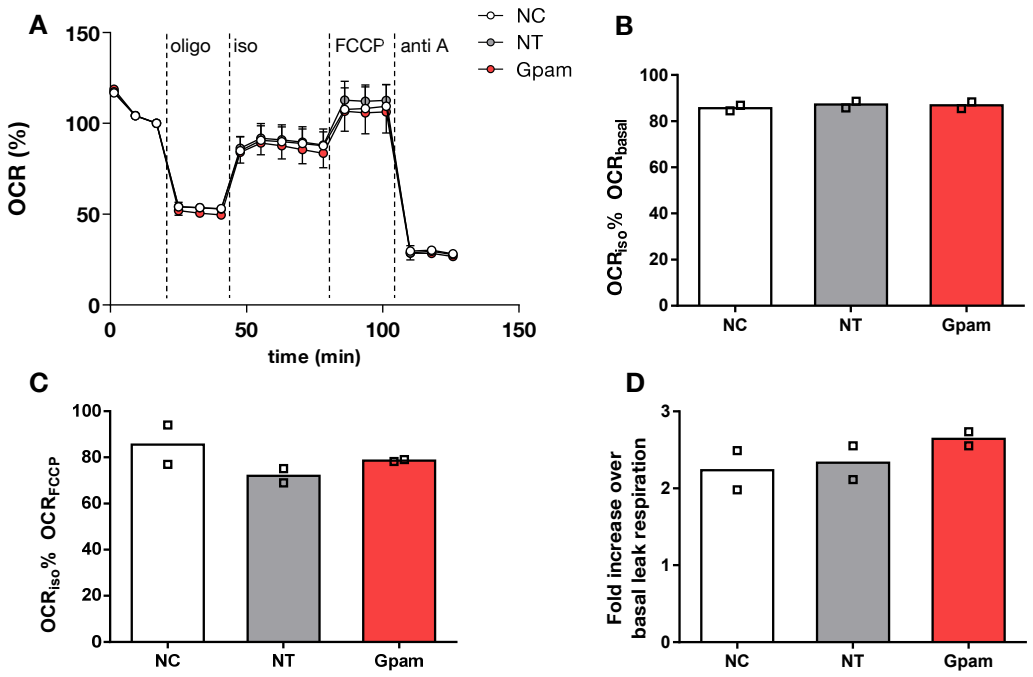

Figure 30: Oxygen consumption rates (OCR) of in siRNA transfected brite adipocytes on differentiation day 8 (dd8). On dd5, cells received only transfection mix (negative control, NC) or transfection mix with non-targeting siRNA (non-targeting control, NT) or siRNA targeting Gpam. Representative time course of OCR. First, basal respiration was detected. Then oligomycin (oligo) was added, to measure basal leak respiration. UCP1 mediated uncoupled respiration was determined after isoproterenol (iso, 0.5 µM) injection. Next FCCP, a chemical uncoupler that allows assessment of maximal respiratory capacity, was added. Finally, antimycin A (anti A) was injected to block complex 3 of the electron transport chain, leaving only non-mitochondrial OCR to be measured. Data of one measurement with 16 – 22 technical replicates. Dots represent mean values ± SD (A). Maximal OCR under iso as a percentage of basal respiration (B) or as a percentage of OCR under FCCP (C). Fold increase of OCR under iso over basal leak respiration (D). Data of B, C and D represent two independent experiments with 16 – 22 technical replicates per group.

Since there was no effect on UCP1 mediated oxygen consumption, the question arose if and when the increase in Ucp1 mRNA expression is translated to protein level. Therefore, another siRNA knockdown experiment was conducted. Again, cells were transfected on dd5. This time RNA and protein was isolated on dd8 and on dd10. The knockdown of Gpam on dd5 was still detectable an dd10 (Figure 31A) and led to an increase in mRNA expression of UCP1 on dd8 and on dd10 (Figure 31B). However, this effect was not visible on the protein level (Figure 32). Increased UCP1 mRNA expression was not translated into increased protein levels.

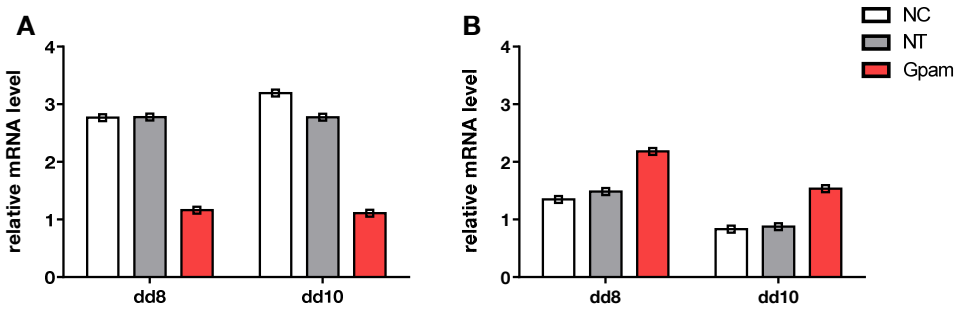

Figure 31: RNA expression of Gpam (A) and Ucp1 (B) in siRNA transfected brite adipocytes on differention day 8 and 10 (dd8, dd10) normalized to Tf2b expression. On dd5 of differentiation, cells received only transfection mix (negative control, NC) or transfection mix with non-targeting siRNA (non-targeting control, NT) or siRNA targeting Gpam.

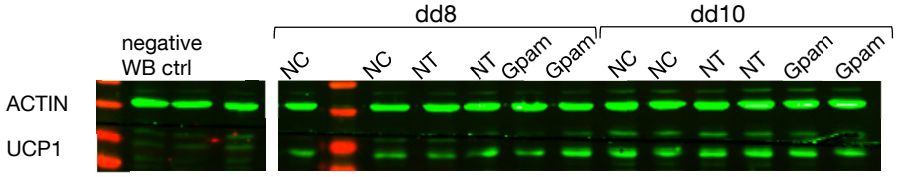

Figure 32: Protein expression of Ucp1 in siRNA transfected brite adipocytes on differention day 8 and 10 (dd8, dd10). On dd5 of differentiation, cells received only transfection mix (negative control, NC) or transfection mix with non-targeting siRNA (non-targeting control, NT) or siRNA targeting Gpam.

In summary, these results show that knockdown of Gpam did not impair thermogenic function of brite adipocytes. However, it increased Ucp1 mRNA levels. Since this effect was not present on the protein level, UCP1 activity was not altered.

3.2 Functional phenotyping of brown adipocytes

Brite adipocytes that express UCP1 in distinct amounts differ in their UCP1 mediated oxygen consumption and thereby also in their thermogenic capacity (3.1.3). However, other functional parameters such as glucose uptake, lipolytic capacity or lactate release are not affected by UCP1 expression. Brown adipocytes express UCP1 in higher amounts than brite adipocytes and a lack of UCP1 in these cells might have a larger impact on a functional phenotype than in brite cells. Although, this hypothesis is not true for glucose uptake, since uptake of glucose also in brown adipocytes was completely independent of presence or activity of UCP1 (3.1.5), other functional parameters such as lipolysis and lactate release as well as oxygen consumption and proton production in brown adipocytes were examined. From measured and deduced parameters a model of metabolic fluxes was created that describes and predicts how an adrenergic stimulus changes metabolic reactions in a brown fat cell.

3.2.1 Release of lipolytic products is diminished by UCP1 activity

FFA represent the primary fuel substrate for thermogenesis. An adequate lipolytic capacity is a perquisite for fueling and activation of UCP1. The lipolytic products FFA and glycerol were measured under basal and isoproterenol (0.5 µM) stimulated conditions. Cells were pretreated with or without 5 µM oligomycin (Figure 33). Under basal conditions, medium of 129SV/S1 UCP $^{+/+}$ and UCP1$^{-/-}$ cultures contained similar amounts of FFA and glycerol after one hour, indicating a comparable basal lipolytic activity. Stimulation of lipolysis by isoproterenol significantly increased the release of FFA and glycerol both in 129SV/S1 UCP1$^{+/+}$ and UCP1$^{-/-}$ cells ($p<0.001$). Interestingly, there was a statistically significant interaction between genotype and treatment ($p<0,001$). Adipocyte cultures from 129SV/S1 UCP1$^{-/-}$ mice released 1.3-fold more FFA and 1.5-fold more glycerol than cultures from UCP1$^{+/+}$ mice when stimulated with isoproterenol. This discrepancy in the response to isoproterenol was even more pronounced, when cells were pretreated with oligomycin. In UCP1$^{-/-}$ cells pretreatment with oligomycin further elevated isoproterenol induced FFA release. In contrast, in UCP $^{+/+}$ cells, it caused a reduced FFA release leading to an almost 3-fold higher FFA concentration after isoproterenol in medium of UCP1$^{-/-}$ compared to medium of UCP1$^{+/+}$ cultures. Oligomycin had no effect on basal FFA or glycerol concentrations. Taken together, there is a negative correlation between UCP1 activity and isoproterenol induced release of FFA into the medium.

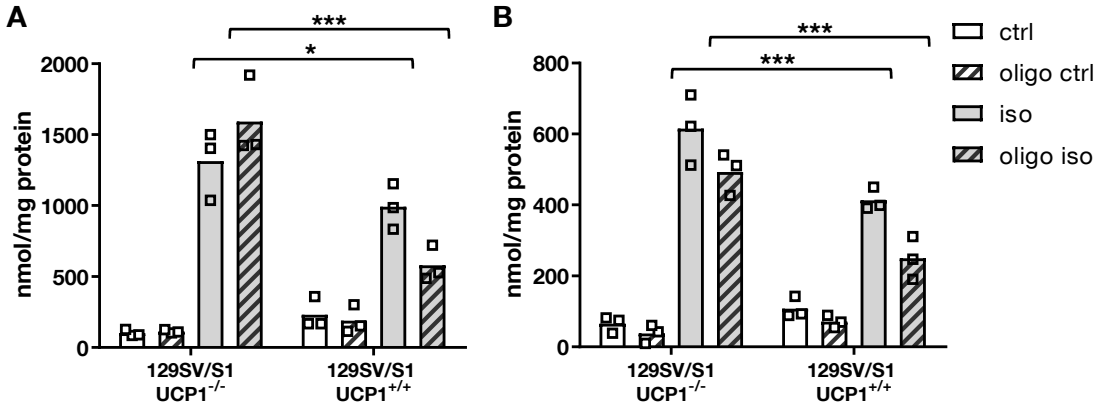

Figure 33: Lipolysis in brown adipocytes. Adipocytes were pretreated with or without 5 µM oligomycin (oligo) and treated with 0.5 µM isoproterenol (iso) and compared to controls (ctrl). Figure A shows measured FFA concentrations, figure B presents detected glycerol levels in medium. Dataset represents three independent experiments, analyzed by Two Way ANOVA and Tukey post-hoc-test (p<0.05, *** p<0.001).*

3.2.2 UCP1 ablation increases release of lactate

Glycolytic ATP generation gets important during mitochondrial uncoupling (Si et al., 2009). The release of lactate can serve as a glycolytic marker (Wu et al., 2007). Lactate release into the supernatant was determined under basal conditions and after stimulation with 0.5 µM isoproterenol with or without pretreatment with 5 µM oligomycin. Lactate release differed between genotypes independently from treatment. 129SV/S1 UCP1$^{-/-}$ cultures released 25 % more lactate than UCP1$^{+/+}$ cultures ($p<0.05$). Stimulation with isoproterenol did not cause any differences in lactate release whereas oligomycin treatment led to a significant increase of lactate under basal as well as under stimulated conditions ($p<0.05$) (Figure 34). In summary, in brown adipocytes, an ablation of UCP1 increased the release of lactate. Furthermore, adrenergic treatment did not affect lactate levels in the medium. In contrast, inhibition of mitochondrial ATP synthesis by oligomycin increased lactate release, indicating an elevated glycolytic ATP production.

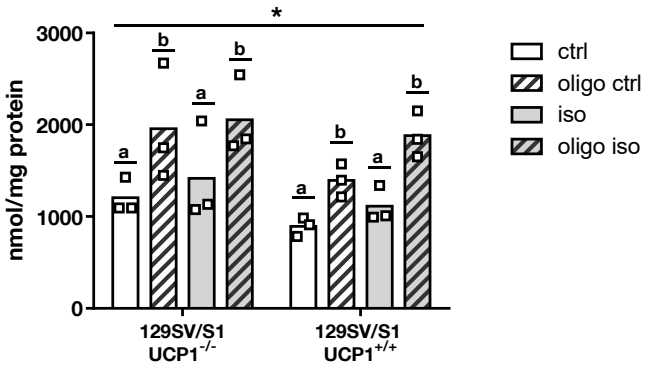

Figure 34: Lactate release in brown adipocytes. Cells were pretreated with or without 5 µM oligomycin (oligo) and treated with 0.5 µM isoproterenol (iso) and compared to controls (ctrl). Dataset represents three independent experiments and was analyzed by Two Way ANOVA and Tukey post-hoc-test (p<0.05). Printed characters indicate differences induced by oligomycin (oligo) treatment (p<0.05).*

3.2.3 Oxygen consumption of brown adipocytes

UCP1 mediated oxygen consumption reflects the thermogenic capacity of cells. Therefore, the oxygen consumption of primary brown adipocytes derived from 129SV/S1 UCP1$^{+/+}$ mice after isoproterenol treatment is expected to be increased in contrast to the oxygen consumption of cells originating from iBAT of 129SV/S1 UCP1$^{-/-}$ mice. To prove that, the established protocol for measuring UCP1 mediated respiration (3.1.3, 3.1.9), was used with slight modifications (Figure 35). First, basal respiration was measured. Then oligomycin was added to half of the cells in order to detect basal leak respiration. UCP1 mediated uncoupled respiration was induced by isoproterenol (0.5 µM) injection. Next FCCP was added followed by antimycin A to reveal non-mitochondrial oxygen consumption. Respiration data under isoproterenol from independent experiments were expressed as a percentage of the respective OCR under basal conditions. Also, the fold change of isoproterenol induced oxygen consumption over basal leak was calculated (Figure 36).

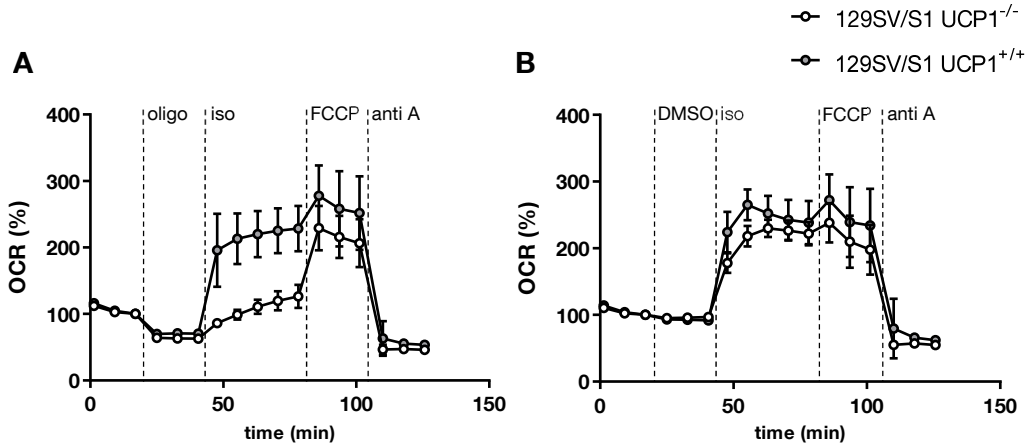

Figure 35: Representative time course of oxygen consumption rate (OCR) of brown adipocytes. First, basal respiration was detected. Then half of the cells received oligomycin (oligo), to measure basal leak respiration (A). The other half of the cells received DMSO (B). UCP1 mediated uncoupled respiration was induced by isoproterenol (iso, 0.5 µM) injection. Next FCCP, a chemical uncoupler that allows assessment of maximal respiratory capacity, was added. Finally, antimycin A (anti A) was injected to block complex 3 of the electron transport chain, leaving only non-mitochondrial OCR to be measured. Medium contained 2 % BSA. Data of one measurement with 7-9 wells per group. Dots represent mean values ± SD.

The established protocol for measuring UCP1 mediated oxygen consumption in cultured adipocytes includes oligomycin injection followed by a subsequent injection of isoproterenol in the presence of 2 % BSA (Li et al., 2014b). As expected, using this protocol, a marked increase in oxygen consumption can be found in cultures from 129SV/S1 UCP1$^{+/+}$ mice, whereas induction of respiration by isoproterenol was impaired in cells from UCP1$^{-/-}$ mice (Figure 35A, Figure36A). The fold increase over basal leak is

more than 2-fold higher in 129SV/S1 UCP1$^{+/+}$ cells compared to UCP1$^{-/-}$ cells ($p<0.001$) (Figure 36B). Surprisingly, when ATP synthase is not inhibited by oligomycin, UCP1$^{-/-}$ cells show a similar OCR under isoproterenol as UCP1$^{+/+}$ cells (Figure 35B, Figure 36A). This observation can be also made in the presence of 3 or 4 % BSA (Figure 36C, Figure 36D), suggesting that the isoproterenol induced OCR in UCP1$^{-/-}$ is not caused by unspecific uncoupling via FFA, a phenomenon which can be observed when BSA concentrations are too low to scavenge FFA.

Overall, these results indicate that in UCP1$^{-/-}$ cells adrenergic stimulation activated a mechanism that consumes large amounts of ATP and that is therefore absent when ATP production is inhibited by oligomycin. Adrenergically increased OCRs could be explained by high oxidative phosphorylation activity, fueling the ATP need of this mechanism in UCP1$^{-/-}$ cells.

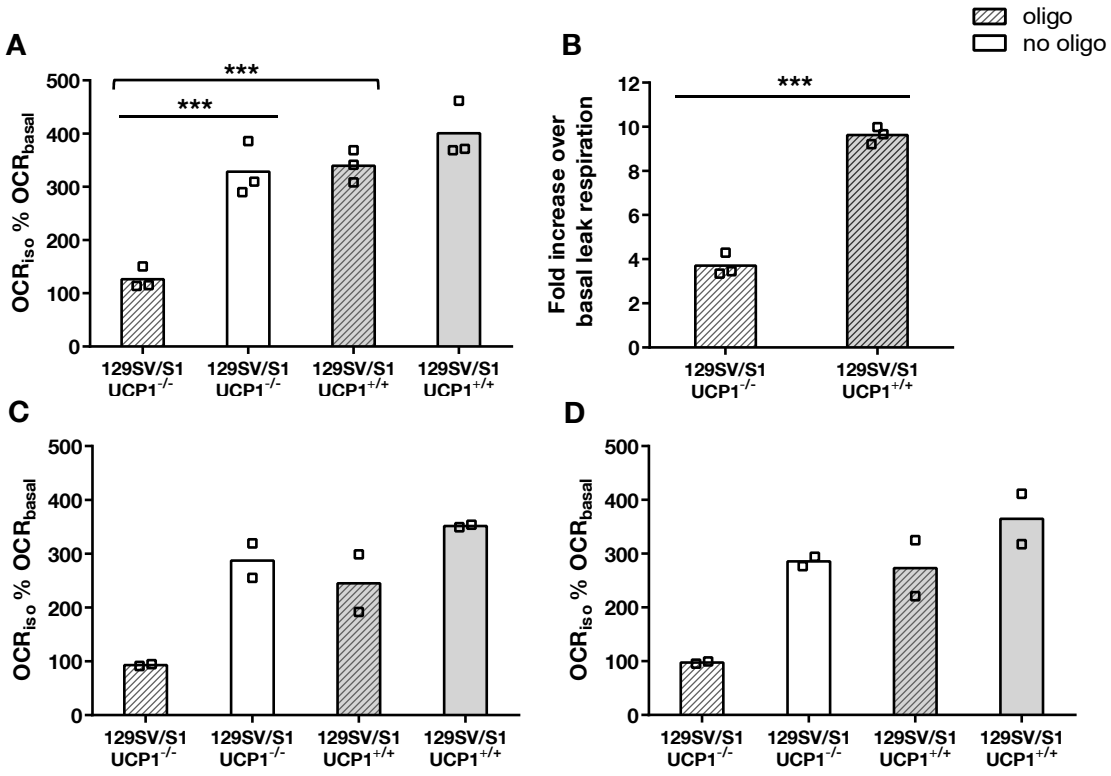

*Figure 36: Oxygen consumption of brown adipocytes. Medium contained either 2 (A, B), 3 (C) or 4 % BSA (D). Graphs represent maximal OCR values under isoproterenol (iso) treatment expressed as a percentage of OCR values under basal conditions (A, C, D) or the fold increase of iso induced OCR over basal leak OCR, were coupled respiration is inhibited through oligomycin (oligo) (B). Bars in A and B represent mean value of 3 independent experiments. Data of A and B were analyzed by Two Way ANOVA and Tukey post-hoc-test or t-test, respectively (*** $p<0.001$).*

3.2.4 *Transcriptome analysis reveals that UCP1 ablation leads to an induction of genes involved in calcium homeostasis*

Adrenergic stimulation activated an ATP consuming mechanism in brown adipocytes derived from UCP1$^{-/-}$ mice. This mechanism can represent an alternative UCP1 independent thermogenic pathway in brown fat. To identify this pathway, NGS based transcriptome analysis of iBAT from C57BL/6J UCP1$^{+/+}$ and UCP1$^{-/-}$ as well as of *in vitro* differentiated brown adipocytes from 129SVS1 UCP1$^{+/+}$ and UCP1$^{-/-}$ mice were performed. In a first step, the expression of brown fat marker genes was checked to clarify if iBAT and brown adipocytes from 129SVS1 UCP$^{-/-}$ mice still express a BAT signature. Brown adipocyte selective markers Cox7a1, Cidea, Eva-1 homolog a (Eva1a) and zinc finger protein of the cerebellum 1 (Zic1) as well as the differentiation marker Fabp4 were not differentially expressed between UCP$^{-/-}$ and UCP1$^{+/+}$ samples neither in tissue nor on the cell culture level. However, iBAT of C57BL/6J UCP1$^{+/+}$ mice significantly expressed more Prdm16 than iBAT of C57BL/6J UCP1$^{-/-}$ mice ($p<0.001$). This difference was not observed between the genotypes of *in vitro* differentiated brown adipocyte cultures (Figure 37).

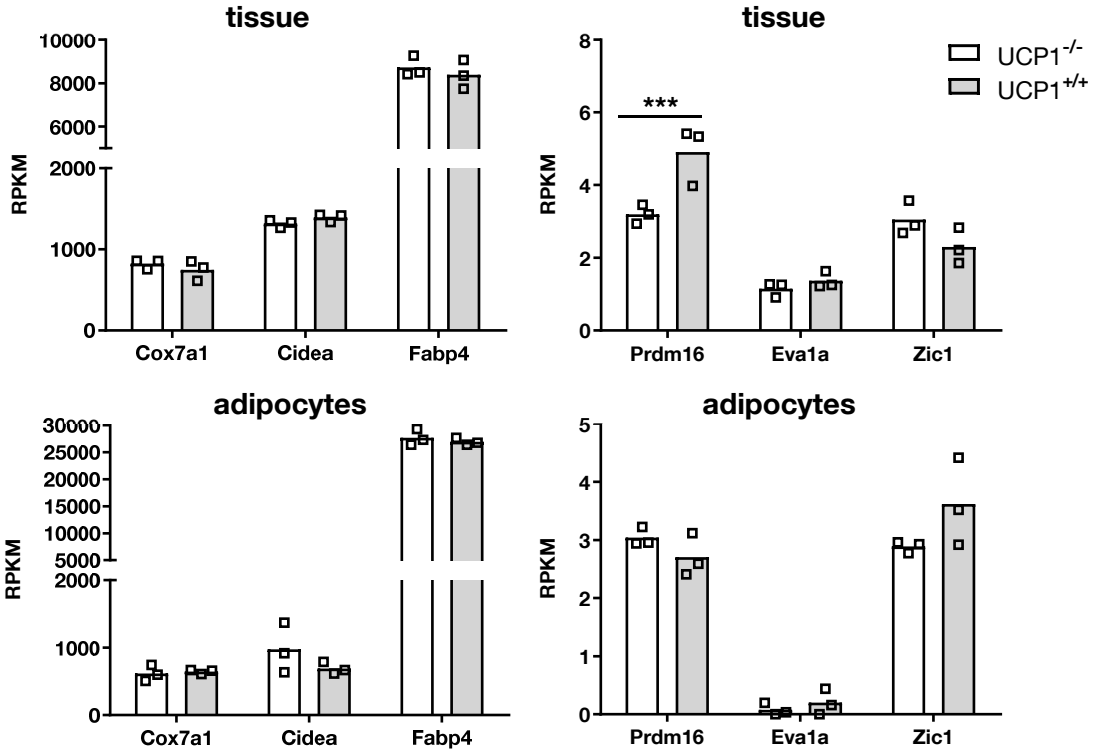

*Figure 37: Expression of BAT marker genes. Cox7a1, Cidea. Prdm16, Eva1a and Zic1 were used as brown marker genes, whereas Fabp4 was used as differentiation marker. Bars represent mean of 3 independent biological samples. RNA expression analysis was performed with DESeq algorithm of the genomatix genome analyzer with a p-value threshold of 0.05 corrected for multiple testing (*** p<0.001).*

Differential RNA expression analysis (DESeq algorithm, Genome Analyzer, Genomatix, Munich, Germany) was performed applying a log2 fold change of > 0.5 (upregulation) or<- 0.5 (downregulation) with a p-value threshold of 0.05 corrected for multiple testing. This analysis revealed that 832 genes are differentially expressed between iBAT of C57BL/6J UCP1$^{-/-}$ and UCP1$^{+/+}$ mice. From these genes, 642 genes were upregulated and 190 were downregulated in tissue of UCP$^{-/-}$ compared to UCP1$^{+/+}$ mice (Figure 38).

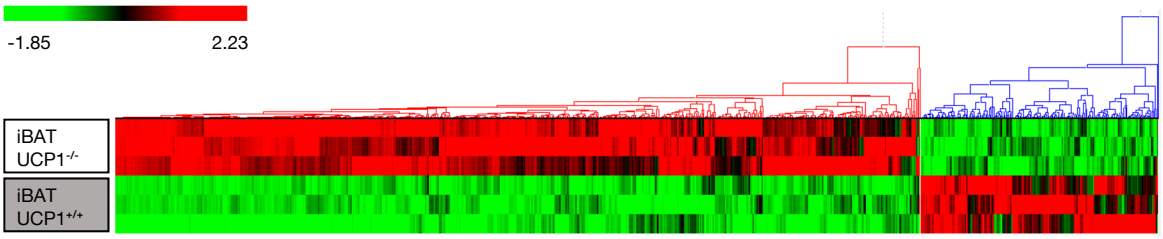

Figure 38: Hierarchical clustering following transcriptome analysis of iBAT of C57BL/6J UCP1$^{+/+}$ and UCP1$^{-/-}$ mice. 832 genes were used for clustering analysis. Three different biological samples per genotype were included. Similarity measures were based on Pearson Correlation Coefficient. Clusters correspond to a minimum similarity value of 0.5.

It has been hypothesized that futile cycles also known as substrate or metabolic cycles contribute to thermogenesis. Futile cycles result from the coupling of opposing reactions such as lipogenesis and lipolysis, glycolysis and gluconeogenesis or active import and export of substances. These reactions dissipate ATP, leading to ADP generation and consequently to stimulation of oxidative phosphorylation and therefore to increased oxygen consumption (Cannon and Nedergaard, 2004; Silva, 2006). In order to identify futile cycles which could explain the adrenergically stimulated, ATP dependent oxygen consumption of UCP$^{-/-}$ cells a pathway and network analysis was conducted (Pathway System tool, Genomatix, Munich, Germany). This analysis showed that genes of several pathways linked to calcium transport and signaling were differentially expressed between genotypes (Table 7). The majority of pathways linked to calcium transport were significantly upregulated in iBAT of C57BL/6J UCP1$^{-/-}$ compared to UCP1$^{+/+}$ mice.

Table 7: Calcium linked pathways associated with genotype dependent expressed genes of iBAT of C57BL/6J UCP1$^{-/-}$ and UCP1$^{+/+}$ mice. Genes which were differentially expressed with a log2 fold change > 0.5 (upregulation) or<-0.5 (downregulation) were subjected to a pathway analysis. Listed are calcium related pathways for which the number of differentially expressed genes between genotypes exceeded the statistically expected number.

Pathway	P-value	Observed genes (#)	Total genes (#)
ryanodine receptor	9.27E-07	13	48
ryanodine sensitive calcium channel activity	3.08E-03	2	3
calmodulin binding	7.03E-08	17	148
calcium tranmembrane transporter activity	2.30E-04	12	109
calcium channel regulator activity	4.79E-04	5	21
calcium release channel activity	7.73E-03	3	13
calcium channel inhibitor activity	1.45E-02	2	8
high voltage calcium channel activity	3.28E-02	2	9
calcium ion transport	1.31E-10	33	280
regulation of calcium ion transmembrane transporter activty	7.34E-06	8	33
regulation of calcium ion transport into cytosol	1.40E-05	10	58

Further analysis revealed which genes were regulated within these pathways. In total 51 genes were found to be significantly differentially expressed between iBAT of C57BL/6J UCP1$^{-/-}$ and UCP1$^{+/+}$ mice (Table 8). From the given log2 fold change of tissue samples it can be observed that from 51 genes 49 genes a significantly upregulated in tissue of C57BL/6J UCP1$^{-/-}$ mice. Although these genes are not significantly differentially expressed between brown UCP1$^{-/-}$ and UCP1$^{+/+}$ cultures, in most cases the log2 fold change of brown adipocytes has the same tendency as the log2 fold change between iBAT UCP1$^{-/-}$ and UCP1$^{+/+}$ samples (Table 8).

Table 8: Differentially expressed genes associated with calcium pathways. Listed are calcium linked genes which were found to be significantly differential expressed between iBAT of C57BL/6J UCP1$^{-/-}$ and UCP1$^{+/+}$ mice. Besides the p-value and log2 fold change (FC) of tissue also the log2 fold change between UCP1$^{-/-}$ and UCP1$^{+/+}$ brown adipocyte cultures are shown.

Symbol	Name	P-value tissue	Log2 FC tissue	Log2 FC adipocytes
Mylk2	myosin light chain kinase 2, skeletal/cardiac muscle	1.03E-46	3.65	1.55
Ryr2	ryanodine receptor 2	6.54E-23	3.28	0.24
Dhrs7c	dehydrogenase/reductase sdr family member 7c	6.60E-10	2.72	
Jsrp1	junctional sarcoplasmic reticulum protein 1	8.61E-17	2.63	-0.26
Cacna1s	voltage-dependent l-type calcium channel subunit alpha-1s	7.17E-15	2.63	1.51
Ryr1	ryanodine receptor 1	2.08E-22	2.54	3.17
Cacng1	voltage-dependent calcium channel gamma-1 subunit	7.56E-06	2.44	0.76
Cacng6	voltage-dependent calcium channel gamma-6 subunit	1.44E-14	2.43	-0.25
Camk2a	calcium/calmodulin-dependent protein kinase type-6-subunit alpha	4.72E-18	2.41	-1.98
Cav3	caveolin-3	2.11E-05	2.36	2.48
Myh1	myosin-1	5.40E-09	2.22	2.16

Table 8 continued

Jph2	junctophilin-2	1.33E-29	2.22	-0.64
Casr	extracellular calcium-sensing receptor	2.42E-04	2.20	
Pvalb	parvalbumin alpha	3.78E-04	2.19	0.19
Casq1	calsequestrin-1	1.30E-04	2.19	-0.40
Crhr2	corticotropin-releasing factor receptor 2	2.47E-04	2.17	
Atp2a1	sarcoplasmic/endoplasmic reticulum calcium ATPase 1	2.97E-04	2.12	0.84
Trdn	triadin	5.17E-04	2.10	2.12
Ttn	titin	9.04E-10	2.07	1.92
Cacna2d1	voltage-dependent calcium channel subunit alpha-2/delta-1	1.99E-30	2.00	-0.21
Myh4	myosin-4	2.29E-03	2.00	2.19
Hrc	sarcoplasmic reticulum histidine-rich calcium-binding protein	8.47E-04	1.96	0.74
Smtnl1	smoothelin-like protein 1	4.38E-03	1.94	
Ramp1	receptor activity-modifying protein 1	7.95E-07	1.93	-0.01
Slc8a3	sodium/calcium exchanger 3	2.35E-04	1.93	-0.51
Tmem38a	trimeric intracellular cation channel type a	4.22E-23	1.87	-0.23
Myh7	myosin-6-related	2.20E-03	1.87	
Capn3	calpain-3	5.22E-07	1.74	-0.02
Nrxn2	neurexin-2	1.84E-02	1.72	1.53
Phkg1	phosphorylase b kinase gamma catalytic chain, skeletal muscle/heart isoform	5.97E-11	1.63	-0.42
Nos1	nitric oxide synthase, brain	6.40E-04	1.62	-0.17
Asph	aspartyl/asparaginyl beta-hydroxylase	3.46E-09	1.53	-0.14
Obscn	obscurin	1.15E-07	1.49	1.21
Cacnb1	voltage-dependent l-type calcium channel subunit beta-1	1.06E-06	1.45	-0.23
Akap6	a-kinase anchor protein 6	4.15E-03	1.26	-0.06
Cth	cystathionine gamma-lyase	2.22E-04	1.17	0.06
Prkcb	protein kinase c beta type	2.69E-02	1.07	1.85
Coro1a	coronin-1a	2.98E-02	0.88	0.84
F2r	proteinase-activated receptor 1	3.52E-03	0.82	-0.32
Dapk1	death-associated protein kinase 1	5.02E-03	0.68	0.11
Dmd	dystrophin	1.05E-03	0.64	0.18
Atp2a3	sarcoplasmic/endoplasmic reticulum calcium ATPase 3	2.92E-02	0.59	0.73
Pacsin3	protein kinase c and casein kinase substrate in neurons protein 3	1.25E-02	0.59	-0.38
Phka1	phosphorylase b kinase regulatory subunit alpha, skeletal muscle isoform	1.57E-04	0.57	0.15
Srl	sarcalumenin	1.34E-04	0.56	-0.02
Ero1l	ero1-like protein alpha	1.02E-02	0.52	-0.53
Slc8b1	sodium/potassium/calcium exchanger 6, mitochondrial	4.02E-02	0.52	0.21
Slc30a1	zinc transporter 1	1.41E-02	-0.52	-0.06
Pde4d	camp-specific 3',5'-cyclic phosphodiesterase 4d	2.81E-02	-0.54	0.20
Myo5b	unconventional myosin-vb	8.66E-03	-0.59	0.25
Pik3r1	phosphatidylinositol 3-kinase regulatory subunit alpha	1.10E-04	-0.72	0.18

Taken together the gene expression data indicate that in iBAT and brown adipocytes of UCP1$^{-/-}$ mice an ATP consuming calcium transport cycle is active. We hypothesize that

calcium is cycling between ER and mitochondria. Calcium could be released from the ER by ryanodine receptor (RYR; gene: Ryr1, Ryr2) or inositoltriphoshate receptor (IP3R; gene: Itpr1-3). Then, calcium could enter mitochondria through voltage-dependent anion channel (VDAC) and mitochondrial calcium transporter (MCU; gene: Mcu). Via mitochondrial sodium calcium transporter (NCLX; gene: Slc8b1) and VDAC, calcium would be exported and again taken up by sarcoplasmic/endoplasmic reticulum calcium ATPase (SERCA; gene: Atp2a1-3) into the ER in an ATP dependent manner. The required ATP would be produced in the mitochondria and released by adenine nucleotide translocators (ANT; gene: Slc25a4,5). The expression of the genes involved in this pathway are shown in Figure 40 (brown adipose tissue) and Figure 41 (cultured brown adipocytes). In tissue, the genes Atp2a1 and Atp2a3 coding for SERCA as well as Ryr genes and Slc8b1 were significantly upregulated in UCP$^{-/-}$ samples. Interestingly, also several genes linked to regulation of ryanodine receptor function were overexpressed in iBAT of UCP$^{-/-}$ mice (Figure 39). This finding further supports and strengthens the hypothesis of calcium cycling in iBAT of UCP$^{-/-}$ mice.

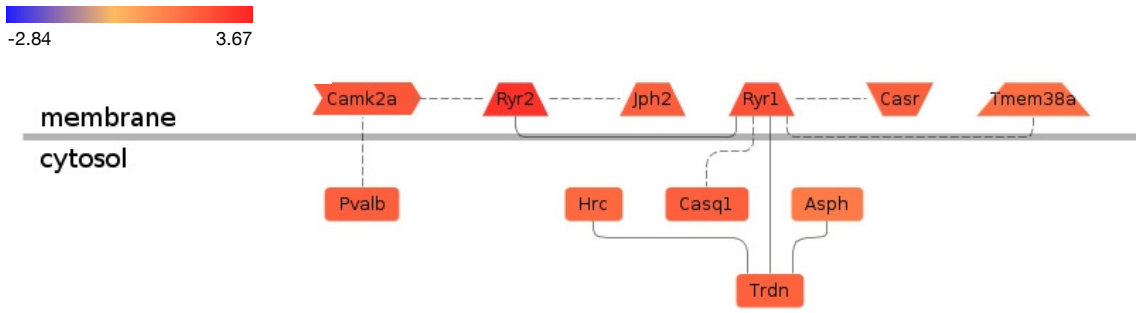

Figure 39: Differentially expressed genes linked to ryanodine receptor (Ryr1, 2) function. Listed genes were found to be significantly upregulated in iBAT of C57BL/6J UCP1$^{-/-}$ compared to UCP1$^{+/+}$ mice.

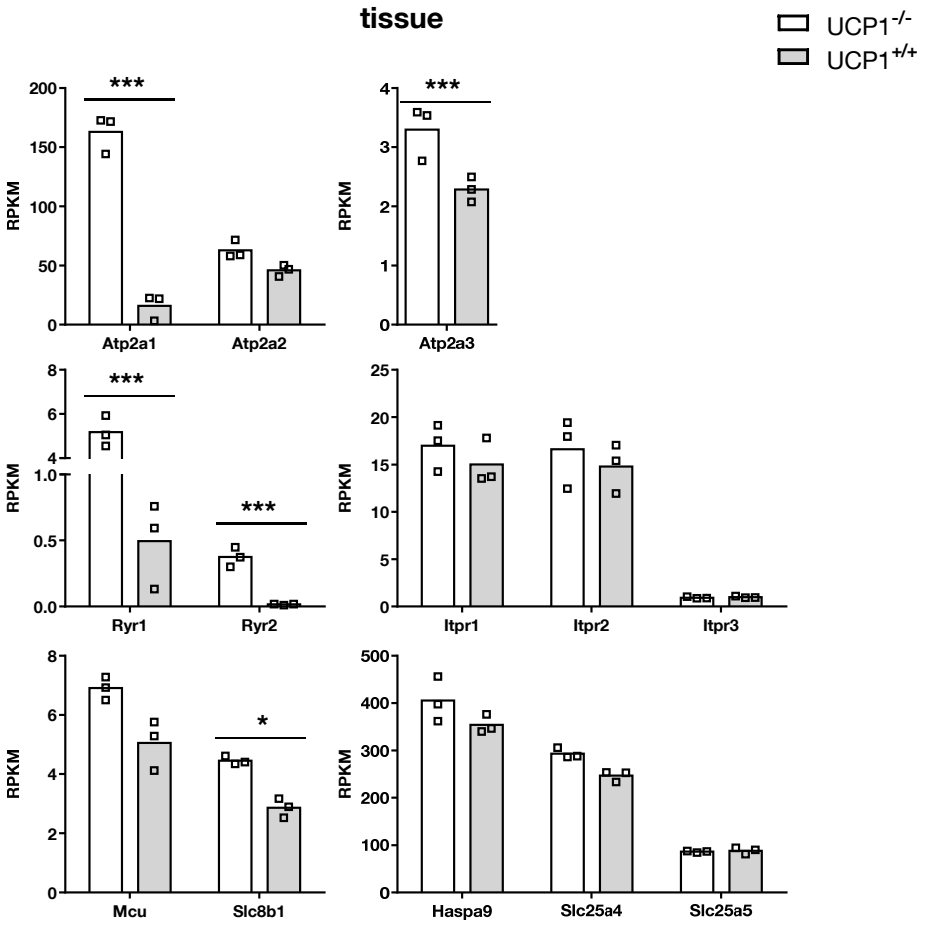

Figure 40: Expression of genes involved in calcium cycling in iBAT of C57BL/6J UCP1$^{-/-}$ and UCP1$^{+/+}$ mice. RNA expression analysis was performed with DESeq algorithm of the genomatix genome analyzer) with a p-value threshold of 0.05 corrected for multiple testing (p<0.05, *** p<0.001).*

In contrast to tissue samples, no significant differences between the expression of calcium cycling related genes of UCP1$^{-/-}$ and UCP1$^{+/+}$ adipocyte cultures were evident (Figure 41). A possible explanation for this might be that tissue samples were acquired from RT acclimated mice. RT represents a mild cold challenge and an elevated sympathetic tone could be expected. Thus, mice hold under these conditions show a recruitment of thermogenic capacity. Contrary to tissue, RNA expression data from cells are derived in a basal, non-thermogenic state.

Besides calcium cycling, also other futile cycles such as creatine-dependent substrate, FA/TAG, or FA oxidation/FA synthesis cycling could contribute to isoproterenol induced ATP consuming oxygen consumption observed in UCP$^{-/-}$ cultures. Thus, transcript levels of putative genes involved in other futile cycles were analysed. In iBAT mitochondrial only creatine kinase Ckmt2 and muscel type creatine kinase Ckm as well as carnitine O-

palmitoyltransferase 1a (Cpt1a), muscle type ATP-dependent 6-phosphofructokinase, Pfkm as well as Na/K-ATPase Atp1b1were significantly upregulated in iBAT of UCP1$^{-/-}$ mice compared to iBAT derived from UCP1$^{+/+}$ mice (Table 9).

Table 9: Differentially expressed genes associated with other possible futile cycles. Listed are genes which were found to be significantly differential expressed between iBAT of C57BL/6J UCP1$^{-/-}$ and UCP1$^{+/+}$ mice. Besides the p-value and log2 fold change (FC) of tissue also the log2 fold change between UCP1$^{-/-}$ and UCP1$^{+/+}$ brown adipocyte cultures are shown.

Symbol	Name	P-value tissue	Log2 FC tissue	Log2 FC adipocytes
Ckmt2	creatine kinase s-type, mitochondrial	0.00	2.03	0.08
Ckm	creatine kinase muscle type	0.00	2.17	0.35
Cpt1a	carnitine o-palmitoyltransferase 1, liver isoform	0.01	0.51	-0.06
Pfkm	ATP-dependent 6-phosphofructokinase, muscle type	0.00	0.60	-0.01
Atp1b1	sodium/potassium-transporting atpase subunit beta-1	0.01	0.56	0.06

In summary, although contribution of other futile cycles cannot be excluded, transcriptome data showed strongest evidence for futile calcium cycling between ER and mitochondria.

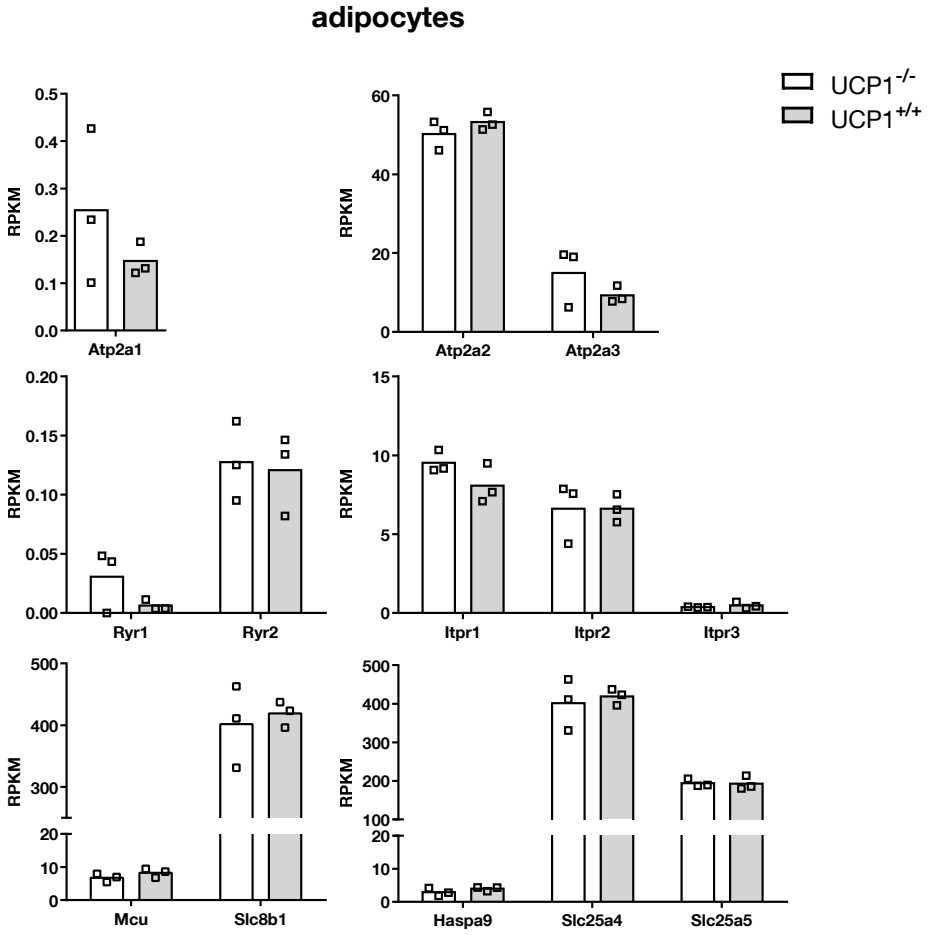

Figure 41: Expression of genes involved in calcium cycling in brown adipocytes from 129SV/S1 UCP1$^{+/+}$ and UCP1$^{-/-}$ mice.

3.2.5 Identification of extracellular acidification mechanisms

Extracellular acidification rate (ECAR) and proton production rate (PPR) can be measured simultaneously with oxygen consumption in multiplate respirometry (XF Analyzer, Agilent Technologies, Santa Clara, USA). Although extracellular acidification provides valuable information that helps to understand the cellular metabolism of brown adipocytes, it has not been studied extensively in these cells. Therefore, we assessed ECAR and PPR together with OCR (Figure 42).

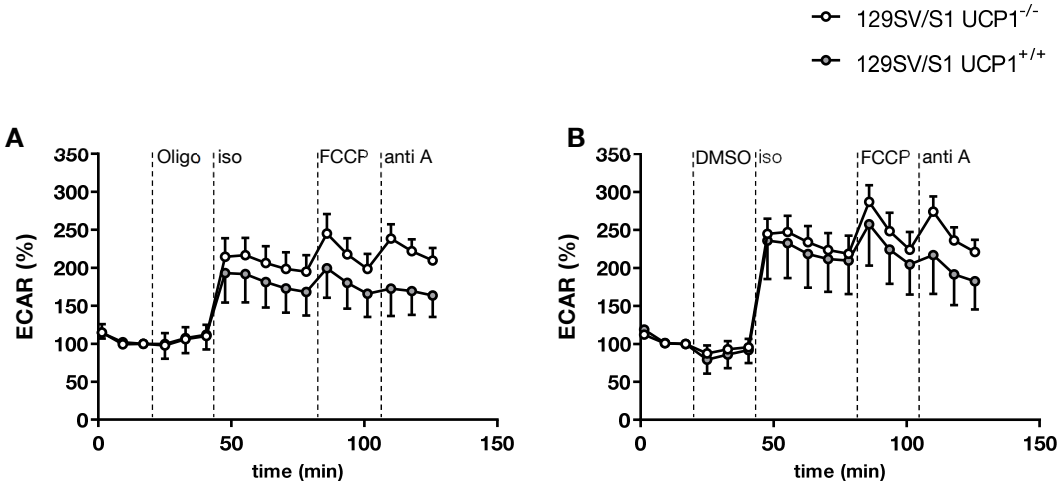

Figure 42: Representative time course of extracellular acidification rate (ECAR) of brown adipocytes. ECAR was measured simultaneously with OCR (chapter 3.2.3).

Injection of oligomycin led to a slight increase in acidification, which was not observed in control cells. Interestingly, isoproterenol incremented ECAR by 100-150 %. Thus, the question arose which acidifying compounds cause this increase in extracellular acidification. Generally, glycolytic produced lactic acid is considered as the major source of medium acidifying protons (Wu et al., 2007) and extracellular acidification rate (ECAR) is commonly used as a direct and quantitative measure of glycolytic rate (Mookerjee et al., 2015; Nadanaciva et al., 2012; Wu et al., 2007). However, besides lactic acid, also other acidification mechanisms such as release of CO_2 or FFA have to be taken into account. To address the question of the responsible acidifying mechanism in brown adipocytes, PPR was determined and expressed as nmol/min/cm^2. In aqueous solution, under physiological pH conditions it can be expected, that lactatic acid (pKa = 3.86) or FFA (pKa ≈ 4.8-5) dissociate into their conjungated base and release stoichiometrically one proton. Therefore, the already measured lactate and FFA concentrations were expressed in nmol/min/cm^2. Furthermore, assuming a RQ of 0.7, the amount of

metabolically produced CO_2 was predicted from OCR data and expressed in the same way as PPR, lactate and FFA (Figure 43).

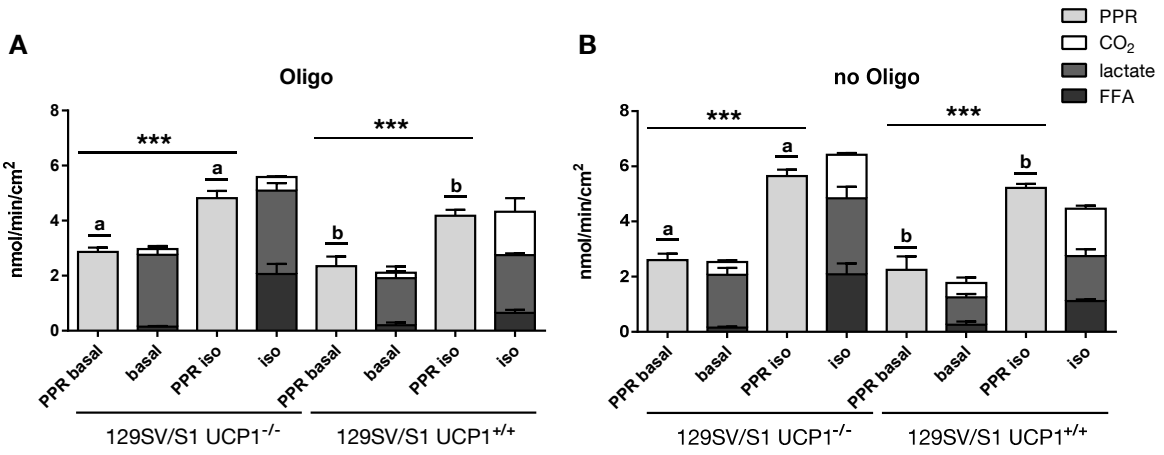

*Figure 43: Proton production rates (PPR) and protons derived from CO_2, free fatty acids (FFA) and lactic acid (stacked bars). Extracellular acidification caused by lactic acid and FFA release and subsequent dissociation was calculated from data shown in 3.2.1 and 3.2.2. Protons released from CO_2 were calculated from OCR data (3.2.3). Bars represent mean of three independent biological replicates ± SD. Data was analyzed by Two Way ANOVA and Tukey post-hoc-test (*** p<0.001). Printed characters indicate differences induced by genotype (p<0.001).*

Under basal as well as under isoproterenol treatment PPR can be explained by dissociation of released lactic acid, FFA and CO_2 (Figure 43). Under basal conditions, the majority of protons are indeed derived from lactic acid. As already observed in the ECAR data, an elevated PPR was detected when cells were stimulated with isoproterenol ($p<0.001$). This increase in extracellular protons is, however, not caused by an elevated lactate export, but nearly completely due to the release of FFA and CO_2. Treatment with oligomycin resulted in higher levels of lactate in all conditions, which was already visible in lactate data in 3.2.2 and could be explained by an upregulated anaerobic glycolytic ATP production, since oxidative phosphorylation is inhibited. The overall PPR under isoproterenol was significantly altered under oligomycin ($p<0.001$), which was partially caused by reduced basal CO_2 production in cells of both genotypes and predominantly the result of reduced CO_2 production of UCP1$^{-/-}$ cells in the isoproterenol stimulated state. Independently from treatment, PPR significantly differed by genotype ($p<0.001$). An overview of the percentage contribution of each acidifying mechanism is given in Table 10. In summary, these results clearly show that in thermogenically active adipocytes the major source of acidification was the release of FFA and metabolically produced CO_2, not lactate export.

Table 10: Contribution of different acidifying mechanisms to proton production rate (PPR). $PPR_{measured}$ represents the PPR assessed in the XF Flux analyzer. $PPR_{calculated}$ is the calculated sum of protons derived from FFA, lactate and CO_2.

Genotype	Treatment	$PPR_{measured}$ nmol/min/cm²	$PPR_{calculated}$ nmol/min/cm²	FFA %	Lactate %	CO_2 %
129SVS1 UCP1$^{-/-}$	basal	2.60	2.53	6.24	75.54	18.21
	iso	5.65	6.42	32.46	43.07	24.47
	oligo basal	2.86	2.97	4.85	88.07	7.08
	oligo iso	4.81	5.58	36.89	54.23	8.88
129SVS1 UCP1$^{+/+}$	basal	2.25	1.77	14.48	56.01	29.52
	iso	5.22	4.46	24.95	36.67	38.38
	oligo basal	2.34	2.10	9.25	81.66	9.09
	oligo iso	4.18	4.33	14.81	48.67	36.52

3.2.6 A metabolic flux model of thermogenically active brown adipocytes

From measured and deduced crucial parameters of chapter 3.2.1-3.2.2 and 3.2.5 a model of metabolic fluxes was created that describes and predicts how an adrenergic stimulus changes metabolic reactions in a brown fat cell. Relevant details are graphically displayed in the form of a comprehensive model of an active brown 129SV/S1 UCP1 $^{+/+}$ cell under isoproterenol stimulation (Figure 44). A complete overview of results of the model calculation with values of basal and adrenergic stimulated state in UCP1$^{+/+}$ and UCP1$^{-/-}$ cells is given in Table 11.

Adrenergic stimulation leads to an increase in intracellular cAMP levels that activate PKA and promote lipolysis. Thereby, around 0.13 µg TAG/min/cm² were hydrolyzed. In contrast, under basal conditions only around 0.03 µg TAG were degraded. Released FFA can activate and fuel thermogenesis. Assuming a RQ of 0.7, 0.12 nmol FFA/min/cm² were broken down in β-oxidation. These are three times more FFA than in the basal state. A major part of FFA, 1.11 nmol/min/cm², was released to the medium. Thus, 10 times more FFA are exported than oxidized. Released glycerol ranged around 0.47 nmol/min/cm². However, after conversion to glycerol-3-phosphate, glycerol could be reesterified with FFA, a metabolic fate that could not be calculated in this model. Glycolytically produced and released lactate concentrations were around 1.64 nmol/min/cm². Glucose uptake was about 0.06 nmol/min/cm². Overall, adrenergic stimulation increased O_2 consumption from 0.84 to 2.76 nmol/min/cm² and led to a CO_2 production of 1.71 nmol/min/cm². That represents a more than 3-fold increase of this metabolite. Taken together, this model provides an important insight into adrenergic mediated metabolic flux changes in brown fat cells.

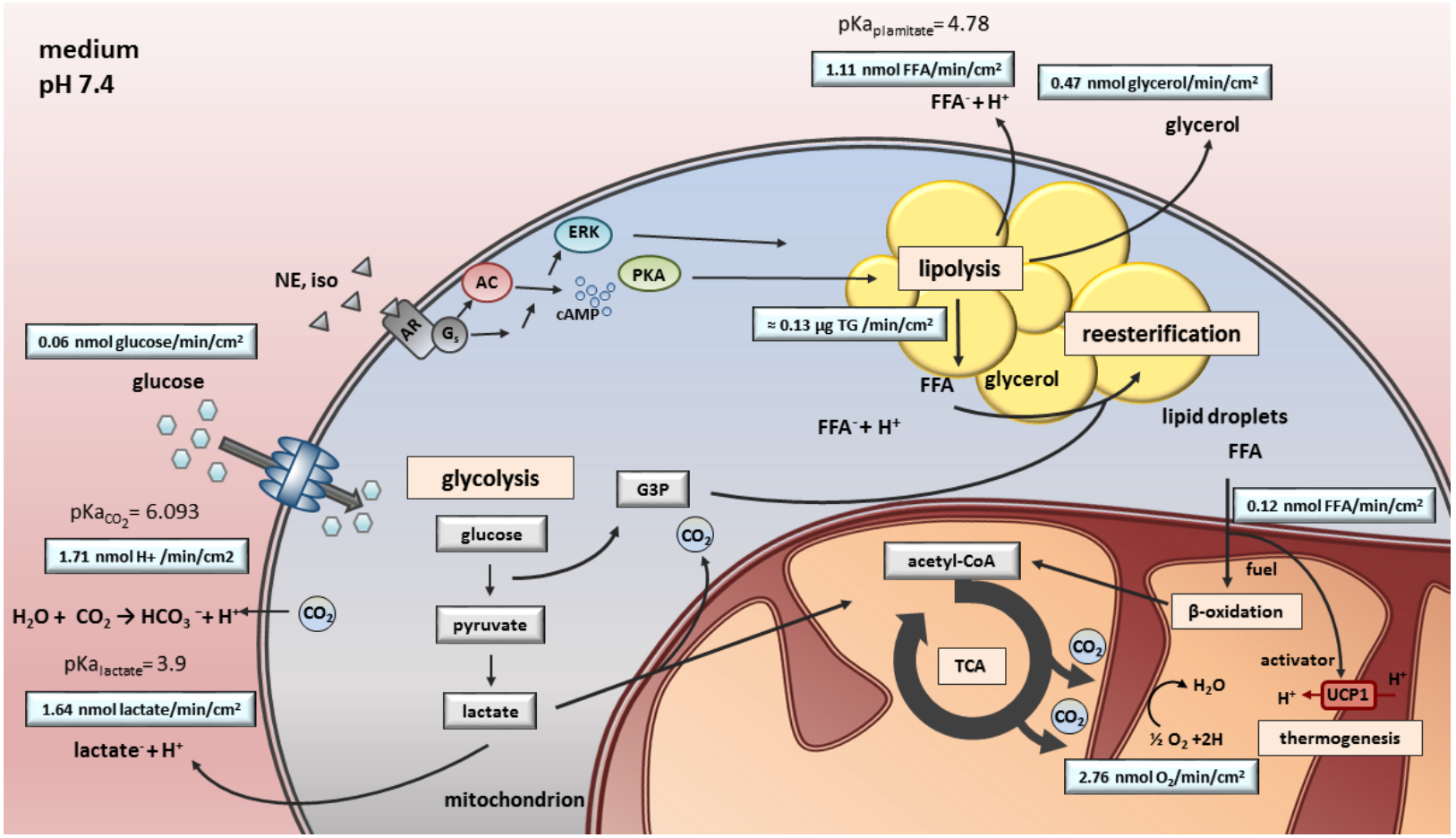

Figure 44: Model of metabolic flux of thermogenic active brown adipocytes. Adrenergic stimulation causes an increase in cyclic AMP (cAMP) which activates protein kinase A (PKA) and subsequently induces lipolysis. Released FFA can act as activator and fuel of thermogenesis. Furthermore, lipolytic products can be released or reesterified. Glycolytically produced pyruvate can either enter the tricarboxylic acid (TCA) cycle or is converted to lactate. Norepinephrine (NE), isoproterenol (iso), adrenergic receptor (AR), adenosine cyclase (AC).

Table 11: Model calculations. Calculations are based on three independent experiments. Shown are mean values ±SD. Glycerol, FFA and lactate levels were measured in the medium. OCR was measured in a XF96 Extracellular Flux Analyzer. CO2, oxidized FFA and hydrolyzed TAG were predicted from OCR data and are based on an RQ value of 0.7. Values used for Figure 44 are printed in bold.

	129SVS1 UCP1$^{-/-}$			129SVS1 UCP1$^{+/+}$		
basal						
glycerol nmol/min/cm^2	0.10	±	0.03	0.12	±	0.03
FFA nmol/min/cm^2	0.16	±	0.03	0.26	±	0.12
lactate nmol/min/cm^2	1.91	±	0.25	0.99	±	0.12
glucose nmol/min/cm^2	0.04	±	0.00	0.04	±	0.00
CO_2 nmol/min/cm^2 (RQ = 0.7)	0.46	±	0.07	0.52	±	0.20
O_2 nmol/min/cm^2	0.74	±	0.11	0.84	±	0.32
FFAox nmol/min/cm^2	0.03	±	0.00	0.04	±	0.01
TAG µg	0.02			0.03		
iso						
glycerol nmol/min/cm^2	0.97	±	0.15	**0.47**	±	0.09
FFA nmol/min/cm^2	2.08	±	0.40	**1.11**	±	0.06
lactate nmol/min/cm^2	2.76	±	0.41	**1.64**	±	0.24
glucose nmol/min/cm^2	0.06	±	0.01	**0.06**	±	0.01
CO_2 nmol/min/cm^2 (RQ = 0.7)	1.57	±	0.07	**1.71**	±	0.11
O_2 nmol/min/cm^2	2.53	±	0.11	**2.76**	±	0.18
FFAox nmol/min/cm^2	0.11	±	0.00	**0.12**	±	0.01
TAG µg	0.22			**0.13**		
oligo basal						
glycerol nmol/min/cm^2	0.05	±	0.04	0.07	±	0.02
FFA nmol/min/cm^2	0.14	±	0.03	0.19	±	0.10
lactate nmol/min/cm^2	2.61	±	0.32	1.71	±	0.42
CO_2 nmol/min/cm^2 (RQ = 0.7)	0.21	±	0.05	0.19	±	0.07
O_2 nmol/min/cm^2	0.34	±	0.08	0.31	±	0.11
FFAox nmol/min/cm^2	0.01	±	0.00	0.01	±	0.00
TAG µg	0.02			0.02		
oligo iso						
glycerol nmol/min/cm^2	0.64	±	0.11	0.27	±	0.06
FFA nmol/min/cm^2	2.06	±	0.36	0.64	±	0.12
lactate nmol/min/cm^2	3.03	±	0.27	2.11	±	0.06
CO_2 nmol/min/cm^2 (RQ = 0.7)	0.50	±	0.02	1.58	±	0.49
O_2 nmol/min/cm^2	0.80	±	0.04	2.54	±	0.78
FFAox nmol/min/cm^2	0.04	±	0.00	0.11	±	0.03
TAG µg	0.21			0.08		

4 Discussion

Recruitment and activation of brite and brown adipocytes represent an attractive treatment strategy against an increasing prevalence of obesity and associated comorbidities including type 2 diabetes. The functional and metabolic characteristics, especially of brite adipocytes are not fully understood. However, a good understanding of the basic biology of these target cells is fundamental to the development of successful therapeutic tools. *In vitro* differentiated primary cells are a useful model for studying basic biology under controlled conditions. The objective of this PhD thesis was to characterize brite and brown primary adipocytes in terms of their functional phenotype and metabolic properties.

4.1 Browning can be phenocopied *in vitro*

In mice, the extent of browning varies between inbred strains (Kozak and Koza, 2010; Lasar et al., 2013; Vitali et al., 2012; Xue et al., 2007). Mice of the 129SV strain have a higher browning propensity than mice of the C57BL/6J strain (Vitali et al., 2012). In this work, strain specific differences in brite adipogenesis observed *in vivo* could be phenocopied in primary cultures *in vitro* (Figure 6, Figure 7). It is of interest that the differential Ucp1 expression between brite cultures was independent of the brown adipocyte markers Cidea and Cox7a1 (Figure 6). These observations are in line with published data by Li et al. (2014a) who found that strain differences in brite adipogenesis are maintained in cultured primary adipocytes and are caused by intrinsic factors of progenitor cells. Taken together these molecular results confirm that the *in vitro* model of the present study is appropriate for studying the effect of differential UCP1 abundance and activity on the functional phenotype and metabolic properties of brite adipocytes.

4.2 Lipid droplet size is affected by UCP1 abundance

Cellular morphology may influence the functional phenotype of adipocyte cultures. Especially the differentiation capacity of cells should be similar between different adipocyte cultures if functional parameters are assessed and compared. Brite adipocyte cultures derived from 129SV/S6, C57BL/6J UCP1$^{+/+}$ and C57BL/6J UCP1$^{-/-}$ mice showed a similar degree of adipocyte differentiation and cellular lipid accumulation (Figure 8). However, cultures differed in the mean lipid droplet (LD) size and in the LD size distribution (Figure 10, Figure11). In C57BL/6J UCP1$^{-/-}$ adipocyte cultures, more small (<40 μm^2) and less big LDs (>230 μm^2) were abundant, whereas cultures from 129SV/S6 mice showed

the lowest and the highest percentage of these respective classes of LDs. Cultures from C57BL/6J UCP1$^{+/+}$ mice had an intermediate LD phenotype.

LDs are essential for storing and mobilizing intracellular fat. Within these dynamic cell organelles neutral lipids, such as triacylglycerides (TAG), steryl esters and retinyl esters are stored which can be mobilized for energy generation, lipid signaling or membrane component synthesis (Brasaemle, 2007; Walther and Farese, 2012). LDs are surrounded by a monolayer of phospholipids (PL) that protects other intracellular organelles from the cytotoxic effects of FA and contains structural proteins and enzymes (Girousse and Langin, 2012; Londos et al., 1999). They are thought to bud and to return ER in a cyclic manner, thereby existing in ER-associated and cytosolic form (Murphy and Vance, 1999; Zehmer et al., 2009). LD number and size can vary, depending on cell type as well as metabolic state and cellular needs (Martin et al., 2005; Walther and Farese, 2012). Furthermore, within a cell, LDs are heterogeneous in size and possibly also in their function (Zhang et al., 2016). Variation of number and size can arise from several processes like *de novo* formation or fusion and fission processes of LDs. Lipid content and thereby size of a LD can also decrease due to lipolytic processes and interaction with other organelles. Contrarily, LDs grow through additional neutral lipids deposition (Boschi et al., 2015).

In the present work, LD size and distribution was assessed in the basal state, without any stimulation. Abundance of large LDs correlated positively with UCP1 expression. A possible explanation for this is an induction of LD growth processes. The LD proteins CIDEA and CIDEC, promote LD enlargement in adipocytes (Puri et al., 2007; Wu et al., 2014) by facilitating LD fusion (Barneda et al., 2015; Gong et al., 2011; Jambunathan et al., 2011). Cidea expression is high in brown adipose tissue (BAT) (Hallberg et al., 2008; Zhou et al., 2003) and elevated upon browning. It was proposed that LD enlargement through LD-LD transference of fat is an important process during white adipose tissue (WAT) browning and is mediated via elevated Cidea and Cidec expression. (Barneda et al., 2013). However, in the present study, Cidea mRNA level was not significantly different between brite adipocyte cultures (Figure 6). Growth of lipid droplets is also regulated by CDP-diacylglycerol (DAG) synthases (CDSs). Knocking down either CDS1or CDS2 in 3T3L1 cells resulted in the formation of giant or supersized LDs (Qi et al., 2016). Interestingly, Cds2 shows a negative correlation with UCP1 expression on transcript level (Li, 2013). Distinct expression of Cds2 might explain the UCP1 dependent enlarged LD size.

4.3 Cultured brite and brown adipocytes are thermogenically active

Thermogenic UCP1, located in the IMM of brite and brown adipocytes, uncouples respiration from ATP synthesis and dissipates energy as heat to maintain core body temperature in a cold environment (Heaton et al., 1978; Lin and Klingenberg, 1982; Rafael and Heldt, 1976). During active non shivering thermogenesis (NST), BAT becomes the major oxygen consuming organ (Cannon and Nedergaard, 2004). In mice, BAT accounts for only 1 to 4 % of total body mass. However, activation of NST leads to a 3 to 4 fold increase in oxygen consumption (Meyer et al., 2010). The high oxidative capacity is facilitated by mitochondrial abundance and an enriched content of oxidative enzymes. Oxygen cannot be efficiently stored within the cell and must be continuously delivered by circulation (Li et al., 2014c; Orava et al., 2011). Hence, the oxygen consumption of cells can be used as an indirect measure of their thermogenic capacity.

In this study, oxygen consumption rates (OCRs) of brite and brown adipocytes were measured using a microplate-based respirometry in the presence of 2 % BSA. First, basal respiration was detected. Then basal leak respiration was measured by adding oligomycin. UCP1 mediated uncoupled respiration was determined after isoproterenol injection. Next FCCP mediated uncoupled respiration was assessed. Finally, antimycin A was injected to identify non-mitochondrial oxygen consumption.

Primary cultures from 129SV/S6 compared to cultures from C57BLB/6J mice showed a significantly higher UCP1 mediated oxygen consumption. Respiration rates under isoproterenol were higher in C57BLB/6J UCP1$^{+/+}$ than in C57BLB/6J UCP1$^{-/-}$ cultures. However, this difference was only significant when isoproterenol induced respiration was expressed as a percentage of basal respiration. Nevertheless, in each experiment oxygen consumption under isoproterenol was higher in UCP1$^{+/+}$ than in UCP1$^{-/-}$ cultures. A higher number of biological replicates may have led to statistical significance also when data is expressed as a percentage of the respective OCRs under FCCP or as fold change of isoproterenol induced OCR over basal leak (Figure 12). In accordance with published data of murine (Li et al., 2014a; Li et al., 2014b; Wu et al., 2012) and human (Barquissau et al., 2016) adipocytes, UCP1 in brite adipocytes was thermogenically active. The differences observed on the molecular level (Figure 6, Figure 7) were also present on the functional level (Figure 12). 129SV/S6 cultures showed the highest expression and activity of UCP1. These results are in agreement with those obtained by Li et al. (2014a), who observed that adipocytes from 129SV/S6 mice express more UCP1 mRNA and protein and show a

higher capacity for isoproterenol induced uncoupled respiration than adipocytes from C57BLB/6J mice.

In brown adipocytes cultures from 129SV/S1 UCP1$^{+/+}$ mice, a steep increase in isoproterenol induced respiration was present whereas induction of respiration by isoproterenol was impaired in cells from UCP1$^{-/-}$ mice (Figure 35A, Figure 36A). The fold increase over basal leak was much more elevated in 129SV/S1 UCP1$^{+/+}$ cells compared to UCP1$^{-/-}$ cells (Figure 36B). Surprisingly, when ATP synthase was not inhibited by oligomycin, UCP $^{-/-}$ cells showed a similar respiration rate under isoproterenol as UCP1$^{+/+}$ cells (Figure 35B, Figure 36A). Importantly, this phenomenon was also present in the presence of 3 or 4 % BSA, suggesting that the isoproterenol induced oxygen consumption in UCP1$^{-/-}$ is not caused by unspecific uncoupling via intracellular free fatty acids (FFA), a process which can be observed when BSA concentrations are too low to scavenge FFA (Li et al., 2014b). Instead, these results indicate an adrenergically induced ATP consuming mechanism in UCP1$^{-/-}$ cells that is impaired when oxidative ATP production is inhibited by oligomycin. Increased respiration rates could be explained by high oxidative phosphorylation activity, fueling the ATP need of this mechanism. This pathway could represent an alternative UCP1 independent NST mechanism in BAT of UCP$^{-/-}$ mice. This phenomenon could have been overlooked previously since, classically, NST in BAT is thought to be exclusively mediated via UCP1.

Although UCP$^{-/-}$ mice are sensitive to acute cold exposure (Enerbäck et al., 1997), when gradually adapted to cold, they are able to defend their body temperature (Golozoubova et al., 2001; Meyer et al., 2010; Shabalina et al., 2010; Ukropec et al., 2006a; Ukropec et al., 2006b). They can adapt to the cold, accompanied by increased oxygen consumption and substrate oxidation (Ukropec et al., 2006a). Thereby they exhibit almost 50 % of the UCP1$^{+/+}$ increase in maximal cold-induced heat production (Meyer et al., 2010). Thus, stepwise cold acclimated UCP1$^{-/-}$ mice recruit thermogenic mechanisms in the absence of UCP1. Such UCP1-independent mechanisms were proposed in WAT (Granneman et al., 2003; Ukropec et al., 2006a) and skeletal muscle (Bal et al., 2012).

In WAT of UCP1 $^{-/-}$ mice, UCP1 negative adipocytes with elevated oxidative capacity appear during cold exposure (Meyer et al., 2010). It was postulated that WAT contributes to energy expenditure and NST via a futile substrate cycling based on lipolytic release of FA and their reesterification into TAG as well as *de novo* FA synthesis (Flachs et al., 2017; Flachs et al., 2013). Another research group hypothesized that in brite adipocytes a creatine-dependent substrate cycling is active (Bertholet et al., 2017; Kazak et al., 2015).

Also, ATP consuming futile cycling of calcium between ER and cytosolic compartments driven by increased oxidative phosphorylation capacity was proposed as an alternative thermogenic pathway in iWAT (Ukropec et al., 2006a; Ukropec et al., 2006b) as well as in skeletal muscle of UCP1$^{-/-}$ mice (Bal et al., 2012; Rowland et al., 2015). All these alternative NST mechanisms were suggested in other tissues and not in BAT itself. However, the phenomenon observed in this study must be due to a brown adipocyte intrinsic mechanism.

NST may be contributed by futile cycles, resulting from coupling of opposing reactions such as lipogenesis and lipolysis, glycolysis and gluconeogenesis or active import and export of substances. Since these reactions are ATP dependent they lead to elevated ADP levels, stimulation of oxidative phosphorylation and consequently to increased oxygen consumption (Cannon and Nedergaard, 2004; Silva, 2006). A pathway and network analysis revealed that genes of several pathways linked to calcium transport were significantly upregulated in iBAT of C57BL/6J UCP1$^{-/-}$ compared to UCP1$^{+/+}$ mice. Due to elevated gene expression of the sarcoplasmic/endoplasmic reticulum calcium ATPase (SERCA) isoforms (Atp2a1, Atp2a3), ryanodine receptor (RYR) isoforms (Ryr1, Ryr2) and sodium calcium transporter NCLX (Slc8b1) together with several genes involved in RYR regulation in iBAT of UCP1$^{-/-}$ mice, it is possible that in these mice a futile calcium cycle is present in BAT which represents an alternative NST mechanism.

Isoproterenol treatment increases cytosolic calcium levels through the release of calcium from the ER in cultured rat brown adipocytes (Leaver and Pappone, 2002). We hypothesize that calcium is released from ER upon an adrenergic stimulus and then cycles between ER and mitochondria. In such a scenario, calcium, released from the ER by RYR or IP3R could enter mitochondria through voltage-dependent anion channel (VDAC) and mitochondrial calcium transporter (MCU). Via NCLX and VDAC calcium could be exported and could again be taken up by SERCA into the ER in an ATP dependent manner. The required ATP is produced in mitochondria and released via adenine nucleotide translocators (ANT) (Figure 45). Such a futile calcium cycle was described in extraocular muscle fiber derived heater cells of the blue marlin (Block and Franzini-Armstrong, 1988; Morrissette et al., 2003). SERCA, located in the ER membrane, translocates calcium ions across the membrane using the chemical energy derived from ATP hydrolysis. During this process part of the chemical energy is also converted into heat (de Meis, 1998; de Meis, 2002; Mitidieri and de Meis, 1999; Smith et al., 2002). SERCA is present in BAT of rats and

it was hypothesized that SERCA is a source of heat production contributing to the thermogenic function of BAT (de Meis, 2003).

Nevertheless, other futile cycles could also contribute to isoproterenol induced ATP dependent oxygen consumption, observed in UCP$^{-/-}$ cultures. Transcriptome data of putative genes involved in other futile cycles such as creatine-dependent substrate, FA/TAG, or FA oxidation/FA synthesis cycling were analyzed. The genes which were significantly upregulated in iBAT tissue of UCP$^{-/-}$ mice within such pathways were mitochondrial creatine kinase Ckmt2 and muscle type creatine kinase Ckm as well as Cpt1a and Pfkm. Pfkm encodes for a muscle type phosphofructokinase that catalyzes the phosphorylation of D-fructose 6-phosphate to fructose 1,6-bisphosphate by ATP in glycolysis (Newsholme et al., 1962). Cpt1a encodes for a carnitine O-palmitoyltransferase that catalyzes the transfer of the acyl group of LCFA-CoA conjugates onto carnitine, an essential step in mitochondrial uptake of LCFAs and β-oxidation in the mitochondrion (Lee et al., 2011). Both genes were comparably expressed in brown adipocytes of UCP1$^{-/-}$ and UCP1$^{+/+}$ mice. Ckmt2 was proposed to be involved in a creatine substrate cycle that also involves a Na/K-ATPase Atp1b1. However, expression of Ckmt2 was very low in brown adipocytes and similarly expressed in both genotypes. The latter is also true for Atp1b1.

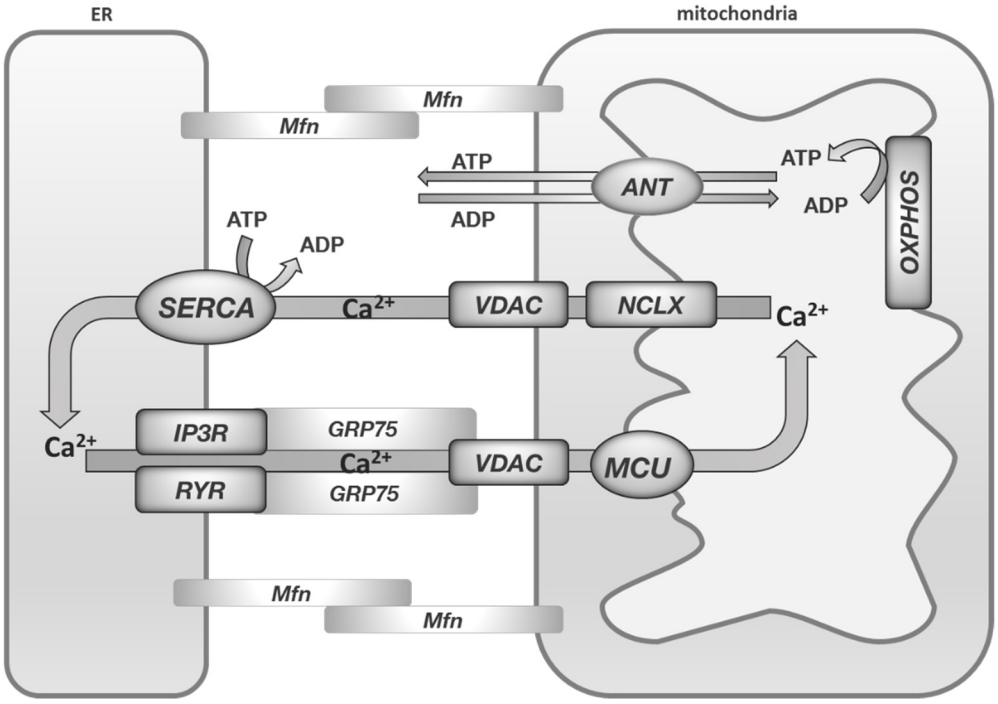

Figure 45: Model of calcium cycling between endoplasmatic reticulum (ER) and mitochondria. ER and mitochondria form contact sites via Mnf and Grp75 proteins. Calcium is released from the Er by ryanodine receptor (RYR) or inositoltriphoshate receptor (IP3R). Calcium enters mitochondria through voltage-dependent anion channel (VDAC) and mitochondrial calcium transporter (MCU). Via mitochondrial sodium calcium transporter (NCLX) and VDAC calcium is exported and can be taken up by SERCA into the ER in an ATP dependent manner. The required ATP is produced in the mitochondria and released by adenine nucleotide translocator (ANT).

Although the contribution of other futile cycles cannot be excluded, transcriptome data showed strongest evidence for futile calcium cycling between ER and mitochondria. Future work should include isolation of mature brown adipocytes from cold acclimated UCP1$^{+/+}$ and UCP1$^{-/-}$ mice. First, this should be done to clarify if differences in gene expression between genotypes in iBAT are also visible on cellular mRNA and protein level. Second, respiration measurements with these cells must be done to clarify if primary mature brown UCP1$^{-/-}$ adipocytes show an ATP dependent thermogenic oxygen consumption. Besides experiments with primary mature adipocytes, chronic isoproterenol treatment of *in vitro* differentiated brown UCP1$^{+/+}$ and UCP1$^{-/-}$ adipocytes has to be performed. Such experiments can elucidate if recruitment of thermogenic capacity through induction of genes involved in calcium cycling occurs *in vitro.* Modification of RYR or SERCA activity using inhibitors, such as dantrolene or thapsigargin, during respiration measurements would be of great interest, since such an approach can directly assess an involvement of these proteins in UCP1 independent NST. However, such modifications will always interfere with intercellular calcium signaling and experimental outcome might be hard to interpret.

4.4 Lipolytic product release is elevated upon UCP1 ablation in brown but not in brite adipocytes

Lipolysis represents the sequential hydrolysis of TAG stored in cell LDs and is catalyzed by ATGL, HSL and monoacylglycerol lipase (MGL) (Bolsoni-Lopes and Alonso-Vale, 2015). Thereby, ATGL and HSL are responsible for more than 90% of TAG hydrolysis in adipose tissue (Schweiger et al., 2006). Lipolysis is a highly regulated process and occurs under non-stimulated, basal conditions as well as after hormonal stimulation. Adrenaline and NE stimulate lipolysis through activation of β-adrenergic receptors (β-ARs) that activate adenylate cyclase (AC). The subsequent rise in cyclic AMP (cAMP) activates protein kinase A (PKA), which phosphorylates hormone sensitive lipase (HSL) and LD-coating protein perilipin as well as the adipose trigyceride lipase (ATGL) co-activator CGI-58 (comparative gene indentification 58) to stimulate lipolysis. On the other hand, catecholamines can also inhibit lipolysis via the activation of α2-AR that mediate AC inhibition and therefore cAMP production. Insulin signaling leads to phosphodiesterase 3B (PDE3B) activation that degrades cAMP and hence reduces PKA activation (Degerman et al., 1997). Furthermore, insulin-induced antilipolytic effects are mediated via lactate and its receptor GPR81 (Ahmed et al., 2010; Liu et al., 2009). ATGL is mainly located in the LD of adipocytes and is considered as the main enzyme responsible for TAG hydrolysis, especially under basal

conditions, since it has direct access to the LDs. Nevertheless, ATGL activity is significantly increased by CGI-58 binding (Ahmadian et al., 2010; Bezaire and Langin, 2009; Yamaguchi et al., 2004).In brite and brown adipocytes, adrenergic UCP1 activation is largely dependent on ATGL rather than HSL and mice with lower expression of ATGL develop severe hypothermia when exposed to cold (Haemmerle et al., 2011; Li et al., 2014b)

FFA are required for fueling and activation of UCP1. Full activity of UCP1 requires an adequate lipolytic rate. Moreover, differences observed in the LD size distribution of brite adipocyte cultures might influence their lipolytic capacities. To investigate the influence of UCP1 abundance and activity on lipolysis, the lipolytic activity was assessed under basal and isoproterenol stimulated conditions in brite and brown adipocyte cultures. The concentrations of the lipolytic products FFA and glycerol were measured in the incubation medium. In the case of brown adipocytes, cells were pretreated with or without oligomycin.

Brite and brown adipocytes released glycerol and FFA in quantitatively significant amounts under basal conditions and especially after treatment with isoproterenol (Figure 13, Figure 33). The lipolytic capacities of 129SV/S6, C57BLB/6J UCP1$^{+/+}$ and C57BLB/6J UCP1$^{-/-}$ cells were comparable and independent from UCP1 abundance or activity. Human hMADS cells, differentiated into brite adipocytes possess a higher lipolytic capacity together with enhanced FA oxidation and FA esterification (Barquissau et al., 2016). Similar to the present work, the brite phenotype was induced by PPAR agonist treatment. PPARγ and PPARα are important regulators of lipolysis. PPARγ activation with rosiglitazone stimulates basal and NE induced lipolysis by increasing the lipolytic potential, including increased ATGL and MGL gene expression in WAT (Festuccia et al., 2006). Palmitoleic acid treatment increases lipolysis *in vivo* and *in vitro* under basal conditions and in response to isoproterenol by increasing phosphorylated ATGL and HSL in adipocyte via PPARα in WAT (Bolsoni-Lopes et al., 2013). Similar effects PPARγ and PPARα agonists were observed in 3T3L1 adipocytes (Bolsoni-Lopes et al., 2013; Goto et al., 2011; Kershaw et al., 2007). Consequently, PPARγ and PPARα mediated elevated lipolytic capacity does not require UCP1. In the present work, lipolytic capacity was assessed in brite adipocytes which were differentiated in the presence of rosiglitazone. Thus, possible UCP1 mediated effects on lipolysis might have been blunted or overlaid by PPARγ agonist treatment. Rosiglitazone can also upregulate the lipolytic machinery of BAT by increasing expression of ATGL, CGI-58 and MGL (Festuccia et al., 2010).

The release of lipolytic products was not only independent from UCP1. The distinct lipid droplet size distribution observed in the basal state of brite adipocytes cultures (Figure 11) did also not cause differences in lipolytic activity. In general, a smaller LD size is assumed to be associated with an increased LD surface/volume ratio which facilitates the rapid lipid degradation and utilization for adaptive thermogenesis (Cinti, 2012). Adrenergic treatment and stimulation of lipolysis activates gradual fragmentation and dispersion of micro-lipid droplets (Brasaemle et al., 2004; Marcinkiewicz et al., 2006). FA can be quickly mobilized and transferred from LD to mitochondria (Rambold et al., 2015). Rapid relocalization of fatty acids to mitochondria is accomplished by direct transfer via contact sites (Welte, 2015; Zhang et al., 2016). Adrenergic induced LD fission processes may rapidly overcome the difference in basal lipid droplet size distribution that might be too small to affect lipolytic activity.

Brown adipocytes derived from 129SV/S1 UCP1$^{+/+}$ and UCP1$^{-/-}$ mice showed a similar glycerol and FFA release under basal conditions, indicating a comparable basal lipolytic activity. However, after isoproterenol treatment adipocyte cultures from 129SV/S1 UCP1$^{-/-}$ mice released significantly more glycerol and FFA than cultures from UCP1$^{+/+}$ mice. This discrepancy was even more pronounced, when cells were pretreated with oligomycin. Pretreatment with oligomycin further elevated isoproterenol induced FFA release in UCP1$^{-/-}$ cells, while it caused a reduced FFA release in UCP1$^{+/+}$ cells. Such an effect of oligomycin was not observed in basal FFA or glycerol concentrations. Thus, there is a negative correlation between UCP1 activity and isoproterenol induced release of FFA into the medium.

A lower release of FFA and glycerol can be explained by an alternative fate of these metabolites. FFA can be combusted in β-oxidation or reesterified with G3P to form TAG. They can be also used for synthesis of other FA and lipids. Glycerol either can serve as energy substrate or can be transformed into G3P, a process that requires GK. GK activity is strongly increased in BAT by cold adaptation (Bertin, 1976). Moreover, during cold exposure glyceroneogenesis is substantially activated in BAT, contributing to G3P generation, which is mostly used to reesterify FFA (Moura et al., 2005). On the one hand UCP1 activity increases substrate oxidation with FFA being the primary fuel for thermogenesis (Ma and Foster, 1986; Nedergaard and Lindberg, 1982; Nicholls and Locke, 1984). On the other hand, brown adipocytes must maintain adequate intracellular TAG stores for constant fuel supply for NST, as observed in cold acclimated rodents, which show a marked increase in BAT TAG (Himms-Hagen, 1965; Moura et al., 2005) an

FA synthesis (Trayhurn, 1979, 1981). Thus, lipid catabolism and anabolism might occur simultaneously upon UCP1 activation and may explain the reduced release of lipolytic products in UCP1 expressing cells under isoproterenol treatment.

4.5 Glucose uptake in brown and brite adipocytes is independent of UCP1

In brown and brite adipocytes, glucose can be used either as energy substrate or as carbon source. It can be utilized for fatty acid synthesis and, after transformation into G3P, it facilitates FA esterification and TAG synthesis (Himms-Hagen, 1965; Knight and Myant, 1970; Ma and Foster, 1986). In the uncoupled state, glucose serves as energy substrate to glycolytically produce cytosolic ATP. The resulting pyruvate can enter the citric acid cycle and serve as energy source (Cannon and Nedergaard, 1979). Although the estimated proportion of glucose as direct oxidative substrate of thermogenesis *in vivo* is rather low (2-12 %) (Ma and Foster, 1986), glucose uptake is elevated under cold exposure (Greco-Perotto et al., 1987; Shibata et al., 1989; Vallerand et al., 1990). In addition, functional BAT and brite fat can improve blood glucose clearance in mice (Stanford et al., 2013; Tharp et al., 2015). Glucose transport into brown adipocytes can be stimulated in two opposite metabolic states. During NST, glucose uptake is triggered by NE whereas in an anabolic state glucose uptake is stimulated by insulin (Cannon and Nedergaard, 2004).

In the present work, glucose uptake was investigated in brite and brown adipocyte with distinct UCP1 expression. The aim was to clarify if adrenergically stimulated glucose uptake is dependent on the presence of UCP1. Radiometric glucose uptake assays are commonly performed without normal D-glucose and with only trace amounts of 2-DG present in the medium. In brite and brown adipocytes, the predominant glucose transporters are GLUT1 and GLUT4 (Burant et al., 1991; Mossenbock et al., 2014; Nishimura et al., 1993; Shimizu et al., 1998). The K_m value of these transporters are in the millimolar range (Burant and Bell, 1992; Zhao and Keating, 2007). This value provides a measure of substrate concentration required for significant transport to occur. Paying attention to this kinetic information, in this study, a glucose uptake assay was established that is conducted in the presence of 5.55 mM D-glucose. To avoid unspecific uncoupling due to a rise in FFA after isoproterenol stimulation, which could lead to an unspecific uptake of glucose, FFA levels were controlled by adding 2 % BSA into the medium. The uptake was assessed under basal conditions and after stimulation with isoproterenol or insulin, or both in combination.

Isoproterenol treatment increased glucose uptake into brite and brown adipocytes. Adrenergically mediated glucose uptake levels were comparable between brite adipocyte cultures from 129SV/S6, C57BL/6J UCP $^{+/+}$ and C57BL/6J UCP1$^{-/-}$ mice (Figure 15). Brown adipocytes derived from UCP1$^{+/+}$ and UCP1$^{-/-}$ mice showed a similar glucose uptake under isoproterenol (Figure 16). Hence, adrenergically stimulated glucose uptake into brite and brown adipocytes is independent from UCP1. The results are in line with published *in vitro* data obtained in brown adipocytes (Hankir et al., 2017; Hutchinson et al., 2005). Although, these studies are based on different protocols the results are consistent. It can be concluded that UCP1 abundance or activity does not affect glucose transport *in vitro.*

In male mice, *in vivo,* NE was found to stimulate uptake of ^{3}H labeled 2-DG in BAT of UCP1$^{+/+}$ but not in UCP1$^{-/-}$ mice (Inokuma et al., 2005). In contrast, in a recent study, investigating glucose uptake after selective β3 adrenergic receptor agonist CL 316 with 18F-FDG PET/magnetic resonance imaging, increased 18F-FDG uptake into BAT of female mice occurred independently of UCP1 function (Hankir et al., 2017). This inconsistency may be due to sex specific differences. A study based on 18F-FDG PET/computed tomography imaging revealed that acute cold exposure (four hours at 4 °C) leads to increased 18F-FDG uptake in UCP $^{+/+}$ mice. It is of interest that this increase was maintained and was even higher in female UCP1$^{-/-}$ mice but not present in male UCP1$^{-/-}$ mice (Jeanguillaume et al., 2013). However, recently it was stated that no such differences between sexes were observable and that glucose uptake, studied with ^{3}H labeled 2-DG, was independent from UCP1 (Olsen et al., 2017). Thus, *in vivo* data on glucose uptake in BAT are heterogeneous and glucose uptake does not seem to be necessarily a consequence of thermogenesis via UCP1.

Cultured brite and brown adipocytes were sensitive to insulin (Figure 15, Figure 16). In both cell types insulin led to a higher glucose uptake compared to the basal or isoproterenol treated state. Interestingly, treatment with a combination of insulin and isoproterenol did not show any synergist effects. Binding of insulin to the extracellular α-subunit of the insulin receptor leads to a conformational change and subsequent autophosphorylation of tyrosine residues of the intracellular β-unit. The activated β-subunit recruits and phosphorylates insulin receptor substrates (IRS) that connect insulin receptor activation with the downstream signaling pathways regulating diverse physiological functions. The effect on glucose uptake is mediated by recruitment and activation of phosphoinositide 3-kinase (PI3K) that converts phosphatidylinositol-(4,5)-bisphosphate to the lipid second messenger phosphatidyl-inositol-(3,4,5)-trisphosphate, inducing the

translocation of 3-phospho-inositide-dependent protein kinase 1 (PDK1) to the plasma membrane. which in turn phosphorylates the protein kinase B (PKB, also Akt) at Thr308. PKB phosphorylates and thereby inactivates AS160 (Akt substrate of 160 kDa), facilitating release and translocation of GLUT4 from intracellular storage vesicles to the plasma membrane (Bryant et al., 2002; Huang and Czech, 2007; Lizunov et al., 2005; Zaid et al., 2008).

Sympathetically stimulated glucose uptake is still not fully understood. NE is able to increase glucose transport into brown adipocytes *in vitro* (Marette and Bukowiecki, 1989; Shimizu et al., 1996) and *in vivo (Liu et al., 1994; Shimizu et al., 1991)* in the absence of insulin. This effect is mediated via actions on GLUT1 and not GLUT4 (Dallner et al., 2006; Shimizu et al., 1998) and was shown to be dependent on activation of mammalian target of rapamycin (mTOR) complex 2 (mTORC2) (Albert et al., 2016; Olsen et al., 2014). Adrenergic stimulated glucose uptake via activation of mTORC2 seems to involve increased cAMP levels, exchange factor directly activated by cAMP 1 (EPAC1) signaling and PI3K activation (Albert et al., 2016). mTORC2 plays a crucial role in adipocyte glucose homeostatsis. As mentioned before, in response to insulin signaling, PKB gets phosphorylated at Thr308. In this state PKB can phosphorylate stress-activated protein kinase interacting protein 1 (SIN1) at Thr86. SIN1 is a component of mTORC2 that regulates mTORC2 activity. mTORC2 phosphorylates downstream targets such as serum- and glucocorticoid-induced protein kinase 1 (SGK1), PKC and negatively feeds back to IRS through Fbw8 (Cai et al., 2016; Kim et al., 2012). mTORC2 also phosphorylates PKB at Ser473, resulting in a positive feedback loop (Yang et al., 2015). It was shown that disruption of mTORC2 causes reduced insulin stimulated PKB phosphorylation at Ser473 and leads to impaired insulin-stimulated GLUT4 translocation to the plasma membrane resulting in decreased glucose transport (Kumar et al., 2010). Thus, mTORC2 activity in adipocytes contributes to insulin as well as adrenergic stimulated glucose uptake via GLUT4 or GLUT1, respectively.

In this work, a relative high dose of insulin (1 µM) was applied. This treatment may result in maximal mTORC2 activity that cannot be further increased by isoproterenol. Indeed, in isolated rat brown adipocytes NE was found to synergistically enhance the effect of insulin only if insulin concentrations were below 0.1 µM. Maximal insulin stimulation was not further potentiated by NE (Marette and Bukowiecki, 1989). It is possible, therefore, that the high dose of insulin used in the present study prevented a synergistic effect of insulin and isoproterenol. Furthermore, a negative cross-talk between insulin and adrenergically

mediated glucose uptake could be present. As already stated, adrenergically induced glucose uptake seems to involve increased cAMP levels. Conversely, insulin signaling reduces cAMP levels by preventing its accumulation through lactate signaling (Ahmed et al., 2010) and promoting its degradation via activation of PDE3B (Degerman et al., 1997).

Taken together, the present work shows that glucose uptake into cultured brite and brown adipocytes could be stimulated by treatment with isoproterenol or insulin. In contrast to some *in vivo* data and in line with published *in vitro* data, the glucose uptake in brite and brown adipocytes was completely independent of presence or function of UCP1. Thus, independent from their metabolic state, regulation of glucose uptake in these cells seems to be not affected by UCP1.

4.6 Lactate release is strain dependent and elevated in brown UCP1 knockout cells

Adipocytes convert glucose not only into CO_2, triglycerides, glycogen and pyruvate but also into lactate, depending on the metabolic state (DiGirolamo et al., 1992; Groff et al., 1992). Conversion of glucose into lactate via glycolysis represents an alternative route for ATP generation. Thereby, the formation of lactate from pyruvate regenerates NAD^+ and facilitates continued glycolysis. Although the yield of ATP per mole of glucose through glycolytic ATP generation is less compared to oxidative phosphorylation this route might become important during mitochondrial uncoupling (Si et al., 2009). Moreover, the release of lactate is commonly used as a glycolytic marker (Wu et al., 2007). Remarkably, lactate induces browning of murine and human white adipocytes (Carriere et al., 2014).

It was hypothesized, that production and release of lactate differs depending on UCP1 activity. Therefore, lactate release into the supernatant was studied in brite and brown adipocyte cultures. Lactate concentrations were determined under basal conditions and after stimulation with isoproterenol. In the case of brown adipocytes, lactate levels were assessed in the presence or absence of oligomycin.

In brite adipocyte cultures, isoproterenol treatment significantly increased lactate release into the supernatant (Figure 17). This effect was independent from UCP1 activity. These results are consistent with data obtained in isolated white adipocytes from epididymal WAT (eWAT) (Crandall et al., 1983). Since UCP1 expression is rather low in this type of adipocytes, it can be concluded that the observed accelerated lactate formation in response to NE does not require UCP1.

Many factors influence the production of lactate. Besides depot specific differences (Newby et al., 1988), the amount of glucose converted into lactate by adipocytes increases with cell size, age, glucose availability and insulin treatment (Crandall et al., 1983; Newby et al., 1988; Sabater et al., 2014). The present work showed that lactate release also differs between mouse inbred strains. Under basal as well as under stimulated conditions 129SV/S6 cultures released more lactate than C57BL/6J cultures.

Basically, a higher lactate output could be the result of 1) a higher glycolytic rate, 2) an increased rate of pyruvate conversion into lactate or 3) an elevated export rate of lactate via MCTs. Between inbred strains of mice, a considerable amount of genetic variation in enzyme activity has been found (Bulfield et al., 1978). Within the glycolytic pathway Hk2 and Gapdh are upregulated in 129SV/S6 compared to C57BL/6J UCP1$^{+/+}$ cells (Li, 2013). Hk2 was shown to be involved in adrenergic stimulated and mTORC2 dependent glucose uptake in brown adipocytes (Albert et al., 2016). Hk2 expression induced by lysophosphatidic acid (LPA) resulted in increased glycolytic rate and lactate production in ovarian cancer cells. Thereby, glucose uptake was not affected (Mukherjee et al., 2015).

LPA (1-acyl-2-hy-droxy-sn-glycero-3-phosphates) exist in various species, dominated by 16-, 18-, and 20- carbon long acyl chains and is intracellularly produced by GPAT, phospholipase A1 and A2 (PLA1, PLA2) (Aoki, 2004; Shen et al., 1998). Gene expression of Gpam (encoding GPAT1) and Pla2g4b, a PLA2, were found to be positively correlated with UCP1 expression (Table 6). These genes are also significantly higher expressed in 129SV/S6 compared to C57BL/6J (Li, 2013). LPA acts through plasma membrane-associated LPAx receptors (Choi et al., 2010) and stimulates Hk2 expression through LPA_2-dependent activation of SREBP (Mukherjee et al., 2015). LPA was shown to be an intracellular target of PPARγ (McIntyre et al., 2003). Hypothetically, increased lactate levels in 129SV/S6 cultures arise from elevated glycolytic flux due to increased expression of Hk2 and Gapdh. Thereby, Hk2 expression might be triggered by elevated LPA levels produced by GPAT1 and Pla2g4b. Since not all glycolytic enzymes are upregulated in 129SV/S6 cultures (Li, 2013) and are additionally subject to post-transcriptional and post-translational regulation (Wang et al., 2017), glycolytic flux experiments should be performed to reveal if a higher glycolytic rate is present in 129SV/S6 cells and contributes to elevated lactate release in these cells.

In contrast to brite adipocytes, isoproterenol did not cause any differences in lactate concentrations in the supernatant of brown adipocytes (Figure 34), supporting previous research in isolated brown adipocytes (Ebner et al., 1987; Isler et al., 1987). In brown

adipocytes, increased lactate release in response to isoproterenol may be prevented due to increased oxidation of pyruvate. Indeed, β-AR-mediated activation of pyruvate dehydrogenase has been demonstrated (Gibbins et al., 1985). Furthermore, expression of this enzyme in iBAT was elevated after cold exposure (Madar and Harel, 1991). Especially in the uncoupled state, pyruvate could enter the TCA cycle and be used as thermogenic substrate. In this state, glycolytically produced NADH could be regenerated to NAD^+ in mitochondria. This process requires net import of NADH into mitochondria via the malate-aspartate shuttle. The genes involved in this transport system malate dehydrogenase 1 (Mdh1) and 2 (Mdh2), glutamate oxaloacetate transaminase 1 (Got1) and (Got2) were higher expressed in iBAT than in iWAT, both in thermoneutrality as well as in cold exposed mice (Hao et al., 2015). This observation might provide a possible explanation for the distinct responses to isoproterenol in brite and brown adipocytes. Also, the pentose phosphate pathway, a metabolic pathway parallel to glycolysis, could represent an alternative fate of glucose in brown adipocytes compared to brite adipocytes. Glucose-6-phosphate dehydrogenase, X-linked (G6pdx), the rate-limiting enzyme of this pathway, was upregulated in iBAT compared to iWAT. However, in the same study it was shown that Ldha and Ldhb RNA levels are higher in iBAT compared to iWAT, especially after cold exposure (Hao et al., 2015).

Interestingly, independently from treatment, lactate release differed between genotypes. 129SV/S1 $UCP1^{-/-}$ cultures released significantly more lactate than $UCP1^{+/+}$ cultures (Figure 34). Oligomycin treatment can elucidate high glycolytic rates (Keuper et al., 2014). Maximal output levels of lactate were also higher in 129SV/S1 $UCP1^{-/-}$ cultures compared to $UCP1^{+/+}$ cultures. Like in brite adipocytes cultures, distinct lactate concentrations independent from treatment could be possibly due to 1) a higher glycolytic rate, 2) an increased rate of pyruvate conversion into lactate or 3) an elevated export rate of lactate via MCTs. An increased rate of pyruvate conversion into lactate might for example be the result of a lower oxidation rate of pyruvate in $UCP1^{-/-}$ cells. Lower glycolytic rates could also arise from alternative use of glucose in $UCP^{+/+}$ cells. Transcriptome analysis did not reveal any differences in the expression of glycolytic enzymes, pyruvate dehydrogenase or MCTs (data not shown), suggesting that the enzymatic and transport activity of these candidates might be mainly modulated on protein level and not on transcript level.

In summary, brite and brown adipocytes release lactate in quantitatively significant amounts. In brite adipocytes, lactate release depends on strain and is elevated in response to isoproterenol independently from UCP1. In brown adipocytes lactate release was not

increased by isoproterenol but UCP1 ablation led to elevated lactate levels. Differences in lactate release could be based on distinct glycolytic rates, lactate production or export. Future work should focus on measuring enzyme activities and glycolytic flux to reveal the underlying mechanisms and test these hypotheses.

4.7 The metabotype of brite adipocytes is dependent on UCP1 activity

Metabolites are endogenously and exogenously derived small-molecule compounds that are products or substrates of chemical reactions within biological systems (Liu and Locasale). They provide a direct functional readout of cellular biochemical activity. Metabolite profiling, also known as non-targeted metabolomics, aims to measure as many metabolites as possible from a biological sample (Patti et al., 2012). Metabolite profiles can reveal a metabolite phenotype, the metabotype of a biological system (Gavaghan et al., 2000; Nicholson, 2006). Cell metabolite profiling is widely used to address fundamental biological questions, identification of biomarkers as well as investigation of cellular responses to stimulants, drugs or toxins (Zhang et al., 2013).

To gain further insights into functional and metabolic properties and potentially reveal a certain metabotype of brite cells, non-targeted metabolite profiling was applied. Brite cultures were treated with isoproterenol to stimulate lipolysis and activate UCP1. Stimulated samples were compared to non-treated controls.

Relative signal intensities of FFA ond lysolipids were increased, whereas those of several amino acids, small peptides and nucleoside triphosphates were reduced (Figure 18, Figure 19). Overall, 14 metabolites could be detected that were elevated specifically in the presence and activity of UCP1 (Figure 23A). Most of these metabolites were polyunsaturated fatty acids (PUFAs), monounsaturated fatty acids (MUFAs), branched chain fatty acids (BCFAs) or odd chain fatty acids (OCFA). Brite cultures with distinct UCP1 expression showed a similar lipolytic capacity (Figure 13). Thus, the observed UCP1 dependent FFA pattern cannot be explained by differences in lipolytic activity. An elevated level of specific FFA with increasing UCP1 activity could be the result of 1) a distinct FA composition of TAG in LDs, 2) a reduced degradation, 3) a lower reesterification rate or 4) reduced binding to FA binding proteins of these FFA in thermogenically active adipocytes.

The enzyme stearoyl-CoA desaturase 1 (Scd1) showed a positive correlation with Ucp1 transcript levels over five inbred strains and was identified as a candidate gene involved in thermogenesis (Table 6). Scd1 catalyzes the rate limiting step for the conversion of saturated FA (SAFA) to MUFAs (Stryjecki et al., 2012) supporting a distinct FA

composition. FA composition in adipose depots varies among anatomical localization (Chacko and Perkins, 1965; Imaichi et al., 1965) sex (Hoene et al., 2014), diet (Llado et al., 1997) and metabolic state (Carneheim et al., 1989; Hollenberg and Douglas, 1962; Nagashima et al., 1995). In rodents, cold acclimatization leads to an increased level of unsaturated FA in total FA content of eWAT but not in BAT (Williams and Platner, 1967). In the present work, the total FA profile (FA of all lipids species and FFA) within brite adipocyte cultures was not altered (Figure 25, Table 5). Acute cold exposure or cold acclimation were shown to change iBAT lipid metabolism, TAG as well as PL content and FA composition in rats (Ogawa et al., 1992). Cold acclimation for four weeks increases saturated FA and reduces MUFA content of TAG, whereas PUFA and arachidonate levels in PL are increased (Ogawa et al., 1987, 1992). Thus, an altered FA composition might be present in different lipid species but not in total FA content.

Thermogenic cells might prefer to oxidize other FA than PUFAs, MUFAs, OCFA or BCFAs, but this cannot explain the UCP1 activity dependent accumulation of palmitate. In addition, rare FA such as homo-γ-linoleate, eicosadienoate and lignocerate have been reported to accumulate during entry into hibernation and to be preferentially utilized during the early phase of arousal in hamster iBAT (Carneheim et al., 1989). However, in rat cold-induced NST in BAT seems to be mainly supported by palmitate, stearate, oleate and linoleate mobilized from TAG (Ogawa et al., 1992).

As stated before, abundance of FFA species could also be influenced by proteins. FA binding proteins intracellularly bind FAs (Weisiger, 2007) but on transcript level, expression of these proteins do not correlate with UCP1 expression (Li, 2013).

The metabolite profile assessed in the present study represents only a static snapshot. To clarify if FA profiles vary among brite adipocyte cultures in a UCP1 dependent manner, analysis of FA composition in TAG before and after adrenergic stimulation should be carried out. Experiments with inhibitors of β-oxidation (e.g. etomoxir) and reesterification (e.g. triacsin c) could reveal which FA are preferentially reesterified or oxidized and if these processes vary among UCP1 abundance and activity. Furthermore, metabolite flux analysis with stable isotopes can provide information on the dynamics of metabolic reactions.

4.8 Novel genes potentially involved in brite thermogenic function

Generation of putative candidate genes implicated in the thermogenic function of brite adipocytes was an objective of this study. The metabolite profile dataset was combined

with seven preexisting NGS based transcriptome analysis data sets from human and murine samples to identify new metabolic pathways involved in the thermogenic function. This approach revealed 33 genes within FA and glycerophospholipid (GPL) metabolism (Table 6). Among these genes, Gpam was identified as a putative candidate gene involved in thermogenic function of brite adipocytes. In primary brite adipocyte cultures from different inbred strains, Gpam expression correlated positively with UCP1 expression. Gpam was also upregulated in iBAT in response to cold exposure. A putative crucial role of Gpam is further supported by the fact that Cpt1 isoforms are differentially expressed between brite adipocytes with distinct browning propensities. Gpam encodes the G3P-acyltransferase GPAT1, located in the outer mitochondrial membrane. GPAT1 and CPT1 compete for acyl-CoAs, thereby determining the fate of a fatty acid, if it is oxidation or used for GPL and TAG synthesis (Faris et al., 2014). GPAT1 catalyzes the esterification of acyl-CoA with G3P to LPA. This conjunction is the first rate limiting step of *de novo* GPL and TAG synthesis via the glycerol phosphate pathway (Faris et al., 2014; Hammond et al., 2002; Igal et al., 2001) (Figure 27).

The role of GPAT1 in browning and thermogenesis was investigated by siRNA mediated knockdown experiments. Interestingly, a knockdown of Gpam resulted in an increased UCP1 expression (Figure 29). However, the increased mRNA expression was not translated into increased protein levels (Figure 32). Knockdown of Gpam had no effect on UCP1 mediated oxygen consumption (Figure 30). Elevated UCP1 expression levels might have been the result of a compensatory reaction. In this study, cells were differentiated in the presence of rosiglitazone. Rosiglitazone is a strong enhancer of Ucp1 expression and WB revealed rather high UCP1 protein levels in brite adipocytes (Figure 32). Thus, treatment with rosiglitazone might already have caused maximal protein expression of UCP1 and an elevated mRNA level could not be further translated into protein. Therefore, knock-down experiments should be repeated without rosiglitazone present in the medium.

4.9 Metabolic flux in brown adipocytes

Brown adipocytes are highly specialized cells with unique metabolic properties. To assess and model concomitant metabolic fluxes, oxygen consumption and proton production data as well as lactate and lipolytic release data of brown $UCP^{-/-}$ or $UCP^{+/+}$ adipocyte cultures under basal conditions as well as after adrenergic stimulation were used. From the measured and deduced parameters, a model of metabolic fluxes that describes and predicts how an adrenergic stimulus changes metabolic reactions in a brown fat cell was created. It provides quantitative information on triacylglycerol degradation and β-oxidation

(Figure 44). Adrenergic treatment led to a dramatic increase in O_2 consumption and FFA release, but did not affect lactate release in all $UCP^{+/+}$ and oligomycin untreated $UCP^{-/-}$ cells. Isoproterenol treatment had only a minor effect on O_2 consumption and CO_2 production in oligo treated $UCP1^{-/-}$ cultures. Measured lactate levels were much higher than detected glucose uptake. The discrepancy could either be explained by alternative glucose sources, such as glycogen, or be due to methodological differences between the two assays. Interestingly, in iBAT of rodents, high concentrations of glycogen are present, second only to those of the liver (Carmean et al., 2013; Farkas et al., 1999). Thus, lactate might have resulted in part from adrenergically stimulated glycogenolysis. The increase in extracellular acidification under adrenergic stimulation was caused by the release of FFA and metabolically produced CO_2 (Figure 43). Since glycolytic produced lactic acid is often considered as the major source of medium acidifying protons (Wu et al., 2007), ECAR is commonly used as a direct and quantitative measure of glycolytic rate (Mookerjee et al., 2015; Nadanaciva et al., 2012; Wu et al., 2007). The present study revealed that ECAR is not an appropriate measure of glycolytic rate in active brown adipocytes. Besides CO_2, which has to be taken into account when using ECAR as a measure for glycolytic activity (Mookerjee et al., 2015), also FFA represent a major acidification source in fat cells.

4.10 Conclusions

In summary, the findings presented in this study support a thermogenic function of UCP1 in cultured brite adipocytes. Regarding the functional phenotype of these cells, lipolytic activity, glucose uptake and lactate release were not affected by UCP1 abundance or activity. In contrast, a UCP1 dependent metabotype mainly characterized by an altered FFA profile was identified. Combining metabolite profiling data and transcriptome data-sets several candidate genes of the PL and FA metabolism were identified which could play a crucial role in thermogenic function. Future work should validate the thermogenic function of these genes using siRNA mediated knockdown and respirometric measurements.

As in brite adipocytes, glucose uptake was completely independent of UCP1 in brown adipocytes. However, UCP1 expressing brown adipocytes showed a reduced lactate release compared to $UCP1^{-/-}$ cells. Furthermore, activity of UCP1 diminished the release of lipolytic products. From measured and deduced parameters, a model of metabolic fluxes was created that describes and predicts how an adrenergic stimulus changes metabolic reactions in a brown fat cell. This model will be helpful for interpretation of any data obtained in brown adipocytes.

Interestingly, an ATP consuming thermogenic mechanism, possibly driven by calcium cycling, was present in brown adipocyte cultures from UCP1$^{-/-}$ mice. This UCP1 independent thermogenic mechanism represents an exciting topic for future research.

In conclusion, the findings presented in this work provide new insights into the thermogenic capacity and functional characteristics of brite and brown adipocytes.

5 Literature

Ahmadian, M., Wang, Y., and Sul, H.S. (2010). Lipolysis in adipocytes. The international journal of biochemistry & cell biology *42*, 555-559.

Ahmed, K., Tunaru, S., Tang, C., Muller, M., Gille, A., Sassmann, A., Hanson, J., and Offermanns, S. (2010). An autocrine lactate loop mediates insulin-dependent inhibition of lipolysis through GPR81. Cell metabolism *11*, 311-319.

Albert, V., Svensson, K., Shimobayashi, M., Colombi, M., Muñoz, S., Jimenez, V., Handschin, C., Bosch, F., and Hall, M.N. (2016). mTORC2 sustains thermogenesis via Akt-induced glucose uptake and glycolysis in brown adipose tissue. EMBO Molecular Medicine.

Alberti, K.G., and Zimmet, P.Z. (1998). Definition, diagnosis and classification of diabetes mellitus and its complications. Part 1: diagnosis and classification of diabetes mellitus provisional report of a WHO consultation. Diabetic medicine : a journal of the British Diabetic Association *15*, 539-553.

Almind, K., Manieri, M., Sivitz, W.I., Cinti, S., and Kahn, C.R. (2007). Ectopic brown adipose tissue in muscle provides a mechanism for differences in risk of metabolic syndrome in mice. Proceedings of the National Academy of Sciences of the United States of America *104*, 2366-2371.

Aoki, J. (2004). Mechanisms of lysophosphatidic acid production. Seminars in cell & developmental biology *15*, 477-489.

Bailey, R.A., Wang, Y., Zhu, V., and Rupnow, M.F.T. (2014). Chronic kidney disease in US adults with type 2 diabetes: an updated national estimate of prevalence based on Kidney Disease: Improving Global Outcomes (KDIGO) staging. BMC Research Notes *7*, 415.

Bal, N.C., Maurya, S.K., Sopariwala, D.H., Sahoo, S.K., Gupta, S.C., Shaikh, S.A., Pant, M., Rowland, L.A., Bombardier, E., Goonasekera, S.A.*, et al.* (2012). Sarcolipin is a newly identified regulator of muscle-based thermogenesis in mammals. Nature medicine *18*, 1575-1579.

Barbatelli, G., Murano, I., Madsen, L., Hao, Q., Jimenez, M., Kristiansen, K., Giacobino, J., De Matteis, R., and Cinti, S. (2010). The emergence of cold-induced brown adipocytes in mouse white fat depots is determined predominantly by white to brown adipocyte transdifferentiation. American Journal of Physiology-Endocrinology and Metabolism *298*, E1244-E1253.

Barneda, D., Frontini, A., Cinti, S., and Christian, M. (2013). Dynamic changes in lipid droplet-associated proteins in the "browning" of white adipose tissues. Biochimica et biophysica acta *1831*, 924-933.

Barneda, D., Planas-Iglesias, J., Gaspar, M.L., Mohammadyani, D., Prasannan, S., Dormann, D., Han, G.S., Jesch, S.A., Carman, G.M., Kagan, V.*, et al.* (2015). The brown adipocyte protein CIDEA promotes lipid droplet fusion via a phosphatidic acid-binding amphipathic helix. eLife *4*.

Barquissau, V., Beuzelin, D., Pisani, D.F., Beranger, G.E., Mairal, A., Montagner, A., Roussel, B., Tavernier, G., Marques, M.A., Moro, C.*, et al.* (2016). White-to-brite conversion in human adipocytes promotes metabolic reprogramming towards fatty acid anabolic and catabolic pathways. Molecular metabolism *5*, 352-365.

Bertholet, A.M., Kazak, L., Chouchani, E.T., Bogaczynska, M.G., Paranjpe, I., Wainwright, G.L., Betourne, A., Kajimura, S., Spiegelman, B.M., and Kirichok, Y. (2017). Mitochondrial Patch Clamp of Beige Adipocytes Reveals UCP1-Positive and UCP1-Negative Cells Both Exhibiting Futile Creatine Cycling. Cell metabolism *25*, 811-822.e814.

Bertin, R. (1976). Glycerokinase activity and lipolysis regulation in brown adipose tissue of cold acclimated rats. Biochimie *58*, 431-434.

Bezaire, V., and Langin, D. (2009). Regulation of adipose tissue lipolysis revisited. The Proceedings of the Nutrition Society *68*, 350-360.

Block, B.A., and Franzini-Armstrong, C. (1988). The structure of the membrane systems in a novel muscle cell modified for heat production. The Journal of cell biology *107*, 1099-1112.

Bolsoni-Lopes, A., and Alonso-Vale, M.I. (2015). Lipolysis and lipases in white adipose tissue - An update. Arch Endocrinol Metab *59*, 335-342.

Bolsoni-Lopes, A., Festuccia, W.T., Farias, T.S., Chimin, P., Torres-Leal, F.L., Derogis, P.B., de Andrade, P.B., Miyamoto, S., Lima, F.B., Curi, R.*, et al.* (2013). Palmitoleic acid (n-7) increases white adipocyte lipolysis and lipase content in a PPARalpha-dependent manner. American journal of physiology Endocrinology and metabolism *305*, E1093-1102.

Bonet, M.L., Oliver, P., and Palou, A. (2013). Pharmacological and nutritional agents promoting browning of white adipose tissue. Biochimica et biophysica acta *1831*, 969-985.

Boschi, F., Rizzatti, V., Zamboni, M., and Sbarbati, A. (2015). Models of lipid droplets growth and fission in adipocyte cells. Experimental Cell Research *336*, 253-262.

Bourne, R.R.A., Stevens, G.A., White, R.A., Smith, J.L., Flaxman, S.R., Price, H., Jonas, J.B., Keeffe, J., Leasher, J., Naidoo, K.*, et al.* (2013). Causes of vision loss worldwide, 1990–2010: a systematic analysis. The Lancet Global Health *1*, e339-e349.

Brasaemle, D.L. (2007). Thematic review series: adipocyte biology. The perilipin family of structural lipid droplet proteins: stabilization of lipid droplets and control of lipolysis. Journal of lipid research *48*, 2547-2559.

Brasaemle, D.L., Dolios, G., Shapiro, L., and Wang, R. (2004). Proteomic analysis of proteins associated with lipid droplets of basal and lipolytically stimulated 3T3-L1 adipocytes. Journal of Biological Chemistry *279*, 46835-46842.

Bryant, N.J., Govers, R., and James, D.E. (2002). Regulated transport of the glucose transporter GLUT4. Nature reviews Molecular cell biology *3*, 267-277.

Bulfield, G., Moore, E.A., and Kacser, H. (1978). GENETIC VARIATION IN ACTIVITY OF THE ENZYMES OF GLYCOLYSIS AND GLUCONEOGENESIS BETWEEN INBRED STRAINS OF MICE. Genetics *89*, 551-561.

Burant, C.F., and Bell, G.I. (1992). Mammalian facilitative glucose transporters: evidence for similar substrate recognition sites in functionally monomeric proteins. Biochemistry *31*, 10414-10420.

Burant, C.F., Sivitz, W.I., Fukumoto, H., Kayano, T., Nagamatsu, S., Seino, S., Pessin, J.E., and Bell, G.I. (1991). Mammalian glucose transporters: structure and molecular regulation. Recent progress in hormone research *47*, 349-387; discussion 387-348.

Busiello, R.A., Savarese, S., and Lombardi, A. (2015). Mitochondrial uncoupling proteins and energy metabolism. Frontiers in Physiology *6*, 36.

Cai, H., Dong, L.Q., and Liu, F. (2016). Recent Advances in Adipose mTOR Signaling and Function: Therapeutic Prospects. Trends in pharmacological sciences *37*, 303-317.

Canettieri, G., Celi, F., Baccheschi, G., Salvatori, L., Andreoli, M., and Centanni, M. (2000). Isolation of Human Type 2 Deiodinase Gene Promoter and Characterization of a Functional Cyclic Adenosine Monophosphate Response Element 1. Endocrinology *141*, 1804-1813.

Cannon, B., and Nedergaard, J. (1979). The physiological role of pyruvate carboxylation in hamster brown adipose tissue. European journal of biochemistry / FEBS *94*, 419-426.

Cannon, B., and Nedergaard, J. (2004). Brown adipose tissue: function and physiological significance. Physiological reviews *84*, 277-359.

Cao, W., Daniel, K.W., Robidoux, J., Puigserver, P., Medvedev, A.V., Bai, X., Floering, L.M., Spiegelman, B.M., and Collins, S. (2004). p38 mitogen-activated protein kinase is the central regulator of cyclic AMP-dependent transcription of the brown fat uncoupling protein 1 gene. Molecular and cellular biology *24*, 3057-3067.

Carmean, C.M., Bobe, A.M., Yu, J.C., Volden, P.A., and Brady, M.J. (2013). Refeeding-induced brown adipose tissue glycogen hyper-accumulation in mice is mediated by insulin and catecholamines. PloS one *8*, e67807.

Carmen, G.-Y., and Víctor, S.-M. (2006). Signalling mechanisms regulating lipolysis. Cellular signalling *18*, 401-408.

Carneheim, C., Cannon, B., and Nedergaard, J. (1989). Rare fatty acids in brown fat are substrates for thermogenesis during arousal from hibernation. The American journal of physiology *256*, R146-154.

Carriere, A., Jeanson, Y., Berger-Muller, S., Andre, M., Chenouard, V., Arnaud, E., Barreau, C., Walther, R., Galinier, A., Wdziekonski, B.*, et al.* (2014). Browning of white adipose cells by intermediate metabolites: an adaptive mechanism to alleviate redox pressure. Diabetes *63*, 3253-3265.

Chacko, G.K., and Perkins, E.G. (1965). Anatomical variation in fatty acid composition and triglyceride distribution in animal depot fats. Journal of the American Oil Chemists' Society *42*, 1121-1124.

Choi, J.W., Herr, D.R., Noguchi, K., Yung, Y.C., Lee, C.W., Mutoh, T., Lin, M.E., Teo, S.T., Park, K.E., Mosley, A.N.*, et al.* (2010). LPA receptors: subtypes and biological actions. Annual review of pharmacology and toxicology *50*, 157-186.

Chondronikola, M., Volpi, E., Borsheim, E., Porter, C., Annamalai, P., Enerback, S., Lidell, M.E., Saraf, M.K., Labbe, S.M., Hurren, N.M.*, et al.* (2014). Brown Adipose Tissue Improves Whole Body Glucose Homeostasis and Insulin Sensitivity in Humans. Diabetes.

Cinti, S. (1999). The adipose organ (Kurtis Milan).

Cinti, S. (2005). The adipose organ. Prostaglandins, leukotrienes, and essential fatty acids *73*, 9-15.

Cinti, S. (2012). The adipose organ at a glance. Disease models & mechanisms *5*, 588-594.

Clark, H. (2013). NCDs: a challenge to sustainable human development. Lancet (London, England) *381*, 510-511.

Coleman, R.A., and Lee, D.P. (2004). Enzymes of triacylglycerol synthesis and their regulation. Progress in lipid research *43*, 134-176.

Coleman, R.A., Lewin, T.M., and Muoio, D.M. (2000). Physiological and nutritional regulation of enzymes of triacylglycerol synthesis. Annual review of nutrition *20*, 77-103.

Collins, S., Daniel, K.W., Petro, A.E., and Surwit, R.S. (1997). Strain-specific response to beta 3-adrenergic receptor agonist treatment of diet-induced obesity in mice. Endocrinology *138*, 405-413.

Cousin, B., Cinti, S., Morroni, M., Raimbault, S., Ricquier, D., Penicaud, L., and Casteilla, L. (1992). Occurrence of brown adipocytes in rat white adipose tissue: molecular and morphological characterization. Journal of cell science *103 (Pt 4)*, 931-942.

Crandall, D.L., Fried, S.K., Francendese, A.A., Nickel, M., and DiGirolamo, M. (1983). Lactate release from isolated rat adipocytes: influence of cell size, glucose concentration, insulin and epinephrine. Hormone and metabolic research = Hormon- und Stoffwechselforschung = Hormones et metabolisme *15*, 326-329.

Cypess, A.M., Lehman, S., Williams, G., Tal, I., Rodman, D., Goldfine, A.B., Kuo, F.C., Palmer, E.L., Tseng, Y.-H., and Doria, A. (2009). Identification and importance of brown adipose tissue in adult humans. New England Journal of Medicine *360*, 1509-1517.

Cypess, A.M., White, A.P., Vernochet, C., Schulz, T.J., Xue, R., Sass, C.A., Huang, T.L., Roberts-Toler, C., Weiner, L.S., Sze, C.*, et al.* (2013). Anatomical localization, gene expression profiling and functional characterization of adult human neck brown fat. Nature medicine *19*, 635-639.

Dallner, O.S., Chernogubova, E., Brolinson, K.A., and Bengtsson, T. (2006). Beta3-adrenergic receptors stimulate glucose uptake in brown adipocytes by two mechanisms independently of glucose transporter 4 translocation. Endocrinology *147*, 5730-5739.

de Jong, J.M.A., Larsson, O., Cannon, B., and Nedergaard, J. (2015). A stringent validation of mouse adipose tissue identity markers. American Journal of Physiology - Endocrinology And Metabolism *308*, E1085-E1105.

de Meis, L. (1998). Control of heat produced during ATP hydrolysis by the sarcoplasmic reticulum Ca 2+-ATPase in the absence of a Ca 2+ gradient. Biochemical and biophysical research communications *243*, 598-600.

de Meis, L. (2002). Ca2+-ATPases (SERCA): energy transduction and heat production in transport ATPases. Journal of Membrane Biology *188*, 1-9.

de Meis, L. (2003). Brown Adipose Tissue Ca2+-ATPase: UNCOUPLED ATP HYDROLYSIS AND THERMOGENIC ACTIVITY. Journal of Biological Chemistry *278*, 41856-41861.

Degerman, E., Belfrage, P., and Manganiello, V.C. (1997). Structure, localization, and regulation of cGMP-inhibited phosphodiesterase (PDE3). Journal of Biological Chemistry *272*, 6823-6826.

DiGirolamo, M., Newby, F.D., and Lovejoy, J. (1992). Lactate production in adipose tissue: a regulated function with extra-adipose implications. Faseb J *6*, 2405-2412.

Ebner, S., Burnol, A.F., Ferre, P., de Saintaurin, M.A., and Girard, J. (1987). Effects of insulin and norepinephrine on glucose transport and metabolism in rat brown adipocytes. Potentiation by insulin of norepinephrine-induced glucose oxidation. European journal of biochemistry / FEBS *170*, 469-474.

Ecker, J., Scherer, M., Schmitz, G., and Liebisch, G. (2012). A rapid GC-MS method for quantification of positional and geometric isomers of fatty acid methyl esters. Journal of chromatography B, Analytical technologies in the biomedical and life sciences *897*, 98-104.

Ellis, J.M., Paul, D.S., Depetrillo, M.A., Singh, B.P., Malarkey, D.E., and Coleman, R.A. (2012). Mice deficient in glycerol-3-phosphate acyltransferase-1 have a reduced susceptibility to liver cancer. Toxicologic pathology *40*, 513-521.

Enerbäck, S., Jacobsson, A., Simpson, E.M., Guerra, C., Yamashita, H., Harper, M.E., and Kozak, L.P. (1997). Mice lacking mitochondrial uncoupling protein are cold-sensitive but not obese. Nature *387*, 90-94.

Faris, R., Fan, Y.Y., De Angulo, A., Chapkin, R.S., deGraffenried, L.A., and Jolly, C.A. (2014). Mitochondrial glycerol-3-phosphate acyltransferase-1 is essential for murine CD4(+) T cell metabolic activation. Biochimica et biophysica acta *1842*, 1475-1482.

Farkas, V., Kelenyi, G., and Sandor, A. (1999). A dramatic accumulation of glycogen in the brown adipose tissue of rats following recovery from cold exposure. Archives of biochemistry and biophysics *365*, 54-61.

Fedorenko, A., Lishko, P.V., and Kirichok, Y. (2012). Mechanism of fatty-acid-dependent UCP1 uncoupling in brown fat mitochondria. Cell *151*, 400-413.

Festuccia, W.T., Blanchard, P.G., Richard, D., and Deshaies, Y. (2010). Basal adrenergic tone is required for maximal stimulation of rat brown adipose tissue UCP1 expression by chronic PPAR-gamma activation. American journal of physiology Regulatory, integrative and comparative physiology *299*, R159-167.

Festuccia, W.T., Laplante, M., Berthiaume, M., Gelinas, Y., and Deshaies, Y. (2006). PPARgamma agonism increases rat adipose tissue lipolysis, expression of glyceride lipases, and the response of lipolysis to hormonal control. Diabetologia *49*, 2427-2436.

Flachs, P., Adamcova, K., Zouhar, P., Marques, C., Janovska, P., Viegas, I., Jones, J.G., Bardova, K., Svobodova, M., Hansikova, J.*, et al.* (2017). Induction of lipogenesis in white fat during cold exposure in mice: link to lean phenotype. International journal of obesity (2005).

Flachs, P., Rossmeisl, M., Kuda, O., and Kopecky, J. (2013). Stimulation of mitochondrial oxidative capacity in white fat independent of UCP1: a key to lean phenotype. Biochimica et biophysica acta *1831*, 986-1003.

Flechtner-Mors, M., Jenkinson, C., Alt, A., Adler, G., and Ditschuneit, H. (2002). In vivo α1-adrenergic lipolytic activity in subcutaneous adipose tissue of obese subjects. Journal of Pharmacology and Experimental Therapeutics *301*, 229-233.

Fricke, K., Heitland, A., and Maronde, E. (2004). Cooperative activation of lipolysis by protein kinase A and protein kinase C pathways in 3T3-L1 adipocytes. Endocrinology *145*, 4940-4947.

Fromme, T. (2013). Transcriptome data set of iBAT samples from 6, 12 and 48 hours cold exposed mice. Unpublished raw data. Chair of Molecular Nutritional Medicine (Prof. Dr. Martin Klingenspor), Technical University Munich.

Fruhbeck, G., Toplak, H., Woodward, E., Yumuk, V., Maislos, M., and Oppert, J.M. (2013). Obesity: the gateway to ill health - an EASO position statement on a rising public health, clinical and scientific challenge in Europe. Obesity facts *6*, 117-120.

Garcia-Ruiz, E., Reynes, B., Diaz-Rua, R., Ceresi, E., Oliver, P., and Palou, A. (2015). The intake of high-fat diets induces the acquisition of brown adipocyte gene expression features in white adipose tissue. International journal of obesity (2005) *39*, 1619-1629.

Garlid, K.D., Orosz, D.E., Modrianský, M., Vassanelli, S., and Jezek, P. (1996). On the mechanism of fatty acid-induced proton transport by mitochondrial uncoupling protein. Journal of Biological Chemistry *271*, 2615-2620.

Garrett, R., and Grisham, C.M. (2009). Biochemistry (Belmont, CA: Thomson Brooks/Cole).

Gavaghan, C.L., Holmes, E., Lenz, E., Wilson, I.D., and Nicholson, J.K. (2000). An NMR-based metabonomic approach to investigate the biochemical consequences of genetic strain differences: application to the C57BL10J and Alpk:ApfCD mouse. FEBS letters *484*, 169-174.

Gerngroß, C., Schretter, J., Klingenspor, M., Schwaiger, M., and Fromme, T. (2017). Active brown fat during 18FDG-PET/CT imaging defines a patient group with characteristic traits and an increased probability of brown fat redetection. Journal of Nuclear Medicine.

Gesta, S., and Kahn, C.R. (2012). White Adipose Tissue. In Adipose Tissue Biology (Springer), pp. 71-121.

Gesta, S., Tseng, Y.-H., and Kahn, C.R. (2007). Developmental origin of fat: tracking obesity to its source. Cell *131*, 242-256.

Gibbins, J.M., Denton, R.M., and McCormack, J.G. (1985). Evidence that noradrenaline increases pyruvate dehydrogenase activity and decreases acetyl-CoA carboxylase activity in rat interscapular brown adipose tissue in vivo. The Biochemical journal *228*, 751-755.

Girousse, A., and Langin, D. (2012). Adipocyte lipases and lipid droplet-associated proteins: insight from transgenic mouse models. International journal of obesity (2005) *36*, 581-594.

Gnaiger, E., and Kemp, R.B. (1990). Anaerobic metabolism in aerobic mammalian cells: information from the ratio of calorimetric heat flux and respirometric oxygen flux. Biochimica et biophysica acta *1016*, 328-332.

Golozoubova, V., Gullberg, H., Matthias, A., Cannon, B., Vennstrom, B., and Nedergaard, J. (2004). Depressed thermogenesis but competent brown adipose tissue recruitment in mice devoid of all hormone-binding thyroid hormone receptors. Molecular endocrinology (Baltimore, Md) *18*, 384-401.

Golozoubova, V., Hohtola, E., Matthias, A., Jacobsson, A., Cannon, B., and Nedergaard, J. (2001). Only UCP1 can mediate adaptive nonshivering thermogenesis in the cold. The FASEB Journal *15*, 2048-2050.

Gong, J., Sun, Z., Wu, L., Xu, W., Schieber, N., Xu, D., Shui, G., Yang, H., Parton, R.G., and Li, P. (2011). Fsp27 promotes lipid droplet growth by lipid exchange and transfer at lipid droplet contact sites. The Journal of cell biology *195*, 953-963.

Gonzalez-Baro, M.R., Granger, D.A., and Coleman, R.A. (2001). Mitochondrial glycerol phosphate acyltransferase contains two transmembrane domains with the active site in the N-terminal domain facing the cytosol. The Journal of biological chemistry *276*, 43182-43188.

Gonzalez-Baro, M.R., Lewin, T.M., and Coleman, R.A. (2007). Regulation of Triglyceride Metabolism. II. Function of mitochondrial GPAT1 in the regulation of triacylglycerol biosynthesis and insulin action. American journal of physiology Gastrointestinal and liver physiology *292*, G1195-1199.

Gordon, C.J. (2012). Thermal physiology of laboratory mice: Defining thermoneutrality. Journal of Thermal Biology *37*, 654-685.

Goto, T., Lee, J.Y., Teraminami, A., Kim, Y.I., Hirai, S., Uemura, T., Inoue, H., Takahashi, N., and Kawada, T. (2011). Activation of peroxisome proliferator-activated receptor-alpha stimulates both differentiation and fatty acid oxidation in adipocytes. Journal of lipid research *52*, 873-884.

Granneman, J.G., Burnazi, M., Zhu, Z., and Schwamb, L.A. (2003). White adipose tissue contributes to UCP1-independent thermogenesis. American journal of physiology Endocrinology and metabolism *285*, E1230-1236.

Greco-Perotto, R., Zaninetti, D., Assimacopoulos-Jeannet, F., Bobbioni, E., and Jeanrenaud, B. (1987). Stimulatory effect of cold adaptation on glucose utilization by brown adipose tissue. Relationship with changes in the glucose transporter system. The Journal of biological chemistry *262*, 7732-7736.

Greenberg, A.S., Shen, W.J., Muliro, K., Patel, S., Souza, S.C., Roth, R.A., and Kraemer, F.B. (2001). Stimulation of lipolysis and hormone-sensitive lipase via the extracellular signal-regulated kinase pathway. The Journal of biological chemistry *276*, 45456-45461.

Greqoir, F., Smas, C., and Sul, H. (1998). Understanding adipocyte differentaion. Physiological reviews *78*, 783-809.

Groff, J.L., Stugard, C.E., Mays, C.J., Koopmans, H.S., and DiGirolamo, M. (1992). Glucose metabolism in isolated rat adipocytes: estimate of total recovery by the product summation method. The Journal of laboratory and clinical medicine *119*, 216-220.

Guerra, C., Koza, R.A., Yamashita, H., Walsh, K., and Kozak, L.P. (1998). Emergence of brown adipocytes in white fat in mice is under genetic control. Effects on body weight and adiposity. The Journal of clinical investigation *102*, 412-420.

Gunawardana, S.C., and Piston, D.W. (2012). Reversal of Type 1 Diabetes in Mice by Brown Adipose Tissue Transplant. Diabetes.

Haemmerle, G., Moustafa, T., Woelkart, G., Buttner, S., Schmidt, A., van de Weijer, T., Hesselink, M., Jaeger, D., Kienesberger, P.C., Zierler, K.*, et al.* (2011). ATGL-mediated fat catabolism regulates cardiac mitochondrial function via PPAR-alpha and PGC-1. Nature medicine *17*, 1076-1085.

Hallberg, M., Morganstein, D.L., Kiskinis, E., Shah, K., Kralli, A., Dilworth, S.M., White, R., Parker, M.G., and Christian, M. (2008). A functional interaction between RIP140 and PGC-1α regulates the expression of the lipid droplet protein CIDEA. Molecular and cellular biology *28*, 6785-6795.

Hammond, L.E., Gallagher, P.A., Wang, S., Hiller, S., Kluckman, K.D., Posey-Marcos, E.L., Maeda, N., and Coleman, R.A. (2002). Mitochondrial glycerol-3-phosphate acyltransferase-deficient mice have reduced weight and liver triacylglycerol content and altered glycerolipid fatty acid composition. Molecular and cellular biology *22*, 8204-8214.

Hankir, M.K., Kranz, M., Keipert, S., Weiner, J., Andreasen, S.G., Kern, M., Patt, M., Kloting, N., Heiker, J.T., Hesse, S.*, et al.* (2017). Dissociation between brown adipose tissue 18F-FDG uptake and thermogenesis in uncoupling protein 1 deficient mice. Journal of nuclear medicine : official publication, Society of Nuclear Medicine.

Hao, Q., Yadav, R., Basse, A.L., Petersen, S., Sonne, S.B., Rasmussen, S., Zhu, Q., Lu, Z., Wang, J., Audouze, K.*, et al.* (2015). Transcriptome profiling of brown adipose tissue during cold exposure reveals extensive regulation of glucose metabolism. American journal of physiology Endocrinology and metabolism *308*, E380-392.

Heaton, G.M., Wagenvoord, R.J., Kemp, A., and Nicholls, D.G. (1978). brown-adipose-tissue mitochondria: photoaffinity labelling of the regulatory site of energy dissipation. European Journal of Biochemistry *82*, 515-521.

Heldmaier, G., and Neuweiler, G. (2004). Vergleichende Tierphysiologie: Band 2 Vegetative Physiologie (Springer).

Hill, J.O., Wyatt, H.R., and Peters, J.C. (2012). Energy Balance and Obesity. Circulation *126*, 126-132.

Himms-Hagen, J. (1965). LIPID METABOLISM IN WARM-ACCLIMATED AND COLD-ACCLIMATED RATS EXPOSED TO COLD. Canadian journal of physiology and pharmacology *43*, 379-403.

Himms-Hagen, J., Melnyk, A., Zingaretti, M.C., Ceresi, E., Barbatelli, G., and Cinti, S. (2000). Multilocular fat cells in WAT of CL-316243-treated rats derive directly from white adipocytes. American journal of physiology Cell physiology *279*, C670-681.

Hoene, M., Li, J., Haring, H.U., Weigert, C., Xu, G., and Lehmann, R. (2014). The lipid profile of brown adipose tissue is sex-specific in mice. Biochimica et biophysica acta *1842*, 1563-1570.

Hofmann, W.E., Liu, X., Bearden, C.M., Harper, M.E., and Kozak, L.P. (2001). Effects of genetic background on thermoregulation and fatty acid-induced uncoupling of mitochondria in UCP1-deficient mice. The Journal of biological chemistry *276*, 12460-12465.

Hollenberg, C.H., and Douglas, D.E. (1962). Effect of adrenaline, corticotropin, fasting, and diabetes on the composition of the long-chain fatty acids of rat epididymal fat. Nature *193*, 1074-1075.

Holm, C. (2003). Molecular mechanisms regulating hormone-sensitive lipase and lipolysis (Portland Press Limited).

Huang, S.-G. (2003). Binding of fatty acids to the uncoupling protein from brown adipose tissue mitochondria. Archives of biochemistry and biophysics *412*, 142-146.

Huang, S., and Czech, M.P. (2007). The GLUT4 glucose transporter. Cell metabolism *5*, 237-252.

Hutchinson, D.S., Chernogubova, E., Dallner, O.S., Cannon, B., and Bengtsson, T. (2005). Beta-adrenoceptors, but not alpha-adrenoceptors, stimulate AMP-activated protein kinase in brown adipocytes independently of uncoupling protein-1. Diabetologia *48*, 2386-2395.

Igal, R.A., Wang, S., Gonzalez-Baro, M., and Coleman, R.A. (2001). Mitochondrial glycerol phosphate acyltransferase directs the incorporation of exogenous fatty acids into triacylglycerol. The Journal of biological chemistry *276*, 42205-42212.

Imaichi, K., Fukuda, J.I., Oyama, K., and Mukawa, A. (1965). Effect of sample site on fatty acid composition of adipose tissue. Journal of biochemistry *58*, 463-469.

Inokuma, K., Ogura-Okamatsu, Y., Toda, C., Kimura, K., Yamashita, H., and Saito, M. (2005). Uncoupling protein 1 is necessary for norepinephrine-induced glucose utilization in brown adipose tissue. Diabetes *54*, 1385-1391.

Isidor, M.S., Winther, S., Basse, A.L., Petersen, M.C.H., Cannon, B., Nedergaard, J., and Hansen, J.B. (2015). An siRNA-based method for efficient silencing of gene expression in mature brown adipocytes. Adipocyte, 1-11.

Isler, D., Hill, H.P., and Meier, M.K. (1987). Glucose metabolism in isolated brown adipocytes under beta-adrenergic stimulation. Quantitative contribution of glucose to total thermogenesis. The Biochemical journal *245*, 789-793.

IUPS (2001). Glossary of terms for thermal physiology. Third edition. Revised by The Commission for Thermal Physiology of the International

Union of Physiological Sciences (IUPS Thermal Commission) (The Japanese Journal of Physiology), pp. 245–280.

Jambunathan, S., Yin, J., Khan, W., Tamori, Y., and Puri, V. (2011). FSP27 promotes lipid droplet clustering and then fusion to regulate triglyceride accumulation. PloS one *6*, e28614.

Jeanguillaume, C., Metrard, G., Ricquier, D., Legras, P., Bouchet, F., Lacoeuille, F., Hindre, F., Morel, O., and Rakotonirina, H. (2013). Visualization of Activated BAT in Mice, with FDG-PET and Its Relation to UCP1. Advances in Molecular Imaging *03*, 19-22.

Jespersen, N.Z., Larsen, T.J., Peijs, L., Daugaard, S., Homoe, P., Loft, A., de Jong, J., Mathur, N., Cannon, B., Nedergaard, J.*, et al.* (2013). A classical brown adipose tissue mRNA signature partly overlaps with brite in the supraclavicular region of adult humans. Cell metabolism *17*, 798-805.

Jonckheere, A.I., Smeitink, J.A.M., and Rodenburg, R.J.T. (2012). Mitochondrial ATP synthase: architecture, function and pathology. Journal of Inherited Metabolic Disease *35*, 211-225.

Kahn, B.B. (1998). Type 2 Diabetes: When Insulin Secretion Fails to Compensate for Insulin Resistance. Cell *92*, 593-596.

Kasuga, M. (2006). Insulin resistance and pancreatic β cell failure. The Journal of clinical investigation *116*, 1756-1760.

Kazak, L., Chouchani, E.T., Jedrychowski, M.P., Erickson, B.K., Shinoda, K., Cohen, P., Vetrivelan, R., Lu, G.Z., Laznik-Bogoslavski, D., Hasenfuss, S.C.*, et al.* (2015). A creatine-driven substrate cycle enhances energy expenditure and thermogenesis in beige fat. Cell *163*, 643-655.

Kelly, T., Yang, W., Chen, C.S., Reynolds, K., and He, J. (2008). Global burden of obesity in 2005 and projections to 2030. International journal of obesity (2005) *32*, 1431-1437.

Kershaw, E.E., Schupp, M., Guan, H.P., Gardner, N.P., Lazar, M.A., and Flier, J.S. (2007). PPARgamma regulates adipose triglyceride lipase in adipocytes in vitro and in vivo. American journal of physiology Endocrinology and metabolism *293*, E1736-1745.

Keuper, M., Jastroch, M., Yi, C.X., Fischer-Posovszky, P., Wabitsch, M., Tschop, M.H., and Hofmann, S.M. (2014). Spare mitochondrial respiratory capacity permits human adipocytes to maintain ATP homeostasis under hypoglycemic conditions. Faseb J *28*, 761-770.

Kim, Sung J., DeStefano, Michael A., Oh, Won J., Wu, C.-c., Vega-Cotto, Nicole M., Finlan, M., Liu, D., Su, B., and Jacinto, E. (2012). mTOR Complex 2 Regulates Proper Turnover of Insulin Receptor Substrate-1 via the Ubiquitin Ligase Subunit Fbw8. Molecular Cell *48*, 875-887.

Kingma, B.R.M., Frijns, A.J.H., Schellen, L., and van Marken Lichtenbelt, W.D. (2014). Beyond the classic thermoneutral zone: Including thermal comfort. Temperature: Multidisciplinary Biomedical Journal *1*, 142-149.

Klingenspor, M., Bast, A., Bolze, F., Li, Y.,, Maurer, S., Schweizer, S., Willershäuser, M.,, and and Fromme, T. (2017). Brown adipose tissue. In Adipose tissue biology, M.E. Symonds, ed. (New York Dordrecht Heidelberg London: Springer), pp. 91-147.

Klingenspor, M., Herzig, S., and Pfeifer, A. (2012). Brown fat develops a brite future. Obesity facts *5*, 890-896.

Knight, B.L., and Myant, N.B. (1970). A comparison between the effects of cold exposure in vivo and of noradrenaline in vitro on the metabolism of the brown fat of new-born rabbits. The Biochemical journal *119*, 103-111.

Kozak, L.P., and Koza, R.A. (2010). The genetics of brown adipose tissue. Progress in molecular biology and translational science *94*, 75-123.

Kumar, A., Lawrence, J.C., Jr., Jung, D.Y., Ko, H.J., Keller, S.R., Kim, J.K., Magnuson, M.A., and Harris, T.E. (2010). Fat cell-specific ablation of rictor in mice impairs insulin-regulated fat cell and whole-body glucose and lipid metabolism. Diabetes *59*, 1397-1406.

Kuryszko, J., Slawuta, P., and Sapikowski, G. (2016). Secretory function of adipose tissue. Polish journal of veterinary sciences *19*, 441-446.

Labbe, S.M., Caron, A., Chechi, K., Laplante, M., Lecomte, R., and Richard, D. (2016). Metabolic activity of brown, "beige," and white adipose tissues in response to chronic adrenergic stimulation in male mice. American journal of physiology Endocrinology and metabolism *311*, E260-268.

Lafontan, M., and Berlan, M. (1993). Fat cell adrenergic receptors and the control of white and brown fat cell function. Journal of lipid research *34*, 1057-1091.

Lasar, D. (2013). Transcriptome data set of postnatal browning rWAT samples from C57BL6/J and 129SV/S6 mice at postnatal day 10, 20 and 30. Unpublished raw data. Chair of Molecular Nutritional Medicine (Prof. Dr. Martin Klingenspor), Technical University Munich.

Lasar, D., Julius, A., Fromme, T., and Klingenspor, M. (2013). Browning attenuates murine white adipose tissue expansion during postnatal development. Biochimica et biophysica acta *1831*, 960-968.

Leaver, E.V., and Pappone, P.A. (2002). β-Adrenergic potentiation of endoplasmic reticulum Ca2+ release in brown fat cells. American Journal of Physiology-Cell Physiology *282*, C1016-C1024.

Lee, K., Kerner, J., and Hoppel, C.L. (2011). Mitochondrial carnitine palmitoyltransferase 1a (CPT1a) is part of an outer membrane fatty acid transfer complex. Journal of Biological Chemistry *286*, 25655-25662.

Lee, Y.H., and Granneman, J.G. (2012). Seeking the source of adipocytes in adult white adipose tissues. Adipocyte *1*, 230-236.

Leto, D., and Saltiel, A.R. (2012). Regulation of glucose transport by insulin: traffic control of GLUT4. Nature reviews Molecular cell biology *13*, 383-396.

Li, Y. (2013). Transcriptome data set of murine in vitro differentiated primary brite adipocyte cultures from different inbred strains. Unpublished raw data. Chair of Molecular Nutritional Medicine (Prof. Dr. Martin Klingenspor), Technical University Munich.

Li, Y., Bolze, F., Fromme, T., and Klingenspor, M. (2014a). Intrinsic differences in BRITE adipogenesis of primary adipocytes from two different mouse strains. Biochimica et Biophysica Acta (BBA) - Molecular and Cell Biology of Lipids.

Li, Y., Fromme, T., Schweizer, S., Schottl, T., and Klingenspor, M. (2014b). Taking control over intracellular fatty acid levels is essential for the analysis of thermogenic function in cultured primary brown and brite/beige adipocytes. EMBO reports *15*, 1069-1076.

Li, Y.G., Lasar, D., Fromme, T., and Klingenspor, M. (2014c). White, brite, and brown adipocytes: the evolution and function of a heater organ in mammals. Canadian Journal of Zoology *92*, 615-626.

Lin, C.S., and Klingenberg, M. (1980). Isolation of the uncoupling protein from brown adipose tissue mitochondria. FEBS letters *113*, 299-303.

Lin, C.S., and Klingenberg, M. (1982). Characteristics of the isolated purine nucleotide binding protein from brown fat mitochondria. Biochemistry *21*, 2950-2956.

Liu, C., Wu, J., Zhu, J., Kuei, C., Yu, J., Shelton, J., Sutton, S.W., Li, X., Yun, S.J., Mirzadegan, T., *et al.* (2009). Lactate inhibits lipolysis in fat cells through activation of an orphan G-protein-coupled receptor, GPR81. The Journal of biological chemistry *284*, 2811-2822.

Liu, X., and Locasale, J.W. Metabolomics: A Primer. Trends in Biochemical Sciences.

Liu, X., Perusse, F., and Bukowiecki, L.J. (1994). Chronic norepinephrine infusion stimulates glucose uptake in white and brown adipose tissues. The American journal of physiology *266*, R914-920.

Lizunov, V.A., Matsumoto, H., Zimmerberg, J., Cushman, S.W., and Frolov, V.A. (2005). Insulin stimulates the halting, tethering, and fusion of mobile GLUT4 vesicles in rat adipose cells. The Journal of cell biology *169*, 481-489.

Llado, I., Pons, A., and Palou, A. (1997). Fatty acid composition of brown adipose tissue in dietary obese rats. Biochemistry and molecular biology international *43*, 1129-1136.

Lo, K.A., and Sun, L. (2013). Turning WAT into BAT: a review on regulators controlling the browning of white adipocytes. Biosci Rep.

Loft, A., Forss, I., Siersbaek, M.S., Schmidt, S.F., Larsen, A.S., Madsen, J.G., Pisani, D.F., Nielsen, R., Aagaard, M.M., Mathison, A.*, et al.* (2015). Browning of human adipocytes requires KLF11 and reprogramming of PPARgamma superenhancers. Genes Dev *29*, 7-22.

Londos, C., Brasaemle, D.L., Schultz, C.J., Segrest, J.P., and Kimmel, A.R. (1999). Perilipins, ADRP, and other proteins that associate with intracellular neutral lipid droplets in animal cells. Seminars in cell & developmental biology *10*, 51-58.

Ma, S.W., and Foster, D.O. (1986). Uptake of glucose and release of fatty acids and glycerol by rat brown adipose tissue in vivo. Canadian journal of physiology and pharmacology *64*, 609-614.

Madar, Z., and Harel, A. (1991). Does the glycogen synthase (EC 2.4.1.21) of brown adipose tissue play a regulatory role in glucose homeostasis? The British journal of nutrition *66*, 95-104.

Marcher, A.B., Loft, A., Nielsen, R., Vihervaara, T., Madsen, J.G., Sysi-Aho, M., Ekroos, K., and Mandrup, S. (2015). RNA-Seq and Mass-Spectrometry-Based Lipidomics Reveal Extensive Changes of Glycerolipid Pathways in Brown Adipose Tissue in Response to Cold. Cell reports *13*, 2000-2013.

Marcinkiewicz, A., Gauthier, D., Garcia, A., and Brasaemle, D.L. (2006). The phosphorylation of serine 492 of perilipin a directs lipid droplet fragmentation and dispersion. The Journal of biological chemistry *281*, 11901-11909.

Marette, A., and Bukowiecki, L.J. (1989). Stimulation of glucose transport by insulin and norepinephrine in isolated rat brown adipocytes. American Journal of Physiology-Cell Physiology *257*, C714-C721.

Martin, S., Driessen, K., Nixon, S.J., Zerial, M., and Parton, R.G. (2005). Regulated localization of Rab18 to lipid droplets: effects of lipolytic stimulation and inhibition of lipid droplet catabolism. The Journal of biological chemistry *280*, 42325-42335.

Martinez de Mena, R., Scanlan, T.S., and Obregon, M.J. (2010). The T3 receptor beta1 isoform regulates UCP1 and D2 deiodinase in rat brown adipocytes. Endocrinology *151*, 5074-5083.

McIntyre, T.M., Pontsler, A.V., Silva, A.R., St Hilaire, A., Xu, Y., Hinshaw, J.C., Zimmerman, G.A., Hama, K., Aoki, J., Arai, H.*, et al.* (2003). Identification of an intracellular receptor for lysophosphatidic acid (LPA): LPA is a transcellular PPARgamma agonist. Proceedings of the National Academy of Sciences of the United States of America *100*, 131-136.

Meyer, C.W., Willershäuser, M., Jastroch, M., Rourke, B.C., Fromme, T., Oelkrug, R., Heldmaier, G., and Klingenspor, M. (2010). Adaptive thermogenesis and thermal conductance in wild-type and UCP1-KO mice. American journal of physiology Regulatory, integrative and comparative physiology *299*, R1396-R1406.

Mitchell, P. (1961). Coupling of phosphorylation to electron and hydrogen transfer by a chemi-osmotic type of mechanism. Nature *191*, 144-148.

Mitidieri, F., and de Meis, L. (1999). Ca2+ Release and Heat Production by the Endoplasmic Reticulum Ca2+-ATPase of Blood Platelets EFFECT OF THE PLATELET ACTIVATING FACTOR. Journal of Biological Chemistry *274*, 28344-28350.

Moisan, A., Lee, Y.K., Zhang, J.D., Hudak, C.S., Meyer, C.A., Prummer, M., Zoffmann, S., Truong, H.H., Ebeling, M., Kiialainen, A.*, et al.* (2015). White-to-brown metabolic conversion of human adipocytes by JAK inhibition. Nature cell biology *17*, 57-67.

Mookerjee, S.A., Goncalves, R.L., Gerencser, A.A., Nicholls, D.G., and Brand, M.D. (2015). The contributions of respiration and glycolysis to extracellular acid production. Biochimica et biophysica acta *1847*, 171-181.

Morrissette, J.M., Franck, J.P., and Block, B.A. (2003). Characterization of ryanodine receptor and Ca2+-ATPase isoforms in the thermogenic heater organ of blue marlin (Makaira nigricans). The Journal of experimental biology *206*, 805-812.

Mossenbock, K., Vegiopoulos, A., Rose, A.J., Sijmonsma, T.P., Herzig, S., and Schafmeier, T. (2014). Browning of white adipose tissue uncouples glucose uptake from insulin signaling. PloS one *9*, e110428.

Moura, M.A., Festuccia, W.T., Kawashita, N.H., Garofalo, M.A., Brito, S.R., Kettelhut, I.C., and Migliorini, R.H. (2005). Brown adipose tissue glyceroneogenesis is activated in rats exposed to cold. Pflugers Archiv : European journal of physiology *449*, 463-469.

Mukherjee, A., Ma, Y., Yuan, F., Gong, Y., Fang, Z., Mohamed, E.M., Berrios, E., Shao, H., and Fang, X. (2015). Lysophosphatidic Acid Up-Regulates Hexokinase II and Glycolysis to Promote Proliferation of Ovarian Cancer Cells. Neoplasia *17*, 723-734.

Murphy, D.J., and Vance, J. (1999). Mechanisms of lipid-body formation. Trends Biochem Sci *24*, 109-115.

Nadanaciva, S., Rana, P., Beeson, G.C., Chen, D., Ferrick, D.A., Beeson, C.C., and Will, Y. (2012). Assessment of drug-induced mitochondrial dysfunction via altered cellular respiration and acidification measured in a 96-well platform. Journal of bioenergetics and biomembranes *44*, 421-437.

Nagashima, Y., Ohno, T., Ogawa, K., and Kuroshima, A. (1995). Effects of fasting and refeeding on some metabolic characteristics of rat brown adipose tissue. Jpn J Physiol *45*, 645-658.

Nedergaard, J., and Cannon, B. (2013). UCP1 mRNA does not produce heat. Biochimica et Biophysica Acta (BBA) - Molecular and Cell Biology of Lipids *1831*, 943-949.

Nedergaard, J., and Lindberg, O. (1982). The brown fat cell. International review of cytology *74*, 187-286.

Newby, F.D., Sykes, M.N., and DiGirolamo, M. (1988). Regional differences in adipocyte lactate production from glucose. The American journal of physiology *255*, E716-722.

Newsholme, E., Randle, P., and Manchester, K. (1962). Inhibition of the phosphofructokinase reaction in perfused rat heart by respiration of ketone bodies, fatty acids and pyruvate. Nature *193*, 270-271.

Nicholls, D.G., and Locke, R.M. (1984). Thermogenic mechanisms in brown fat. Physiological reviews *64*, 1-64.

Nicholson, J.K. (2006). Global systems biology, personalized medicine and molecular epidemiology. Molecular systems biology *2*, 52.

Nishimura, H., Pallardo, F.V., Seidner, G.A., Vannucci, S., Simpson, I.A., and Birnbaum, M.J. (1993). Kinetics of GLUT1 and GLUT4 glucose transporters expressed in Xenopus oocytes. The Journal of biological chemistry *268*, 8514-8520.

Ogawa, K., Ohno, T., and Kuroshima, A. (1987). Muscle and brown adipose tissue fatty acid profiles in cold-exposed rats. Jpn J Physiol *37*, 783-796.

Ogawa, K., Ohno, T., and Kuroshima, A. (1992). Effects of cold acclimation on cold-induced changes in lipid metabolism of rat brown adipose tissue. Jpn J Physiol *42*, 63-73.

Olmsted, J., and Williams, G.M. (1997). Chemistry : the molecular science (Dubuque, IA: Brown).

Olsen, J.M., Csikasz, R.I., Dehvari, N., Lu, L., Sandström, A., Öberg, A.I., Nedergaard, J., Stone-Elander, S., and Bengtsson, T. (2017). β3-Adrenergically Induced Glucose Uptake in Brown Adipose Tissue is Independent of UCP1 Presence or Activity: Mediation through the mTOR Pathway. Molecular metabolism.

Olsen, J.M., Sato, M., Dallner, O.S., Sandström, A.L., Pisani, D.F., Chambard, J.-C., Amri, E.-Z., Hutchinson, D.S., and Bengtsson, T. (2014). Glucose uptake in brown fat cells is dependent on mTOR complex 2–promoted GLUT1 translocation. The Journal of cell biology *207*, 365-374.

Orava, J., Nuutila, P., Lidell, Martin E., Oikonen, V., Noponen, T., Viljanen, T., Scheinin, M., Taittonen, M., Niemi, T., Enerbäck, S.*, et al.* (2011). Different Metabolic Responses of Human Brown Adipose Tissue to Activation by Cold and Insulin. Cell metabolism *14*, 272-279.

Orava, J., Nuutila, P., Noponen, T., Parkkola, R., Viljanen, T., Enerback, S., Rissanen, A., Pietilainen, K.H., and Virtanen, K.A. (2013). Blunted Metabolic Responses to Cold and Insulin Stimulation in Brown Adipose Tissue of Obese Humans. Obesity (Silver Spring, Md).

Pagnon, J., Matzaris, M., Stark, R., Meex, R.C., Macaulay, S.L., Brown, W., O'Brien, P.E., Tiganis, T., and Watt, M.J. (2012). Identification and functional characterization of protein kinase A phosphorylation sites in the major lipolytic protein, adipose triglyceride lipase. Endocrinology *153*, 4278-4289.

Pasnoor, M., Dimachkie, M.M., Kluding, P., and Barohn, R.J. (2013). DIABETIC NEUROPATHY PART 1: OVERVIEW AND SYMMETRIC PHENOTYPES. Neurologic clinics *31*, 425-445.

Patti, G.J., Yanes, O., and Siuzdak, G. (2012). Innovation: Metabolomics: the apogee of the omics trilogy. Nature reviews Molecular cell biology *13*, 263-269.

Patzel, V. (2007). In silico selection of active siRNA. Drug discovery today *12*, 139-148.

Prentki, M. (2006). Islet β cell failure in type 2 diabetes. *116*, 1802-1812.

Puri, V., Konda, S., Ranjit, S., Aouadi, M., Chawla, A., Chouinard, M., Chakladar, A., and Czech, M.P. (2007). Fat-specific protein 27, a novel lipid droplet protein that enhances triglyceride storage. The Journal of biological chemistry *282*, 34213-34218.

Qi, Y., Kapterian, T.S., Du, X., Ma, Q., Fei, W., Zhang, Y., Huang, X., Dawes, I.W., and Yang, H. (2016). CDP-diacylglycerol synthases regulate the growth of lipid droplets and adipocyte development. Journal of lipid research *57*, 767-780.

Rafael, J., and Heldt, H. (1976). Binding of guanine nucleotides to the outer surface of the inner membrane of guinea pig brown fat mitochondria in correlation with the thermogenic activity of the tissue. FEBS letters *63*, 304-308.

Rambold, A.S., Cohen, S., and Lippincott-Schwartz, J. (2015). Fatty acid trafficking in starved cells: regulation by lipid droplet lipolysis, autophagy, and mitochondrial fusion dynamics. Developmental cell *32*, 678-692.

Rauch, J.C., and Hayward, J. (1969). Topography and vascularization of brown fat in a small nonhibernator (deer mouse, Peromyscus maniculatus). Canadian journal of zoology *47*, 1301-1314.

Rich, P.R., and Marechal, A. (2010). The mitochondrial respiratory chain. Essays in biochemistry *47*, 1-23.

Rim, J.S., Xue, B., Gawronska-Kozak, B., and Kozak, L.P. (2004). Sequestration of thermogenic transcription factors in the cytoplasm during development of brown adipose tissue. Journal of Biological Chemistry *279*, 25916-25926.

Robidoux, J., Kumar, N., Daniel, K.W., Moukdar, F., Cyr, M., Medvedev, A.V., and Collins, S. (2006). Maximal beta3-adrenergic regulation of lipolysis involves Src and epidermal growth factor receptor-dependent ERK1/2 activation. The Journal of biological chemistry *281*, 37794-37802.

Rogers, N.H., Landa, A., Park, S., and Smith, R.G. (2012). Aging leads to a programmed loss of brown adipocytes in murine subcutaneous white adipose tissue. Aging cell *11*, 1074-1083.

Rolfe, D., and Brand, M.D. (1996). Contribution of mitochondrial proton leak to skeletal muscle respiration and to standard metabolic rate. American Journal of Physiology-Cell Physiology *271*, C1380-C1389.

Rosenwald, M., Perdikari, A., Rulicke, T., and Wolfrum, C. (2013). Bi-directional interconversion of brite and white adipocytes. Nature cell biology *15*, 659-667.

Rowland, L.A., Bal, N.C., Kozak, L.P., and Periasamy, M. (2015). Uncoupling Protein 1 and Sarcolipin Are Required to Maintain Optimal Thermogenesis, and Loss of Both Systems Compromises Survival of Mice under Cold Stress. The Journal of biological chemistry *290*, 12282-12289.

Sabater, D., Arriarán, S., Romero, M.d.M., Agnelli, S., Remesar, X., Fernández-López, J.A., and Alemany, M. (2014). Cultured 3T3L1 adipocytes dispose of excess medium glucose as lactate under abundant oxygen availability. Sci Rep *4*.

Sanchez-Gurmaches, J., Hung, C.-M., Sparks, C.A., Tang, Y., Li, H., and Guertin, D.A. (2012). PTEN loss in the Myf5 lineage redistributes body fat and reveals subsets of white adipocytes that arise from Myf5 precursors. Cell metabolism *16*, 348-362.

Sarwar, N., Gao, P., Seshasai, S.R., Gobin, R., Kaptoge, S., Di Angelantonio, E., Ingelsson, E., Lawlor, D.A., Selvin, E., Stampfer, M.*, et al.* (2010). Diabetes mellitus, fasting blood glucose concentration, and risk of vascular disease: a collaborative meta-analysis of 102 prospective studies. Lancet (London, England) *375*, 2215-2222.

Scholander, P.F., Hock, R., Walters, V., and Irving, L. (1950). Adaptation to cold in arctic and tropical mammals and birds in relation to body temperature, insulation, and basal metabolic rate. The Biological Bulletin *99*, 259-271.

Schulz, T.J., Huang, T.L., Tran, T.T., Zhang, H., Townsend, K.L., Shadrach, J.L., Cerletti, M., McDougall, L.E., Giorgadze, N., Tchkonia, T.*, et al.* (2011). Identification of inducible brown adipocyte progenitors residing in skeletal muscle and white fat. Proceedings of the National Academy of Sciences of the United States of America *108*, 143-148.

Schweiger, M., Eichmann, T.O., Taschler, U., Zimmermann, R., Zechner, R., and Lass, A. (2014). Measurement of lipolysis. Methods in enzymology *538*, 171-193.

Schweiger, M., Schreiber, R., Haemmerle, G., Lass, A., Fledelius, C., Jacobsen, P., Tornqvist, H., Zechner, R., and Zimmermann, R. (2006). Adipose triglyceride lipase and hormone-sensitive lipase are the major enzymes in adipose tissue triacylglycerol catabolism. The Journal of biological chemistry *281*, 40236-40241.

Seale, P., Bjork, B., Yang, W., Kajimura, S., Chin, S., Kuang, S., Scime, A., Devarakonda, S., Conroe, H.M., and Erdjument-Bromage, H. (2008). PRDM16 controls a brown fat/skeletal muscle switch. Nature *454*, 961-967.

Shabalina, I.G., Hoeks, J., Kramarova, T.V., Schrauwen, P., Cannon, B., and Nedergaard, J. (2010). Cold tolerance of UCP1-ablated mice: a skeletal muscle mitochondria switch toward lipid oxidation with marked UCP3 up-regulation not associated with increased basal, fatty acid- or ROS-induced uncoupling or enhanced GDP effects. Biochimica et Biophysica Acta (BBA)-Bioenergetics *1797*, 968-980.

Shabalina, I.G., Jacobsson, A., Cannon, B., and Nedergaard, J. (2004). Native UCP1 displays simple competitive kinetics between the regulators purine nucleotides and fatty acids. Journal of Biological Chemistry *279*, 38236-38248.

Shabalina, I.G., Petrovic, N., de Jong, J.M., Kalinovich, A.V., Cannon, B., and Nedergaard, J. (2013). UCP1 in brite/beige adipose tissue mitochondria is functionally thermogenic. Cell reports *5*, 1196-1203.

Shen, Z., Belinson, J., Morton, R.E., Xu, Y., and Xu, Y. (1998). Phorbol 12-myristate 13-acetate stimulates lysophosphatidic acid secretion from ovarian and cervical cancer cells but not from breast or leukemia cells. Gynecologic oncology *71*, 364-368.

Shibata, H., Perusse, F., Vallerand, A., and Bukowiecki, L.J. (1989). Cold exposure reverses inhibitory effects of fasting on peripheral glucose uptake in rats. The American journal of physiology *257*, R96-101.

Shimizu, Y., Kielar, D., Minokoshi, Y., and Shimazu, T. (1996). Noradrenaline increases glucose transport into brown adipocytes in culture by a mechanism different from that of insulin. The Biochemical journal *314 (Pt 2)*, 485-490.

Shimizu, Y., Nikami, H., and Saito, M. (1991). Sympathetic activation of glucose utilization in brown adipose tissue in rats. Journal of biochemistry *110*, 688-692.

Shimizu, Y., Satoh, S., Yano, H., Minokoshi, Y., Cushman, S.W., and Shimazu, T. (1998). Effects of noradrenaline on the cell-surface glucose transporters in cultured brown adipocytes: novel mechanism for selective activation of GLUT1 glucose transporters. The Biochemical journal *330 (Pt 1)*, 397-403.

Si, Y., Shi, H., and Lee, K. (2009). Metabolic flux analysis of mitochondrial uncoupling in 3T3-L1 adipocytes. PloS one *4*, e7000.

Silva, J.E. (2006). Thermogenic mechanisms and their hormonal regulation. Physiological reviews *86*, 435-464.

Skulachev, V.P. (1991). Fatty acid circuit as a physiological mechanism of uncoupling of oxidative phosphorylation. FEBS letters *294*, 158-162.

Smith, W.S., Broadbridge, R., East, J.M., and Lee, A.G. (2002). Sarcolipin uncouples hydrolysis of ATP from accumulation of Ca2+ by the Ca2+-ATPase of skeletal-muscle sarcoplasmic reticulum. The Biochemical journal *361*, 277-286.

Stanford, K.I., Middelbeek, R.J., Townsend, K.L., An, D., Nygaard, E.B., Hitchcox, K.M., Markan, K.R., Nakano, K., Hirshman, M.F., Tseng, Y.H.*, et al.* (2013). Brown adipose tissue regulates glucose homeostasis and insulin sensitivity. The Journal of clinical investigation *123*, 215-223.

Steinbring, J., Graja, A., Jank, A.M., and Schulz, T.J. (2017). Flow Cytometric Isolation and Differentiation of Adipogenic Progenitor Cells into Brown and Brite/Beige Adipocytes. Methods Mol Biol *1566*, 25-36.

Stralfors, P., and Belfrage, P. (1983). Phosphorylation of hormone-sensitive lipase by cyclic AMP-dependent protein kinase. The Journal of biological chemistry *258*, 15146-15152.

Stryjecki, C., Roke, K., Clarke, S., Nielsen, D., Badawi, A., El-Sohemy, A., Ma, D.W.L., and Mutch, D.M. (2012). Enzymatic activity and genetic variation in SCD1 modulate the relationship between fatty acids and inflammation. Molecular Genetics and Metabolism *105*, 421-427.

Takeuchi, K., and Reue, K. (2009). Biochemistry, physiology, and genetics of GPAT, AGPAT, and lipin enzymes in triglyceride synthesis. American journal of physiology Endocrinology and metabolism *296*, E1195-1209.

Tharp, K.M., Jha, A.K., Kraiczy, J., Yesian, A., Karateev, G., Sinisi, R., Dubikovskaya, E.A., Healy, K.E., and Stahl, A. (2015). Matrix-Assisted Transplantation of Functional Beige Adipose Tissue. Diabetes *64*, 3713-3724.

Thonberg, H., Fredriksson, J.M., Nedergaard, J., and Cannon, B. (2002). A novel pathway for adrenergic stimulation of cAMP-response-element-binding protein (CREB) phosphorylation: mediation via α1-adrenoceptors and protein kinase C activation. Biochemical Journal *364*, 73-79.

Trayhurn, P. (1979). Fatty acid synthesis in vivo in brown adipose tissue, liver and white adipose tissue of the cold-acclimated rat. FEBS letters *104*, 13-16.

Trayhurn, P. (1981). Fatty acid synthesis in mouse brown adipose tissue. The influence of environmental temperature on the proportion of whole-body fatty acid synthesis in brown adipose tissue and the liver. Biochimica et biophysica acta *664*, 549-560.

Tsigos, C., Hainer, V., Basdevant, A., Finer, N., Mathus-Vliegen, E., Micic, D., Maislos, M., Roman, G., Schutz, Y., Toplak, H.*, et al.* (2011). Criteria for EASO-collaborating centres for obesity management. Obesity facts *4*, 329-333.

Ukropec, J., Anunciado, R.P., Ravussin, Y., Hulver, M.W., and Kozak, L.P. (2006a). UCP1-independent thermogenesis in white adipose tissue of cold-acclimated Ucp1-/- mice. The Journal of biological chemistry *281*, 31894-31908.

Ukropec, J., Anunciado, R.V., Ravussin, Y., and Kozak, L.P. (2006b). Leptin is required for uncoupling protein-1-independent thermogenesis during cold stress. Endocrinology *147*, 2468-2480.

Unger, R.H., and Scherer, P.E. (2010). Gluttony, sloth and the metabolic syndrome: a roadmap to lipotoxicity. Trends in endocrinology and metabolism: TEM *21*, 345-352.

Vallerand, A.L., Perusse, F., and Bukowiecki, L.J. (1990). Stimulatory effects of cold exposure and cold acclimation on glucose uptake in rat peripheral tissues. The American journal of physiology *259*, R1043-1049.

van Marken Lichtenbelt, W.D., Vanhommerig, J.W., Smulders, N.M., Drossaerts, J.M., Kemerink, G.J., Bouvy, N.D., Schrauwen, P., and Teule, G.J. (2009). Cold-activated brown adipose tissue in healthy men. The New England journal of medicine *360*, 1500-1508.

Virtanen, K.A., Lidell, M.E., Orava, J., Heglind, M., Westergren, R., Niemi, T., Taittonen, M., Laine, J., Savisto, N.-J., and Enerbäck, S. (2009). Functional brown adipose tissue in healthy adults. New England Journal of Medicine *360*, 1518-1525.

Vitali, A., Murano, I., Zingaretti, M.C., Frontini, A., Ricquier, D., and Cinti, S. (2012). The adipose organ of obesity-prone C57BL/6J mice is composed of mixed white and brown adipocytes. Journal of lipid research *53*, 619-629.

Waldén, T.B., Hansen, I.R., Timmons, J.A., Cannon, B., and Nedergaard, J. (2012). Recruited vs. nonrecruited molecular signatures of brown,“brite,” and white adipose tissues. American Journal of Physiology-Endocrinology and Metabolism *302*, E19-E31.

Walther, T.C., and Farese, R.V., Jr. (2012). Lipid droplets and cellular lipid metabolism. Annual review of biochemistry *81*, 687-714.

Wang, Q.A., Tao, C., Gupta, R.K., and Scherer, P.E. (2013). Tracking adipogenesis during white adipose tissue development, expansion and regeneration. Nature medicine.

Wang, Y., Chen, Y., and Fang, J. (2017). Post-transcriptional and Post-translational regulation of Central Carbon Metabolic Enzymes in Cancer. Anti-cancer agents in medicinal chemistry.

Weisiger, R.A. (2007). Mechanisms of intracellular fatty acid transport: role of cytoplasmic-binding proteins. Journal of molecular neuroscience : MN *33*, 42-44.

Welte, M.A. (2015). Expanding roles for lipid droplets. Current biology : CB *25*, R470-481.

Wendel, A.A., Lewin, T.M., and Coleman, R.A. (2009). Glycerol-3-phosphate acyltransferases: rate limiting enzymes of triacylglycerol biosynthesis. Biochimica et biophysica acta *1791*, 501-506.

WHO (2009). Global health risks: mortality and burden of disease attributable to selected major risks.

WHO (2016). Obesity and overweight. Fact sheet (World Health Organization).

Williams, D.D., and Platner, W.S. (1967). Cold-induced changes in fatty acids of the rat and hamster. The American journal of physiology *212*, 167-172.

Winder, W.W., and Thomson, D.M. (2007). Cellular energy sensing and signaling by AMP-activated protein kinase. Cell biochemistry and biophysics *47*, 332-347.

Winkler, E., and Klingenberg, M. (1994). Effect of fatty acids on H+ transport activity of the reconstituted uncoupling protein. Journal of Biological Chemistry *269*, 2508-2515.

Wu, J., Boström, P., Sparks, Lauren M., Ye, L., Choi, Jang H., Giang, A.-H., Khandekar, M., Virtanen, Kirsi A., Nuutila, P., Schaart, G.*, et al.* (2012). Beige Adipocytes Are a Distinct Type of Thermogenic Fat Cell in Mouse and Human. Cell *150*, 366-376.

Wu, L., Zhou, L., Chen, C., Gong, J., Xu, L., Ye, J., Li, D., and Li, P. (2014). Cidea controls lipid droplet fusion and lipid storage in brown and white adipose tissue. Science China Life sciences *57*, 107-116.

Wu, M., Neilson, A., Swift, A.L., Moran, R., Tamagnine, J., Parslow, D., Armistead, S., Lemire, K., Orrell, J., Teich, J.*, et al.* (2007). Multiparameter metabolic analysis reveals a close link between attenuated mitochondrial bioenergetic function and enhanced glycolysis dependency in human tumor cells. American journal of physiology Cell physiology *292*, C125-136.

Xue, B., Rim, J.S., Hogan, J.C., Coulter, A.A., Koza, R.A., and Kozak, L.P. (2007). Genetic variability affects the development of brown adipocytes in white fat but not in interscapular brown fat. J Lipid Res *48*, 41-51.

Yamaguchi, T., Omatsu, N., Matsushita, S., and Osumi, T. (2004). CGI-58 Interacts with Perilipin and Is Localized to Lipid Droplets POSSIBLE INVOLVEMENT OF CGI-58 MISLOCALIZATION IN CHANARIN-DORFMAN SYNDROME. Journal of Biological Chemistry *279*, 30490-30497.

Yang, G., Murashige, D.S., Humphrey, S.J., and James, D.E. (2015). A Positive Feedback Loop between Akt and mTORC2 via SIN1 Phosphorylation. Cell reports *12*, 937-943.

Young, P., Arch, J., and Ashwell, M. (1984). Brown adipose tissue in the parametrial fat pad of the mouse. FEBS letters *167*, 10-14.

Zaid, H., Antonescu, C., Randhawa, V., and Klip, A. (2008). Insulin action on glucose transporters through molecular switches, tracks and tethers. Biochemical Journal *413*, 201-215.

Zehmer, J.K., Bartz, R., Bisel, B., Liu, P., Seemann, J., and Anderson, R.G. (2009). Targeting sequences of UBXD8 and AAM-B reveal that the ER has a direct role in the emergence and regression of lipid droplets. Journal of cell science *122*, 3694-3702.

Zhang, A., Sun, H., Xu, H., Qiu, S., and Wang, X. (2013). Cell Metabolomics. OMICS : a Journal of Integrative Biology *17*, 495-501.

Zhang, S., Wang, Y., Cui, L., Deng, Y., Xu, S., Yu, J., Cichello, S., Serrero, G., Ying, Y., and Liu, P. (2016). Morphologically and Functionally Distinct Lipid Droplet Subpopulations. Scientific reports *6*, 29539.

Zhao, F.Q., and Keating, A.F. (2007). Functional Properties and Genomics of Glucose Transporters. Current Genomics *8*, 113-128.

Zhou, Z., Toh, S.Y., Chen, Z., Guo, K., Ng, C.P., Ponniah, S., Lin, S.-C., Hong, W., and Li, P. (2003). Cidea-deficient mice have lean phenotype and are resistant to obesity. Nature genetics *35*, 49-56.

Zingaretti, M.C., Crosta, F., Vitali, A., Guerrieri, M., Frontini, A., Cannon, B., Nedergaard, J., and Cinti, S. (2009). The presence of UCP1 demonstrates that metabolically active adipose tissue in the neck of adult humans truly represents brown adipose tissue. The FASEB Journal *23*, 3113-3120.

6 Appendix

6.1 Supplementary tables

Table S1: Biochemicals from E2 and E3 that show significant interaction of genotype and treatment. Data represent mean values of relative signal intensities of two biological replicates ± SD

BIOCHEMICAL	Adj. p-values	129SV/S6				C57BL/6J UCP1 $^{+/+}$				C57BL/6J UCP1 $^{-/-}$			
		ctrl		iso		ctrl		iso		ctrl		iso	
		mean	SD	mean	SD	mean	SD	mean	SD	mean	SD	mean	SD
1-arachidonoyl-GPE (20:4n6)*	0.04	4.55	0.22	9.97	1.08	3.28	1.31	4.42	0.33	2.73	1.27	4.39	0.80
1-arachidonoyl-GPI (20:4)*	0.03	3.69	0.38	17.11	0.29	2.89	2.22	11.17	0.62	2.08	1.55	7.48	2.82
1-palmitoleoyl-GPC (16:1)*	0.01	4.27	0.97	19.98	3.06	3.43	1.51	10.50	0.92	3.27	2.15	7.99	1.41
10-heptadecenoate (17:1n7)	0.01	3.95	1.46	98.41	13.68	2.18	2.33	102.02	5.77	1.76	1.56	23.02	24.72
15-methylpalmitate	0.01	4.17	1.54	19.69	2.53	2.42	1.82	12.97	1.83	1.42	0.89	5.73	2.09
2-palmitoleoyl-GPC (16:1)*	0.02	4.18	0.72	15.90	1.12	3.34	2.21	8.40	1.21	3.35	2.65	6.73	0.61
5-methylthioadenosine (MTA)	0.01	5.65	0.37	2.87	0.11	4.50	0.75	2.30	0.21	2.91	0.22	2.43	0.32
arachidonate (20:4n6)	0.00	3.90	1.25	33.64	0.92	1.62	1.46	10.38	0.68	1.56	1.38	7.20	4.25
choline phosphate	0.03	7.94	0.59	2.81	0.69	4.78	0.98	1.71	0.47	4.72	0.61	2.87	0.38
coenzyme A	0.05	7.19	0.25	3.90	0.00	6.02	0.76	3.43	0.16	2.00	0.11	2.73	2.14
dihomo-linolenate (20:3n3 or n6)	0.00	1.22	0.18	9.09	0.95	0.84	0.49	3.92	0.26	1.38	1.26	3.85	0.10
docosahexaenoate (DHA; 22:6n3)	0.00	4.20	1.17	18.02	0.79	1.59	1.27	8.95	0.48	1.83	1.76	4.69	1.07
docosapentaenoate (n3 DPA; 22:5n3)	0.00	3.57	0.01	20.54	2.53	1.39	1.07	12.88	0.64	1.45	1.18	5.87	2.42
eicosenoate (20:1)	0.03	3.54	1.34	39.52	8.85	2.02	2.02	48.93	8.67	1.42	1.35	14.52	10.98

Table S1 continued

glycerophosphorylcholine (GPC)	0.02	8.30	1.00	3.89	0.44	4.51	0.14	3.30	0.03	3.61	0.58	2.69	1.05
guanine	0.02	7.03	1.66	3.95	0.29	4.06	1.09	3.23	0.00	2.62	0.93	5.30	1.01
guanosine	0.02	4.64	0.61	8.90	0.29	2.87	0.93	3.31	0.78	3.91	1.58	3.52	0.80
guanosine 5'-monophosphate (5'-GMP)	0.02	3.72	0.04	17.20	0.64	1.54	1.23	15.04	0.80	1.10	0.97	6.50	3.60
hippurate	0.04	4.96	0.39	5.89	0.58	3.04	0.27	5.57	0.20	2.32	0.37	3.39	0.34
linoleate (18:2n6)	0.01	3.03	0.10	21.91	1.50	1.78	1.51	17.29	0.09	1.72	1.04	7.52	4.24
linolenate [alpha or gamma; (18:3n3 or 6)]	0.01	3.40	0.45	17.75	1.85	1.57	0.94	12.11	0.15	1.79	1.02	6.02	2.49
malate	0.00	6.93	0.94	3.99	0.05	4.40	0.41	3.76	0.69	2.90	0.47	4.80	0.52
maltotetraose	0.00	1.85	0.12	2.15	1.26	1.00	0.18	14.63	1.45	1.62	1.11	0.89	0.12
mead acid (20:3n9)	0.01	0.26	0.03	6.49	0.06	0.19	0.03	3.04	0.68	0.73	0.80	4.52	0.66
myristate (14:0)	0.05	4.39	1.64	18.64	1.63	2.61	1.99	17.84	4.49	1.47	0.81	6.55	2.43
myristoleate (14:1n5)	0.00	3.84	1.00	35.52	1.73	1.06	0.95	26.21	5.78	1.76	1.84	6.98	2.79
oleate (18:1n9)	0.02	3.99	1.35	46.43	5.43	2.69	2.78	50.26	0.82	1.82	1.52	15.31	14.17
palmitate (16:0)	0.03	4.27	1.45	23.01	3.36	2.69	2.24	22.80	3.01	1.43	0.88	8.05	4.37
palmitoleate (16:1n7)	0.00	4.02	1.47	71.88	3.97	1.55	1.58	63.46	1.72	1.63	1.50	14.81	14.26
pentadecanoate (15:0)	0.02	4.45	1.82	27.23	5.97	2.70	2.22	24.21	3.35	1.47	0.72	7.85	3.25
phenol red	0.01	6.97	0.28	4.71	0.08	3.99	0.45	3.33	0.18	2.94	0.26	3.32	0.68
phosphopantetheine	0.00	4.14	1.36	30.62	2.40	1.32	0.64	8.40	0.65	0.96	0.57	5.65	2.81
UDP-glucuronate	0.02	7.72	0.20	4.04	0.56	5.59	0.29	2.49	1.00	2.45	0.27	2.91	1.63
uridine	0.00	4.46	0.49	20.57	3.28	1.21	0.79	12.33	1.07	1.61	1.28	4.86	1.25
xanthine	0.00	11.25	2.51	2.41	0.65	2.71	0.90	1.61	0.15	2.34	0.09	1.70	0.23
X - 08893	0.01	5.86	0.03	4.40	0.07	3.83	0.45	3.85	0.34	4.29	0.04	3.24	0.07
X - 11909	0.00	3.40	0.15	17.64	3.69	1.66	1.49	20.30	0.75	1.88	1.71	5.64	0.16
X - 12899	0.01	3.09	2.30	18.72	1.15	2.04	1.35	10.51	1.88	1.52	0.99	5.75	0.93
X - 13372	0.03	7.55	0.42	3.35	0.79	7.09	0.91	2.48	0.08	4.07	0.93	2.87	0.77
X - 16094	0.03	1.90	0.40	13.41	1.80	2.49	2.16	8.36	1.35	3.73	1.40	8.76	0.09

Table S2: Relative signal intensities of metabolites that were altered upon iso treatment independently from UCP1

	129SV/S6						C57BL/6JUCP1 $^{+/+}$						C57BL/6JUCP1 $^{-/-}$					
	ctrl			iso			ctrl			iso			ctrl			iso		
Biochemical	E1	E2	E3	E1	E2	E3	E1	E2	E3	E1	E2	E3	E1	E2	E3	E1	E2	E3
glutamate, gamma-methyl ester	7.22	7.23	6.18	1.51	3.24	3.66	6.77	5.59	6.41	1.93	3.15	3.49	7.66	3.91	4.57	1.92	2.17	3.54
glutathione, oxidized (GSSG)	6.49	4.42	5.08	3.33	3.88	3.59	6.26	4.16	3.92	4.11	3.84	2.99	9.79	4.93	4.68	4.65	3.40	3.83
adenosine 5'-monophosphate (AMP)	5.56	3.89	3.57	6.71	7.97	7.80	3.05	5.32	1.06	5.42	9.65	9.09	3.97	2.23	0.54	6.86	5.50	4.06
10-nonadecenoate (19:1n9)	1.99	0.14	1.20	5.49	6.32	7.36	0.58	1.07	0.10	9.72	6.50	6.19	0.37	1.55	0.20	3.96	5.89	6.24
uridine 5'-triphosphate (UTP)	4.53	12.90	7.46	0.69	1.61	1.79	6.37	4.80	14.39	1.23	1.20	0.99	7.06	5.54	6.88	1.91	0.36	3.72
adenosine 5'-triphosphate (ATP)	3.86	10.78	6.96	0.58	1.64	1.42	5.72	8.21	18.36	1.57	1.57	1.54	6.47	7.07	5.02	2.66	0.34	3.60

Table S3: Relative signal intensities of metabolites present in distinct amounts between mouse strain

	129SV/S6						C57BL/6J UCP1 $^{+/+}$						C57BL/6J UCP1 $^{-/-}$					
	ctrl			iso			ctrl			iso			ctrl			iso		
Biochemical	E1	E2	E3	E1	E2	E3	E1	E2	E3	E1	E2	E3	E1	E2	E3	E1	E2	E3
gamma-glutamylisoleucine*	7.64	5.63	5.39	6.02	5.14	4.25	2.09	3.82	3.29	1.67	2.94	2.23	2.36	3.24	2.54	1.89	3.07	2.87
gamma-glutamylthreonine*	8.54	8.45	5.35	6.64	7.98	5.88	1.85	7.68	3.91	2.21	3.52	2.76	1.56	3.16	3.98	2.02	2.05	3.48
gamma-glutamylvaline	17.58	8.98	6.94	12.60	7.26	7.07	3.93	4.44	3.40	2.97	3.89	3.01	3.27	3.78	3.67	3.18	3.28	3.41
ophthalmate	22.10	8.17	6.81	13.70	6.58	5.22	5.33	5.34	3.53	3.05	2.95	2.48	3.33	3.53	3.84	2.98	2.17	3.13
X - 12776	5.02	5.52	5.98	4.77	4.36	4.34	3.91	4.64	3.85	3.91	3.98	3.15	3.97	3.57	2.17	3.67	3.43	4.06
dihomo-linoleate (20:2n6)	2.33	0.38	0.70	8.42	4.70	5.04	0.80	0.52	0.25	6.74	3.93	3.19	0.78	1.41	0.25	3.71	4.92	4.89

6.2 Chemicals and reagents

Table S4: Chemicals and reagents used in this work

Name	Producer	Order number
100 bp-DNA Ladder Equalized	Carl Roth	T833.1
2-Mercaptoethanol	Carl Roth	4227
2-Propanol	Carl Roth	T910
3,3′,5-Triiodo-L-thyronine (T3)	Sigma	T2752
^{3}H labeled 2-deoxy-D-glucose		
3-Isobutyl-1-methylxanthine (IBMX)	Sigma	I5879
Acetic acid Rotipuran®	Carl Roth	3738.4
Acetone	Carl Roth	9372.4
Acetyl coenzyme A sodium salt	Sigma	A2056-5MG
Agar-Agar	Carl Roth	5210.2
Agarose	Serva	11406.02
Ammoniumperoxy disulfate (AMPS)	Carl Roth	9592.3
Antimycin A	Sigma	A8674
Bovine serum albumin (BSA) fatty acid free	Sigma	A3803
Bovine serum albumin (BSA) Fraction V	Carl Roth	8076.3
Carbonylcyanide-4(trifluoromethoxy)- phenylhydrazone (FCCP)	Sigma	C2920
Chloroform p.a	Carl Roth	Y015.1
Collagenase A	Biochrom	C1-22
D-(+)-Glucose	Carl Roth	
Dexamethasone	Sigma	D1159
Dimethylsulfoxide Rotipuran® (DMSO)	Carl Roth	4720.2
DMEM base	Sigma	D5030
DMEM without glucose or pyruvate	Gibco, Themo scientific	11966025
Dulbecco's Modified Eagle's Medium (DMEM)	Sigma	D5796
Ethanol ≥99.8%	Carl Roth	9065
Ethanol 70%, denaturated	Carl Roth	T913
Ethanol 96 %, denaturated	Carl Roth	T171
Ethylenediamine tetraacetic aciddisodium salt dihydroxide (EDTA)	Carl Roth	8043.2
FBS Superior	Biochrom	S0615
Fungizone (Amphotericin B)	Biochrom	A2612
Glutamax	Life Technologies	35050-061
Glycin Pufferan	Carl Roth	3908.2
Hank"s balanced salt solution (HBSS) w/Mg;Ca	Invitrogen	14025-050
HD Green Plus DNA stain	INTAS	Ba20121127
HEPES Pufferan	Carl Roth	9105.4
Indomethacin	Sigma	I7378
Insulin Solution, human 10 mg/ml	Sigma	I9278
Isoproterenol hydrochloride	Sigma	I6505-500MG
LightCycler® 480 Probes Master	Roche	04707404001
Magnesium chloride hexahydrate (MgCl2)	Carl Roth	2189.2
Magnesium sulfate heptohydrate (MgSO4)	Carl Roth	P027.2
Methanol	Carl Roth	4627
Nonidet® P40	Fluka Analytical	74385
Nuclease-free water	Promega	P119c
Oligomycin	Sigma	O4876
Orange G	Carl Roth	O318.2
Oxaloacetate	Sigma	O4126-1G
PageRulerTM Prestained Protein Ladder	Thermo Scientific	26616
PBS Tablets	Gibco Life Technologies	18912-014
Penicillin/Streptomycin 10,000 µg/ml	Biochrom	A2212
Potassium chloride (KCl)	Carl Roth	6781.1
Protease Inhibitor Cocktail	Sigma	P8340
Rosiglitazone	Biomol (Cayman)	Cay-71740
Rotiphorese® Gel30	Carl Roth	3029.1
SensiMix SYBR No-ROX	Bioline	QT650-05
Sodium chloride (NaCl)	Carl Roth	3957.1
Sodium hydrogen phosphate (Na2HPO4)	Carl Roth	T879.2
Sodium lauryl sulfate (SDS)	Carl Roth	4360.2
Sodium pyruvate 100 mM	Biochrom AG	L0473
TEMED	Carl Roth	2367.3
Trichlormethane/Chloroform	Carl Roth	Y015.1
TRIS Pufferan	Carl Roth	4888.2
TRIS-hydrochlorid Pufferan	Carl Roth	9090.3
TRIsure	Bioline	BIO-38033

Table S4 continued		
Trypsin/EDTA Solution 0.25% in PBS	Biochrom	L2163
Tryptone	Carl Roth	8952.2
Tween® 20	Carl Roth	9127.2
XF Calibrant	Agilent Technologies	100840-000

6.3 Kit systems

Table S5: Kit systems used in this work

Name	Producer	Order number
Free glycerol reagent	Sigma-Aldrich	F6428
Glycerol standard solution	Sigma-Aldrich	G7793
NEFA standard solution	Wako Chemicals	270-77000
NEFA-HR (2) R1	Wako Chemicals	436-91795
NEFA-HR (2) R2	Wako Chemicals	436-91995
Pierce® BCA Protein Assay Kit	Thermo Scientific	23227
QuantiTect® Reverse Transcription Kit	Qiagen	205315
RNA 6000 Nano Kit	Agilent Technologies	5067-1511
SensiFast cDNA Synthesis Kit	Bioline	BIO-65054
Stranded TNA LT kit	Illumina	RS-122-220
SV Total RNA Isolation System	Promega	Z3105
TruSeq SR Cluster Kit v3	Illumina	GD-401-3001
TruSeq SBS Kit v3-HS	Illumina	FC-401-300
XF96 extracellular fluxPak	Agilent Technologies	102310-001

6.4 Antibodies

Table S6: Antibodies used in this work

Name	Species	Producer	Order number
Primary antibodies			
Anti UCP1	Rabbit	Abcam	Ab10983
Anti-Actin, clone C4	Mouse	Millipore	MAB1501
Otto3 antiUCP1	Rabbit		
Secondary antibodies			
IRDye 680CW Donkey Anti-Mouse IgG		LI-COR	926-32222
IRDye 800CW Donkey Anti-Mouse IgG		LI-COR	926-32212
IRDye 800CW Goat Anti-Rabbit IgG		LI-COR	926-32213

6.5 Disposables

Table S7: Disposables used in this work

Name	Producer	Order number
Cell culture dish 100x20 mm	Sarstedt	83.1802
Cell culture dish 150x20 mm	Sarstedt	83.1803
Cell culture dish 35x10 mm	Sarstedt	83.3900
Cell culture dish 60x15 mm	Sarstedt	83.1801
Cell culture plates, 12-well	Sarstedt	83.3921
Cell culture plates, 24-well	Sarstedt	83.3922
Cell culture plates, 6-well	Sarstedt	83.3920
Cell strainer, 40 µM	BD Bioscience	352340
Frame Star 384-well	4titude	4ti-0382
Nitrocellulose	LI-COR	926-31092
Nunc 96F untreated	Thermo Scientific	260895
XF96 cell culture microplate	Agilent Technologies	101085-004
XF96 extracellular flux assay kit	Agilent Technologies	102310-001

6.6 Devices and other equipment

Table S8: Disposables and other equipment used in this work

Name	Producer
2010-GC-MS system	Shimadzu
AxioVert 40 Microscope	Zeiss
Bioanalyzer	Agilent Technologies
Centrifuge 5417R	Eppendorf
Centrifuge 5804R	Eppendorf
DFC360FX	Leica
DMI 4000B	Leica
Eppendorf Research plus 10-100, 8-Channel	Eppendorf
Eppendorf Research plus 30-300, 8-Channel	Eppendorf
HeraCell240	Heraeus, Thermo Scientific
HiSeq 2500 platform	Illumina
Infinite® M200 Microplate Reader	Tecan
Light Cycler® 480	Roche
Matrix electronic 384 equalizer pipette	Thermo Scientific
Metabolomics platform	
Mini-PROTEAN System	BioRad
Multipette®stream	Eppendorf
NanoQuant Plate	Tecan
Odyssey Infrared Imaging System	LI-COR
Odyssey Nitrocellulose Membrane	LI-COR
Peltier Thermal Cycler PTC-200	MJ Research
Pierce® Concentrators 7ml/9K MWCO	Thermo Scientific
Power Pac Basic	BioRad
RNA Seq	
Thermomixer comfort	Eppendorf
Thermo-Shaker	Universal Labortechnik
TransBlot SD	BioRad
Ultra-Turrax D-1	Miccra GmbH
XF Prep Station	Agilent Technologies
XF96 Extracellular Flux Analyzer	Agilent Technologies

6.7 Software and bioinformatics resources

Table S9: Software and bioinformatics resources

Name	Producer, Resources
GraphPad Prism 6	Graphpad Software, Inc.
Office Excel 2016	Microsoft
HCE	http://www.cs.umd.edu/hcil/hce/
MeV	https://sourceforge.net/projects/mev-tm4/
Incromap	Center for Bioinformatics Tübingen (ZBIT)
Mining Station	Genomatix
Genome Analyzer	Genomatix
Wave 2.2.0	Seahorse Bioscience
Odyssey V3.0	LI-COR
i-control 1.4	TECAN
LightCycler® 480 SW 1.5	Roche
SigmaPlot 12.5	SYSTAT Software Inc.
Leica Application Suite V3.8	Leica Microsystems

VI. Acknowledgements

An dieser Stelle möchte ich mich bei allen bedanken, die auf wissenschaftlicher und persönlicher Ebene zum Gelingen dieser Arbeit beigetragen haben.

Mein Dank gilt zunächst Prof. Dr. Martin Klingenspor für die Bereitstellung des Themas, die Betreuung, die Unterstützung und all die Anregungen und Ratschläge die diese Doktorarbeit ermöglicht haben.

Ebenso möchte ich mich bei meinem Zweitprüfer Prof. Dr. Martin Hrabě de Angelis für die Möglichkeit an diesem Projekt arbeiten zu dürfen und für den wissenschaftlichen Input bedanken.

Ich danke meinen Kooperationspartnern vom Genome Analysis Center des Helmholtz Zentrums München, Prof. Dr. Jerzy Adamski und Dr. Anna Artati für das Metabolite Profiling. Bei Dr. Josef Ecker möchte mich für die Lipidomics-Messungen bedanken.

Ein großes Dankeschön geht an Tobi für seine Betreuung und Unterstützung. Vielen Dank für all die hilfreichen Ratschläge, guten Ideen und den ansteckenden Enthusiasmus sowie für das Korrekturlesen dieser Arbeit.

Ich möchte mich bei allen Kollegen, mit denen ich im Laufe der Jahre zusammenarbeiten durfte, für die angenehme Arbeitsatmosphäre und die große Hilfsbereitschaft bedanken. Insbesondere danke ich Sabine, Anika und Philipp für ihre Hilfe im Labor und Flo und Yongguo für ihre wissenschaftlichen Ideen und Ratschläge.

Ein besonderer Dank gilt meiner Familie, die stets für mich da ist und mich immer bedingungslos unterstützt hat. Bei David bedanke ich mich herzlich für das Korrekturlesen. Johannes danke ich für den starken emotionalen Rückhalt und die liebevolle Unterstützung. Zuletzt möchte ich mich bei all meinen Freunden bedanken, die mich stets aufgebaut haben und für die erforderliche Abwechslung sorgten.

Dieses Projekt wurde vom Deutschen Zentrum für Diabetesforschung gefördert.

VII. Eidesstattliche Erklärung

Ich erkläre an Eides statt, dass ich die bei der promotionsführenden der Fakultät Wissenschaftszentrum Weihenstephan für Ernährung, Landnutzung und Umwelt der TUM zur Promotionsprüfung vorgelegte Arbeit mit dem Titel:

Functional phenotype and metabolic properties of brite and brown adipocytes

am Lehrstuhl für Molekulare Ernährungsmedizin unter der Anleitung und Betreuung durch Univ.-Prof. Dr. Martin Klingenspor ohne sonstige Hilfe erstellt und bei der Abfassung nur die gemäß § 6 Abs. 6 und 7 Satz 2 angegebenen Hilfsmittel benutzt habe.

Ich habe keine Organisation eingeschaltet, die gegen Entgelt Betreuerinnen und Betreuer für die Anfertigung von Dissertationen sucht, oder die mir obliegenden Pflichten hinsichtlich der Prüfungsleistungen für mich ganz oder teilweise erledigt.

Ich habe die Dissertation in dieser oder ähnlicher Form in keinem anderen Prüfungsverfahren als Prüfungsleistung vorgelegt.

Die vollständige Dissertation wurde noch nicht veröffentlicht.

Ich habe den angestrebten Doktorgrad noch nicht erworben und bin nicht in einem früheren Promotionsverfahren für den angestrebten Doktorgrad endgültig gescheitert.

Die öffentlich zugängliche Promotionsordnung der TUM ist mir bekannt, insbesondere habe ich die Bedeutung von § 28 (Nichtigkeit der Promotion) und § 29 (Entzug des Doktorgrades) zur Kenntnis genommen. Ich bin mir der Konsequenzen einer falschen Eidesstattlichen Erklärung bewusst.

Mit der Aufnahme meiner personenbezogenen Daten in die Alumni-Datei bei der TUM bin ich einverstanden

München, den ....

Unterschrift